UNIVERSITY OF
KWAZULU-NATAL

1,4,7,10,13,16-Hexaazacyclooctadecane (Hexacyclen) Induced Nitrosative Stress and Downregulated NF-κB Cell Survival Pathway in Human Embryonic Kidney (Hek293) and Colorectal Adenocarcinoma (Caco2) Cells

by

Mthokozisi Nxumalo (217001271)

BSc, BMedSc (Hons) (UKZN)

Submitted in fulfilment of the requirements for the degree of

Master of Medical Science

in the Discipline of Medical Biochemistry and Chemical Pathology

School of Laboratory Medicine and Medical Sciences

College of Health Sciences

University of KwaZulu-Natal

Durban

2022

DECLARATION

I Mthokozisi Bongani Nxumalo, declare that:

This dissertation contains original work done by the author and has not been submitted to UKZN or any other tertiary institution for the purposes of obtaining an academic qualification, whether by myself or any other party. The use of work by others has been duly acknowledged in the text. The research described in this study was carried out in the Department of Medical Biochemistry and Chemical Pathology, School of Laboratory Medicine and Medical Science, Faculty of Health Sciences, University of KwaZulu-Natal, Durban, under the supervision of Dr RB Khan.

_____ 28 June 2022

SIGNED : Mthokozisi Nxumalo DATE

ACKNOWLEDGEMENTS

God

All praise and thanks be to Him, who causes all things to work together for good to those who love Him and are called according to His purpose.

My family

To my late great grandmother (J.B Nyandeni) and grandfather (J.M Mnyandu), I cannot express enough how thankful and how much I appreciate you for the learning opportunities that you provided me with and for your wise words that encouraged me up until this day, may your souls continue resting in peace.

My grandmother (A.B Mnyandu), my mother (N.N Nxumalo), and the rest of my family would like to thank them for their support in my daily life and for having them by my side to guide me always. Their prosperity and unconditional love for me is truly a blessing.

Dr Khan

I am truly honoured to be your student. I am grateful for all the motivation, inspiration and support that you have given me all this time. I offer my sincere appreciation for the learning opportunity that you have granted me. The completion of this project could not have been accomplished without your support.

Dr Khumalo

Thank you for your advice, suggestions and corrections towards this project, I am also grateful for your time to make me a better scientist.

Dr Letty

Your guidance and your assistance in and out of the laboratory has made me a better person, thank you for everything there is still a lot that I want to learn from you.

Friends and colleagues of Medical Biochemistry

Thank you to my friends for their friendship and willingness to assist me. A special thanks to Nosipho Ntanzi and Siphosethu Mndebele for your laughter, jokes, those sleepless nights we had and those times we felt like giving up, thank you for standing by me and showing me that hard work and dedication pays off.

TABLE OF CONTENTS

Contents

LIST OF ABBREVIATIONS

B	Beta
μM	Micrometre
ΔΨM	Mitochondrial membrane potential
%	Percentage
$^{\bullet}OH$	Hydroxyl radicals
$^{\bullet}ONOO$	Peroxynitrite
5-FU	5-fluorouracil
A431	Epidermoid carcinoma cells
ACD	Autophagic cell death
ADP	Adenosine diphosphate
AFP	Alpha-fetoprotein
AIF	Apoptosis-inducing factor
Apaf-1	apoptotic protease-activating factor-1
APC	Adenomatous polyposis coli
APS	Ammonium persulfate
ARE	Antioxidant response element
ATM	Ataxia Telangiectasia Mutated
ATP	Adenosine triphosphate
ATR	Ataxia Telangiectasia and Rad3-related
BAFFR	B-cell activation factor receptor
BCA	Bicinchoninic acid
Bcl-2	B-cell-lymphoma protein 2
Caco2	Colorectal adenocarcinoma
CAT	Catalase
CCM	Complete culture medium
CDKs	Cyclin-dependent kinases
CEHRs	Crown ether host-rotaxanes (CEHRs
Chk2	Checkpoint Kinase 2
CO_2	Carbon dioxide
cPARP	Cleaved Poly (ADP-ribose) polymerase
CRC	Colorectal cancer
CT	Computed tomography
CTC	Computed tomographic colonography

dATP	Deoxyadenosine triphosphate
DFO	Deferoxamine
dH_2O	De-ionised water
DISC	death-inducing signalling complex
DISC	Death-inducing signalling complex
DKK1	Dickkopf-1
DMED	Dulbecco's Modified Eagle Medium
DNA	Deoxyribonucleic acid
DPA	Di(2-picolyl) amine
DTNB	Sulfhydryl reagent 5,5′-dithio-bis (2-nitrobenzoic acid)
ECM	Extracellular matrix
EDTA	Ethylenediaminetetraacetic acid
endoG	Endonuclease G
ETC	Electron transport chain
FADD	Fas-associated death domain
$FADH_2$	Flavin adenine dinucleotide
FAP	Familial adenomatous polyposis
Fas-L	Fas ligand
Fe^{2+}	Ferrous ion
Fe-S	Iron-sulphur cluster
FITs	Faecal immunochemical tests
FMN	Flavin mononucleotide
FOLFIRI	Irinotecan
FOLFOX	Oxaliplatin
GF	Glomerulus filtration
GFR	Glomerulus filtration rate
GPC3	Glypican-3
GPx	Glutathione peroxidases
GSH	Glutathione
GSH	Glutathione
GSSG	Glutathione disulphide
GST	Glutathione-S-transferase
H_2O	Water
H_2O_2	Hydrogen peroxide

HaCaT	Human keratinocyte cell line
HBV	Hepatitis B virus
HCC	Hepatocellular carcinoma
HCl	Hydrochloric acid
HCT116	Human colorectal carcinoma cell line
HCV	Hepatitis C virus
Hek293	Human embryonic kidney
HepG2	Human hepatocellular carcinoma
HNPCC	Hereditary non-polyposis colorectal cancer
HO-1	Heme oxygenase-1
HOCl	Hypochlorous acid
HRP	Horse-radish peroxidase
Hrs	Hours
HSP70	Heat shock protein 70
IAP	Inhibitors of apoptosis protein
IBD	Inflammatory bowel disease
IC_{50}	Half-maximal inhibitory concentration
IFNRs	IFN receptors
IKK	IκB kinase
IL	Interleukin
IL-1R	Interleukin-1 receptor
iNOS	Inducible nitric oxide synthase
INT	Iodonitrotetrazolium or 2-(4-iodophenyl) -3-(4-nitrophenyl) -5-phenyl-2H-tetrazolium
JAK	Janus kinase
K562	Erythroleukemia cells
KCl	Potassium chloride
kDa	Kilodalton
LDH	Lactate dehydrogenase
LPS	Lipopolysaccharide
LTβR	lymphotoxin β-receptor
MAPK	Mitogen-activated protein kinase
MDA	Malondialdehyde
MDM2	Mouse double minute 2 homolog
Mg^{+}	Magnesium cation

MLKL	Mixed lineage kinase domain-like protein
Mn^{2+}	Manganese
MOMP	mitochondrial outer membrane permeabilization
MRI	magnetic resonance imaging
MRI	magnetic resonance imaging
MTT	3-(4,5-dimethylthiazol-2-yl)-2,5-diphenyl tetrazolium bromide
MTT	3-(4,5-Dimethylthiazol-2-yl)-2,5-Diphenyltetrazolium Bromide
NaCl	Sodium chloride
NADH	Nicotinamide adenine dinucleotide
NADPH	Nicotinamide adenine dinucleotide phosphate
NAFLD	Non-alcoholic fatty liver disease
NEDD	N-(1-naphthyl) ethylenediamine
NEMO	NF-κB essential modulator
NFE2-	nuclear factor erythroid 2-
NF-κB	Nuclear factor-kappa B
NIK	NF-κB inducing kinase
Nm	Nanometre
NO_2	Nitrogen dioxide
NOS	Nitric Oxide Synthase
NRF2	Nuclear-factor-erythroid 2 p45-related factor 2
O_2	Oxygen
$O_2^{\bullet}$	Superoxide
OD	Optical density
OXPHOS	Oxidative phosphorylation
PARP	Poly (ADP-ribose) polymerase
PBS	Phosphate-buffered saline
PCR	Polymerase chain reaction
p-p53	Phosphorylated p53
PRRs	pathogen recognition receptors
PRRs	Pathogen recognition receptors
PRX	Peroxiredoxin
PRX	Peroxiredoxin
PS	Phosphatidylserine
RANK	Receptor activator for nuclear factor kappa B

RBD	Relative band density
RHD	Receptor homology domain
RIPK	Receptor-interacting protein kinases
RLU	Relative light unit
RNS	Reactive nitrogen species
ROS	Reactive oxygen species
RT	Room temperature
SCGE	Single-cell gel electrophoresis
SDH	Succinate dehydrogenase
SDS-PAGE	Sodium dodecyl sulphate-polyacrylamide gel electrophoresis
SOD	Superoxide dismutase
SOD2	Superoxide dismutase 2
STA3	Signal transducer and activator of transcription 3
SULF	Sulfanilic acid
TACN	1,4,7-Triazacyclononane
TBA	Thiobarbituric Acid
TBARS	Thiobarbituric Acid Reactive Substances
TEMED	Tetramethyl ethylenediamine
TLRs	Toll-like receptors
TNB	5′-thio-2-nitrobenzoic acid
TNF	Tumour necrosis factor
TNFR	Tumour necrosis factor receptor
TNFR1	TNF receptor 1
TNFR1	TNF receptor 1
TPEN	N, N, N', N' -Tetrakis(2-pyridylmethyl) ethylenediamine
TRADD	TNF receptor-associated death domain
TRAIL	TNF-related apoptosis-inducing ligand
TTBS	Tris-buffered saline containing Tween20
WHO	World Health Organisation
XIAP	X-linked Inhibitor of Apoptosis
Zn^{2+}	Zinc ion

LIST OF FIGURES

CHAPTER 2

CHAPTER 3

CHAPTER 4

CHAPTER 5

ABSTRACT

Colorectal cancer (CRC) is the third most common malignancy detected and the second leading cause of cancer-related mortality. Mammalian cells require metals for the physiological process as they are part of the structure or co-factor of many proteins. However, excessive accumulation may manifest in toxicity. In addition, the promotion of oncogenesis and tumour growth has been associated with an increased presence of metals. Promising anticancer compounds that disrupt the onset and progression of carcinogenesis are currently being intensely investigated by the scientific community. Hexacyclen, a nitrogen electron donor and a potent metal ion chelator that binds various metal and transition metal cations, is one such anticancer drug. The cytotoxic effects of Hexacyclen on human colorectal adenocarcinoma cells (Caco2) and normal embryonic kidney cells (Hek293) were investigated in this work after acute exposure (48 hours). The toxicity of Hexacyclen was studied in Hek293 and Caco2 cells at different concentration ranges [(0-500 μM) and (0-50 μM), respectively]. The MTT (to determine IC_{20} and IC_{50}), ATP and mitochondrial membrane potential ($\Delta\Psi M$) assays were used to assess metabolic activity, while TBARS, NOS and GSH assays were used to assess oxidative activity. Caspase activity (-8, -9, -3/7), phosphatidylserine externalisation and LDH leakage were used to assess cell death by apoptosis. In addition, western blotting was used to examine the expression of antioxidant (SOD2, GPx, catalase), pro-and anti-apoptotic (p-p53, Bcl-2, HSP70, PARP, cPARP) and inflammatory (NF-κB, STAT3 and p-STAT3) proteins. From the dose-dependent MTT curve, an IC_{20} and IC_{50} of 6μM and 38μM (Hek293) and 1.2μM and 5μM (Caco2 cells) were determined. The decreased ATP concentration in Hek293 ($p<0.05$) and Caco2 ($p>0.05$) cells for both treatments was consistent with altered $\Delta\Psi M$ in both cell lines, indicating reduced metabolic activity. Elevated RNS was implied by increased iNOS particularly at the Caco2 IC_{50} ($p<0.05$) that promoted nitric oxide production at the IC_{20} ($p>0.05$) and IC_{50} ($p<0.05$) for Hek293 and Caco2 cells respectively. The decreased MDA in Hek293 cells ($p>0.05$) was associated with increased SOD2 ($p<0.05$) and GPx ($p<0.05$), while slightly increased MDA in Caco2 cells ($p>0.05$) accompanied increased SOD2 ($p>0.05$) and GPx ($p<0.05$ at the IC_{50} only). Furthermore, GSH levels were increased significantly in IC_{50}-treated Hek293 and Caco2 cells ($p<0.05$), but downregulation of catalase in Hek293 and Caco2 cells was not significant. In this study, apoptosis was initiated by an increase in caspase-9 (IC_{50}, $p<0.05$) but not caspase 8, which was decreased for both treatments in Hek293 cells ($p<0.05$). In Caco2 cells, caspase-8 ($p<0.05$) and caspase 9 ($p>0.05$) were increased. Anti-apoptotic Bcl-2 ($p<0.05$) and HSP70 ($p<0.05$ for Caco2 cells) were downregulated in both cell lines. The activity of p-p53 was not affected in IC_{20}, whereas it was significantly reduced in IC_{50}-treated ($p<0.05$) in Hek293 and Caco2 cells. Apoptosis was executed as caspase 3/7 was increased in all treatments ($p<0.05$), albeit non-significantly for IC_{20}-treated Hek293 cells. Moreover, phosphatidylserine externalisation, an early apoptosis marker, was increased in both cell lines ($p<0.05$ for IC_{50}-treated

Hek293 cells), while LDH (a late marker) was increased for Hek293 cells ($p<0.05$) but not Caco2 cells ($p>0.05$). Interestingly, decreased cPARP/PARP activity was observed for IC_{50}-treated cells ($p<0.05$) in both cell lines. Finally, the inflammatory markers NF-κB ($p>0.05$ for IC_{20}-treated Hek293 cells) and p-STAT3/STAT3 ($p>0.05$ for IC_{20}-treated Caco2 cells) were downregulated in this study. Hexacyclen induced apoptosis in Hek293 and Caco2 cells via an RNS-mediated mechanism. Intrinsic apoptosis was noted in Hek293 cells, while both pathways facilitated apoptosis in Caco2 cells. Interestingly, apoptosis proceeded concurrently with a reduction in the NF-κB cell survival pathway.

Keywords: 1, 4, 7, 10, 13, 16-hexaazacyclooctadecane (Hexacyclen), inflammation, oxidative stress, apoptosis, Hek293 cells, Caco2 cells.

CHAPTER 1 : INTRODUCTION

1.1 BACKGROUND

The term cancer is used to describe a large group of diseases characterized by the abnormally rapid growth of cells that can spread to the surrounding tissues by metastasis (Hausman, 2019). Cancer is ranked as one of the diseases that cause high rates of death throughout the world (Bray *et al.*, 2018). The World Health Organisation (WHO) has estimated that approximately 9.3 million new cancer cases and 10.0 million cancer-associated deaths occurred in 2020 alone (Sung *et al.*, 2021). The number of new colorectal cancer cases predicted to have occurred in 2020 were beyond 1.9 million and 935,000 deaths (Sung *et al.*, 2021). Colorectal cancer (CRC) or bowel cancer is a form of malignancy that affects the colon and rectum of the large intestine (Rawla *et al.*, 2019). Risk factors associated with the development of CRC include overconsumption of alcohol, tobacco smoking, high ingestion of red meat and fats, and obesity (Kuipers *et al.*, 2015). Additionally, males have a higher risk of developing CRC than females. The study by Abancens and co-workers noted the difference in sex dimorphism in CRC global incidence of young women between the age of 18-44 years and males of same age. The better survival rate in female was linked to the steroid hormone oestrogen which regulate genes and cellular signalling (Abancens *et al.*, 2020). Genetic mutations such as familial adenomatous polyposis (FAP), Lynch syndrome or hereditary non-polyposis CRC (HNPCC) and Cowden syndrome are hereditary forms of risk factors linked to CRC (Aghabozorgi *et al.*, 2020). Furthermore, chronic inflammatory bowel disease (IBD) patients have an increased risk of colitis, a coexistent primary sclerosing cholangitis and severity of bowel inflammation. Chronic exposure to these risk factors induces proliferative growth of non-cancerous cells called polyps, which may take up to 10–20 years before transforming into cancerous cells (Rawla *et al.*, 2019).

Present anti-CRC therapeutics may involve a combination of approaches that may encompass surgery to prevent the risk of spreading to healthy tissues (Kuipers *et al.*, 2015). Unfortunately, due to the aggressive nature of this form of cancer coupled with late diagnosis, there is a high probability that cancer may have infiltrated other parts of the body such as the regional lymph nodes; in this case, adjuvant chemotherapy and radiation therapy are also performed as treatment (Baur *et al.*, 2019). Current available CRC treatments are associated with severe side effects, and many chemotherapeutic drugs are nephrotoxic causing acute kidney injury and nephritis (Heidari-Soreshjani *et al.*, 2017, Barnett and Cummings, 2018). In addition, non-specificity to cancer treatment and resistance contribute to a low 5-year survival rate of patients (Spearman and Sonderup, 2014). Therefore, there is still an urgent need for the discovery and design of new, potently effective anticancer agents that

exert minimal to no side effects thus preserving the health of cancer patients. In recent years, scientists have focused their attention on synthetic macrocyclic polyether molecules as potential anticancer agents (Bader and Bukhzam, 2014).

A class of synthetic macrocyclic polyether molecules called crown ethers was first introduced in the 1960s as a treatment for cancer (Kralj *et al.*, 2008, Iqbal *et al.*, 2022). This was due to the remarkable features such as their ability to sequester metal ions and form complexes with drugs to pass through cell membranes (Bader and Bukhzam, 2014). The macrocyclic compound 1, 4, 7, 10, 13, 16-hexaazacyclooctadecane, also known as Hexacyclen or 18-aza crown-6, is a multidentate amine macrocycle and an analogue of 18-crown-6 ether; it is reported to bind different metal cations and transition metal cations (Austin and Rodgers, 2014). Hexacyclen preferentially binds alkali and alkaline earth metal cations including tin (Sn^{2+}), cobalt (Co^{3+}) and mercury (Hg^{2+}), and transition metal cations such as copper (Cu^{2+}), Manganese (Mn^{2+}), cobalt (Co^{2+}), iron (Fe^{2+}), nickel (Ni^{2+}) and zinc (Zn^{2+}) (Austin and Rodgers, 2014). Crown ethers have been shown to enhance the activity of antioxidant molecules during instances of oxidative stress and induce apoptosis without the occurrence of necrosis (Boojar and Goodarzi, 2006b, Wong *et al.*, 2010, Iqbal *et al.*, 2022). Oxidative stress, accelerated cell cycle, avoidance of apoptosis and inflammation are hallmarks of cancer (Aggarwal *et al.*, 2019). Therefore, it is essential to understand molecular signalling pathways responsible for cancer progression to discover a unique therapeutic strategy to target this disease.

Previous studies reported that cancer initiation, promotion and progression are linked to oxidative stress (Hayes *et al.*, 2020). Oxidative stress is described as a condition where the balance between the production and removal of free radicals is disrupted (Sies, 2015, Hayes *et al.*, 2020). Free radicals are molecules produced by the body and are essential for normal cell signalling processes. However, the overproduction of free radicals causes damage to the molecules of the cells including DNA, proteins and lipids (Jat and Nahar, 2017). Free radicals are divided into reactive oxygen species (ROS) such as superoxide ($O_2^{\bullet}$), hydroxyl radicals ($^{\bullet}OH$) and hydrogen peroxide (H_2O_2), and reactive nitrogen species (RNS) such as nitric oxide (NO) and peroxynitrite ($^{\bullet}ONOO$) (Lushchak, 2014, Hayes *et al.*, 2020). Intracellular balance mechanisms are mediated by antioxidants, which prevent free radicals from damaging the cell by removing them (Adwas *et al.*, 2019). Antioxidant enzymes include superoxide dismutase (SOD) that converts $O_2^{\bullet}$ to H_2O_2, which is further neutralised by catalase to water or interacts with reduced glutathione (GSH) in a reaction catalysed by glutathione peroxidases (GPx-1) (Sharma *et al.*, 2018). Several studies have noted that increased ROS production enhances cell survival and proliferation (Arfin *et al.*, 2021)

The cell cycle controls growth and proliferation by dividing the parent cell into two identical daughter cells by mitosis. The cell cycle events are highly regulated by cyclin-dependent kinases (CDKs) associated with diverse types of cyclins, to allow the cell to proceed from one phase to another (Otto and Sicinski, 2017). Cell movement to another phase is determined by checkpoints that inhibit the cell cycle if DNA damage is encountered (Otto and Sicinski, 2017). The tumour suppressor proteins, p53 and retinoblastoma (pRb), play a vital role in regulating the cell cycle and preventing cancer development and progression (Ebata *et al.*, 2016). The p53 and pRb are targeted mainly by carcinogens and mutated causing continuous cell proliferation despite DNA damage, thus eventually lowering the apoptosis rate (Williams and Schumacher, 2016).

Damaged, aberrant or excess cells are removed by apoptosis. Unlike other types of cell death, such as autophagy and necrosis, apoptosis eliminates unnecessary cells without triggering an immune or inflammatory response (Szondy *et al.*, 2017). There are two apoptosis pathways; the intrinsic (mitochondrial) and the extrinsic or receptor-dependent pathway (Pfeffer and Singh, 2018). The extrinsic pathway is initiated by extracellular binding signals such as tumour necrosis factor-alpha (TNF-α) and Fas ligand to their respective receptors, resulting in the activation of initiator caspase -8/10 in the death inducing signalling complex by induced proximity (Yuan *et al.*, 2018). The intrinsic pathway is prompted by an internal stimulus such as free radicals that cause upregulated oncogenes or damaged DNA within cells (Singh *et al.*, 2019b). The internal stimulus that results in the damage of DNA, coupled with the failure of p53 to repair the damage will enable the transcription of Noxa and Puma. These proteins bind anti-apoptotic Bcl-2 to free pro-apoptotic Bax and Bak, thereby inducing mitochondrial outer membrane permeabilization to facilitate cytochrome c release and the activation of initiator caspase 9 (Pfeffer and Singh, 2018, Singh *et al.*, 2019b). Both initiator caspases can cleave and activate caspases 3/7, resulting in the execution of cell death. The dismantling of the cell is accomplished by cleavage of caspase-associated DNase causing DNA fragmentation, endonucleases that degrade nuclear materials and/or activating proteins for cytoskeleton degradation (Pfeffer and Singh, 2018). Most human cancer malignancies have a decreased ability to undergo apoptosis since the p53 tumour suppressor gene is inactivated (Aubrey *et al.*, 2018). Dysfunction of p53 in tumours can also enhance chronic inflammation to promote tumour progression (Shi and Jiang, 2021).

Inflammation is the cellular process that involves the recruitment, activation and action of innate and adaptive immunity (Greten and Grivennikov, 2019). Inflammation plays a vital role in host defence against pathogens and is involved in tissue repair, renewal and remodelling (Greten and Grivennikov, 2019). However, chronic inflammation is often associated with several steps involved in

carcinogenesis including alteration of the cell, promotion, proliferation, survival, invasion, angiogenesis and metastasis (Singh *et al.*, 2019a). One of the ways that chronic inflammation is linked to cancer is by consequent activation of inflammatory signalling pathways such as nuclear factor (NF)-κB, an inhibitor of NF-κB (IκB) and IκB kinase (IKK) pathway that plays a significant role in the activation of pro-inflammatory cytokines and protein (Liu *et al.*, 2017b). In tumours, NF-κB is continuously activated and contributes to cancer by accelerating cell proliferation, inhibiting apoptosis, promoting the initiation and progression of tumours as well as stimulating angiogenesis and metastasis (Yang *et al.*, 2020). Furthermore, inflammation is linked to oxidative stress, which also contributes to cancer (Sharma *et al.*, 2018).

To date, there is a lack of literature regarding the biochemical effects of Hexacyclen on different cancer and normal cell lines. Hence, this study investigated the cytotoxic effects underlying the mechanism of Hexacyclen on human colorectal adenocarcinoma (Caco2) and normal embryonic kidney cells (Hek293) over a 48-hour acute exposure.

1.2 PROBLEM STATEMENT / RATIONALE

Cancer is ranked among the leading causes of death across the globe. Two types of cancer, hepatocellular carcinoma and colorectal cancers, are significant contributors to cancer incidence and mortality (Sung *et al.*, 2021). The prognosis for liver and colorectal cancer is poor, with a low 5-year survival rate and few patients surviving for more than a year after diagnosis (Spearman and Sonderup, 2014). The treatment for cancer includes chemotherapy, radiotherapy, ablation and surgery (Yamashita and Kaneko, 2016). However, these treatments come with adverse side effects and are not specific to cancer cells. In addition, many chemotherapeutics are nephrotoxic (Heidari-Soreshjani *et al.*, 2017, Barnett and Cummings, 2018). Side effects associated with chemotherapeutic agents include papillary necrosis, cystic change, urothelial changes, infarction, interstitial nephritis, acute tubular necrosis and haemorrhagic cystitis (Jia *et al.*, 2015). For this reason, new and effective anti-cancer therapies with minimal toxic side effects exerted on normal healthy non-cancer cells are vital to overcoming the economic and healthcare expenses of cancer. In addition, effective treatment for CRC is required.

1.3 SIGNIFICANCE / IMPLICATIONS

It is essential to develop effective cancer treatment to reduce the global burden associated with cancer. Current available cancer treatments are expensive while associated with adverse side effect. This further increase cost for the health sectors and to patients. Additionally, these treatments are often

effective to patients for a short period with high recurrence rates. For this reason, it is essential to discover, design and develop new effectively potent cancer treatments that have the potential to reduce financial burden for both health department and patients while increasing survival rates for colorectal cancer patients without compromising the health of normal non-cancer cells or organs.

1.4 RESEARCH QUESTION

What are the antioxidant and anti-proliferative effects of Hexacyclen on proliferation, apoptosis, oxidative stress and inflammation in colorectal adenocarcinoma (Caco2) cells and human embryonic kidney (Hek293) cells?

1.5 AIM

The study aims to investigate the cytotoxic, apoptotic, antioxidant and anti-inflammtory effect of 1,4,7,10,13,16-Hexaazacyclooctadecane (Hexacyclen) in colorectal adenocarcinoma (Caco2) cells and human embryonic kidney (Hek293) cells.

1.6 NULL HYPOTHESIS

Hexacyclen will not induce apoptosis or alleviate oxidative stress and inflammation in Caco2 and Hek293 cells.

1.7 HYPOTHESIS

Hexacyclen will alleviate oxidative stress and inflammation in Caco2 and Hek293 cells, but will induce apoptosis in Caco2 cells only.

1.8 OBJECTIVES

The objectives of this study were to

- evaluate cell viability of Caco2 and Hek293 cells treated with Hexacyclen by
    - using the 3-(4,5-dimethylthiazol-2-yl)-2,5-diphenyl tetrazolium bromide (MTT) assay to obtain an IC_{20} and IC_{50} to be used in subsequent assays.
    - quantifying ATP using luminometry.
    - assessing the mitochondrial membrane potential using JC-10 dye.
- assess the effect of Hexacyclen on the protein expression of key cell cycle regulators, p53 and pRb.
- Determine whether Hexacyclen induced cell death in Caco2 and Hek293 cells by

    - assessing phosphatidylserine externalisation using the annexin V assay as an early marker of apoptosis to quantify apoptotic cells (luminometry).
    - measuring the activity of different caspases to elaborate pathways of apoptosis (luminometry).
    - detecting the presence of pro- or anti-apoptotic proteins (BCl_2, Bax, HSP70, PARP and cPARP) using the western blot.
- evaluate the induction of oxidative stress in Caco2 and Hek293 cells by Hexacyclen using
    - the TBARS and NOS assay for detection of oxidant production
    - luminometry for GSH
    - western blot for antioxidant enzymes (SOD2, GPx1 and catalase)
- assess the effect of Hexacyclen on inflammation in Caco2 and Hek293 cells using western blot for genes and proteins expressions (NF-κB, STAT3, p-STAT3).

CHAPTER 2 : LITERATURE REVIEW

2.1 CANCER

The term cancer is used to describe a large group of diseases characterized by the rapid growth of abnormal cells that may spread to the surrounding tissues by a process known as metastasis (Hausman, 2019). The World Health Organisation (WHO) ranks cancer as one of the leading diseases that cause death across the globe (Bray *et al.*, 2018). The recent data from GLOBOCAN (2021) show that cancer is now estimated to be the first or second leading cause of death before 70 years of age in 112 of 183 countries, and ranks third or fourth in 23 other countries (Sung *et al.*, 2021). The WHO estimated that 19.3 million new cancer cases and 10.0 million cancer deaths occurred in 2020 (Figure 2.1) (Sung *et al.*, 2021). These figures are expected to increase by 45%, possibly exceeding 13 million cases by 2030, with most deaths occurring in low- to medium-income countries like South Africa (Bray *et al.*, 2018). To date, lung malignancies remain the leading cause of cancer-related death (Figure 2.1). It is estimated to cause approximately 1.8 million deaths (18%), followed by colorectal (9.4%), liver (8.3%), stomach (7.7%), and female breast (6.9%) cancers (Figure 2.1) (Sung *et al.*, 2021).

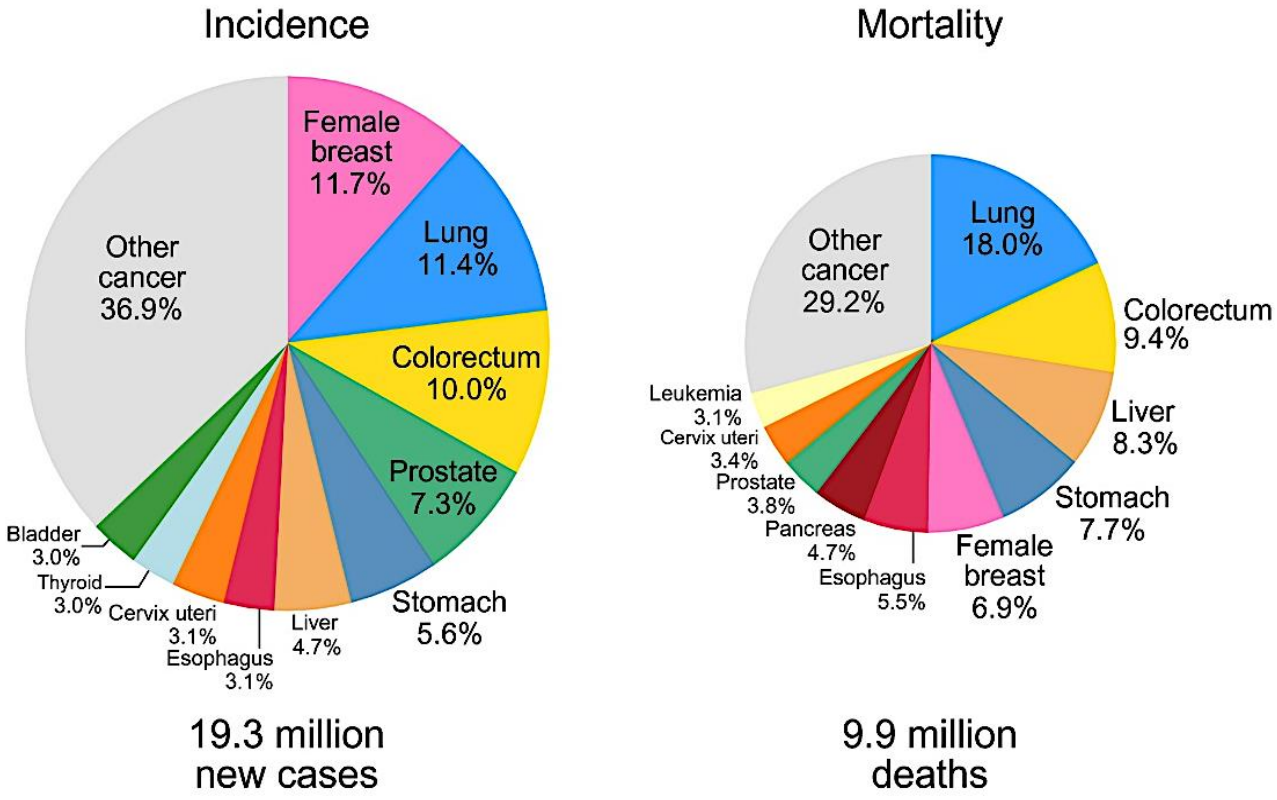

Figure 2.1: Ranking of the estimated 2020 cancer incidence and mortality by the International Agency for Research on Cancer (Sung *et al.*, 2021).

2.2 COLORECTAL CANCER

Colorectal cancer (CRC) is also referred to as bowel cancer, which is a form of malignancy that affects the colon and rectum part of the large intestine (Rawla *et al.*, 2019).

2.2.1 Colon and rectum

The colon and rectum are part of the large intestine (Kuipers *et al.*, 2015). The colon is the longest part of the large intestine which extends from the cecum of the small intestine. The roles of the colon include absorption of the remaining water and salts from undigested food, lubrication of waste products and storing waste temporally before it is passed to the rectum (Britannica, 2018). The rectum is the last potion that extends to the anus. Waste enters the rectum and within the distended rectal cavity, the pressure builds up for elimination (Kuipers *et al.*, 2015, Britannica, 2018). In the inner lining of the colon and rectum, a growth called polys can develop (Figure 2.3), and over time it can turn into cancer (Kuipers *et al.*, 2015). Together, colon and rectum cancer are referred to as colorectal cancer (CRC) or bowel cancer (Rawla *et al.*, 2019).

2.2.2 Incidence of CRC

Colorectal cancer has been ranked third as the most common cancer detected globally with 10.0% compared to other types of cancer, while it is the second place in terms of mortality rate with 9.4% (Figure 2.1) (Sung *et al.*, 2021). The number of new colorectal cancer cases predicted to have occurred in 2020 were beyond 1.9 million and 935,000 deaths (Sung *et al.*, 2021). In 10 of 191 countries nationwide, CRC is the most diagnosed type of cancer in males in comparison to females (Rawla *et al.*, 2019). There are low rates of colon and rectal cancer incidence in most regions of Africa (Rawla *et al.*, 2019). The incidence rate of colon cancer in Southern Africa for males and females is 8.7% and 7.3% respectively, and the rate for rectum cancer is 7.2% and 5.0% in males and females (Figure 2.4 A and B) (Sung *et al.*, 2021). The data about CRC in low– and middle–income countries (LMIC) like South Africa is limited (Graham *et al.*, 2012). A study by Motsuku *et al.* (2021) reported 33,232 incident CRC cases and 26,836 CRC deaths from 2002 to 2014 (Motsuku *et al.*, 2021). According to gender, 54% male and 46% female incident CRC cases, and 47% male and 53% female CRC deaths were reported (Motsuku *et al.*, 2021).

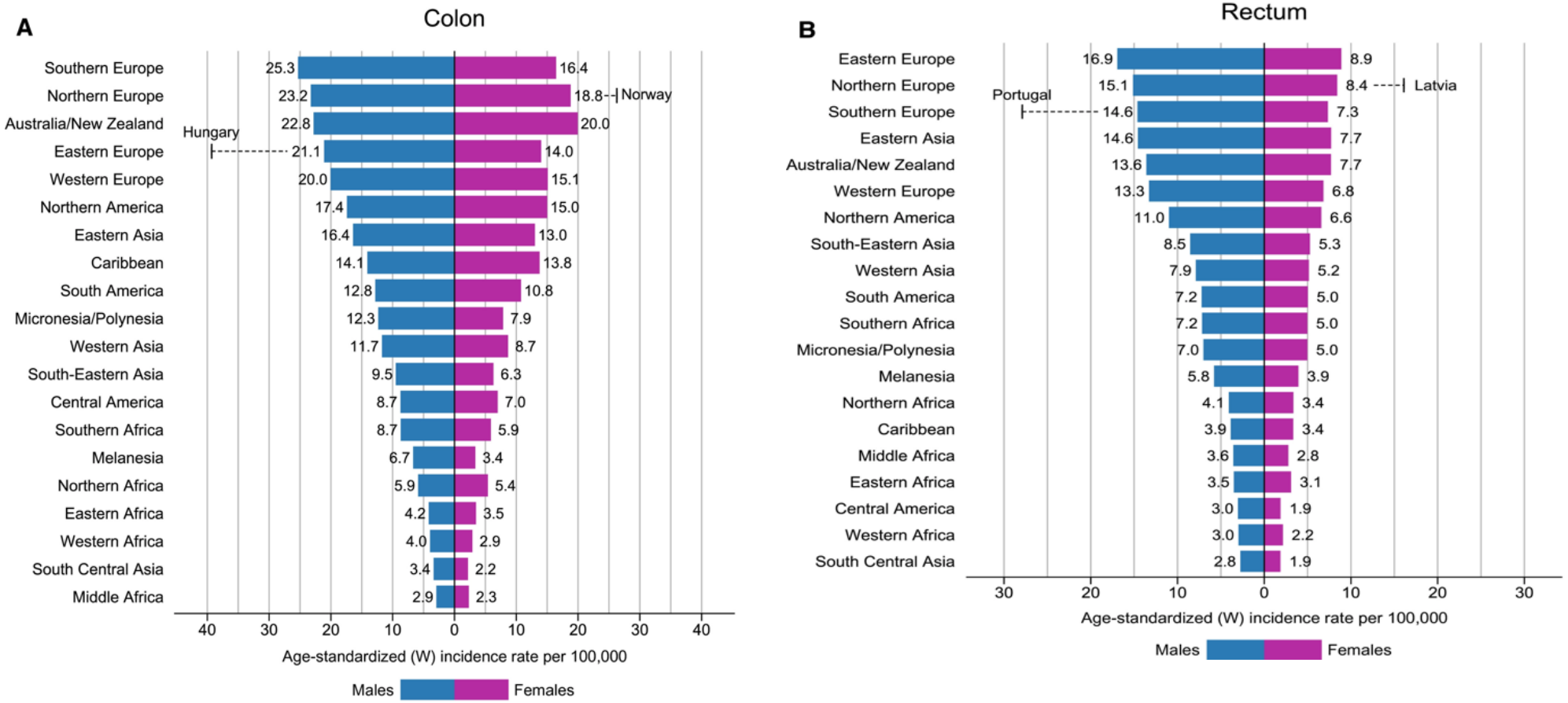

Figure 2.2: The incidence rate of colorectal cancer in different regions across the globe (Sung *et al.*, 2021).

2.2.3 Risk factors associated with CRC

It is predicted that greater than 80% of people with CRC were exposed to risk factors such as older age, male gender, high consumption of red meat and fats and obesity (Kuipers *et al.*, 2015). Notably, overconsumption of alcohol and tobacco smoking increases CRC risk by more than 20% (Rawla *et al.*, 2019). Genetic mutations such as familial adenomatous polyposis (FAP), Lynch syndrome or hereditary non-polyposis CRC (HNPCC) and Cowden syndrome are hereditary forms of risk factors linked to CRC (Aghabozorgi *et al.*, 2020). Particularly, FAP and HNPCC disorders cause about 5-10% of all CRCs. The FAP accounts for nearly 1% and is characterised by the presence of polyps throughout the intestine which may be attributed to the mutated adenomatous polyposis coli (APC) gene which is inherited (Toma *et al.*, 2012). On the other hand, HNPCC contributes to approximately 3-4% of all CRC cases and is due to mutations in DNA lesion repairing genes. It is distinguished by the early deposition of numerous metachronous and synchronous colorectal tumours, accompanied by skin lesions and extracolonic tumours (Toma *et al.*, 2012, Aghabozorgi *et al.*, 2020). Furthermore, chronic inflammatory bowel disease (IBD) patients have an increased risk of colitis, a coexistent primary sclerosing cholangitis and severity of bowel inflammation.

Generally, CRC starts in the mucosal epithelial cells as the non-cancerous proliferation growth called polyps; this growth can take about 10–20 years before progressing into cancer (Rawla *et al.*, 2019). These polyps are constrained growths of abnormal cells located within the intestinal mucosa that project into the lumen (Figure 2.3). Polyps generate enough genetic changes, allowing them to enter the bowel wall, the hallmark of CRC (Simon, 2016). Hyperproliferation of started polyps leads to developing a precancerous adenomatous polyp, or adenoma, which arises from epithelial cells (Figure 2.3) (Simon, 2016). An adenoma is classified as the obligated precursor of adenocarcinomas. Still, only about 10% of adenomatous polyps grow while mutations and epigenetic changes may occur leading to the transformation into malignant and adenocarcinoma cells (stage I) (Figure 2.3) (Baur *et al.*, 2019). An adenocarcinoma is characterised by increased tumour volume that accounts for approximately 96 % of all CRCs and it eventually invades other tissues such as the serosa (Stage II) and visceral peritoneum (Stage III) (Pickhardt *et al.*, 2013). Stage IV of CRC is characterised by adenocarcinoma metastasis via blood and/or lymphatic vessels to distant body sites, as seen in Figure 2.3 (Baur *et al.*, 2019).

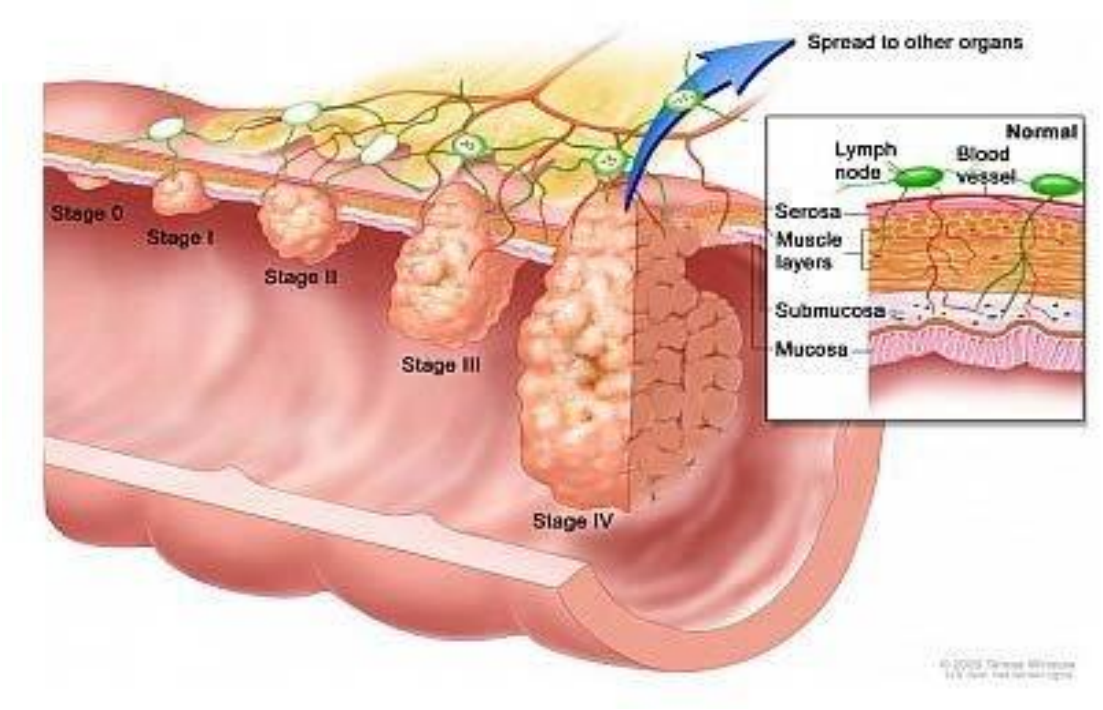

Figure 2.3: Different stages of CRC, showing the initial polyp transformation into an adenocarcinoma (stage I) that invades the surrounding tissue as it extends into the lumen (stages II and III) and eventually starts to metastasise (stage IV) (Baur *et al*., 2019).

2.2.4 Diagnosis and treatment of CRC

The best way of early detection and preventing further pre-cancerous polyps into CRC is by screenings (Baur *et al.*, 2019). Screening for CRC is performed by examining the structure of the colon and rectum using computed tomographic colonography (CTC), colonoscopy, sigmoidoscopy or stool tests such as the faecal occult blood test (FOBT) (Baur *et al.*, 2019). The faecal immunochemical tests (FITs) and FOBT are frequently used to detect CRC by detecting haemoglobin as a marker of occult blood in the stool (Simon, 2016). Normally, surgery may be performed once CRC has been positively detected to prevent further risk of spreading, by removing affected malignant tumours and nearby lymph nodes (Kuipers *et al.*, 2015). Once cancer has already spread to regional lymph nodes, adjuvant chemotherapy and/or radiation therapy is performed as the treatment (Baur *et al.*, 2019). Chemotherapeutic drugs such as 5-fluorouracil (5-FU)-based drug (methotrexate, 5-FU) are used for treatment in stage II and stage III CRC (Baur *et al.*, 2019). Advanced stages of CRC can be treated with drugs like 5-FU and irinotecan (FOLFIRI), or folinic acid, 5-FU and oxaliplatin (FOLFOX) (Baudino, 2015). Over the years, it has been recognised that patients on cancer treatment may also present with symptoms associated with kidney disease, which occurred after receiving

anticancer treatment. This link between cancer and kidney disease is now referred to as one-nephrology (Lameire, 2014).

2.2.5 Nephrotoxicity: one-nephrology

The kidney is a vital organ that plays an essential role in maintaining homeostasis, excretion of toxic metabolites and drugs, and detoxification (Kim and Moon, 2012, Al-Naimi *et al.*, 2019). The functional unit of the kidney, the nephron, is made up of the glomerulus and tubules including the proximal and distal convoluted tubules connected by the loop of Henle. One of the kidneys are functions to remove drugs from the renal capillaries mainly through glomerular filtration (GF) and tubular secretion pathways. The GF excretes metabolites according to size, thus unbound protein molecules can pass the capillary wall of the glomerulus (Breshears and Confer, 2017). Protein-bound molecules in circulation are eliminated through urine by secretion in the proximal tubule (Małyszko *et al.*, 2016). Cancer treatment via chemotherapy is reported to be helpful; however, it is associated with renal disease in about 60% of patients with cancer (Horie *et al.*, 2018). Nephrotoxicity arising from chemotherapy may cause a deterioration in kidney function (Al-Naimi et al., 2019).

Chemotherapeutic drugs cause damage to the excretory pathways of the kidney. Mechanisms of kidney injury include inflammation, renal tubular toxicity, glomerular damage, thrombotic microangiopathy and crystal nephropathy (Al-Naimi *et al.*, 2019). Side effects associated with chemotherapeutic agents comprise papillary necrosis, cystic change, urothelial changes, infarction, interstitial nephritis, acute tubular necrosis and haemorrhagic cystitis (Jia *et al.*, 2015). Other complications involve reduced total body water, which is linked to lowered glomerular filtration rate (GFR), renal oxidative stress and excessive angiotensin-II/endothelin which further increases nephrotoxicity. Moreover, detoxification of some drugs by the kidney favours the production of toxic metabolites and ROS that causes harm via DNA strand breaks, lipid peroxidation, nucleic acid alkylation or oxidation and protein damage (Perazella, 2012).

Cisplatin, the most toxic anti-cancer drug injures the S3 segment of the proximal tubule, thereby decreasing GFR (Małyszko *et al.*, 2016). The kidney responds by increasing the expression of several pro-inflammatory cytokines such as interleukin-6, tumour necrosis factor-alpha, caspases and interferon-gamma (Ramesh and Reeves, 2002, Małyszko *et al.*, 2016). These molecules endorse the growth and maturation of T cells and neutrophils, mitogen-

activated protein kinase (MAPK) activation and p53 signalling. Alternately, inflammation and oxidative stress allied with cellular injuries are triggered (Małyszko *et al.*, 2016). Eventually, this leads to kidney failure and dysfunction.

Due to the downfall of current treatments, the medicinal chemistry and pharmaceutical industry focused their efforts on anticancer drugs that inhibit pathways that drive the onset and development of carcinogenesis. These anticancer agents are considered potent metal ion chelators (Gaur *et al.*, 2018, Kontoghiorghes, 2020).

2.2 CROWN ETHERS

Crown ethers were first synthesized in the 1960s as synthetic macrocyclic polyether molecules comprising a ring containing several ether groups (Kralj *et al.*, 2008, Tan *et al.*, 2017). Figure 2.4 depicts these macromolecules referred to as crown ethers; they are compared to a crown sitting on one's head with the structure of a crown ether bound to a cation (Bader and Bukhzam, 2014). There are a variety of important crown ether members, but the most common are 12-crown-4 (12C4), 15-crown-5 (15C5) and 18-crown-6 (18C6) (Morrison *et al.*, 2017). These molecules have been reported to have remarkable binding properties, the ability to sequester metal ions and the ability to form complexes with drugs to allow movement through cell membranes (Bader and Bukhzam, 2014, Morrison *et al.*, 2017). The complexing ability of crown ethers depends on selectivity, size of the compound, number and type of heteroatom (Kralj *et al.*, 2008). For example, 12-Crown-4 tends to be complex with Li^+, while 18-crown-6 selects K^+ (Bader and Bukhzam, 2014). Crown ethers are widely used in biology, chemistry and industrial and pharmacological research (Kralj *et al.*, 2008, Tan *et al.*, 2017). Notably, crown ethers play an essential role in drug delivery due to the ability to cross cellular membranes after sequestering metals and are also used in other therapeutic areas, such as antitumour treatment (Chehardoli and Bahmani, 2019).

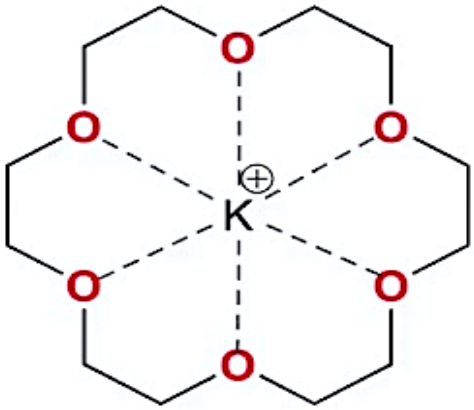

Figure 2.4: An example of 18-crown-6 (18C6) ether complexing the potassium (K+) ion (Chehardoli and Bahmani, 2019).

2.3.1 1,4,7,10,13,16-Hexaazacyclooctadecane (Hexacyclen)

The repetitive oxygen units found in crown ethers (Figure 2.4) are replaced by other atoms, such as nitrogen to form novel crown ethers including aza-crown ethers (Chehardoli and Bahmani, 2019). The macrocyclic compound 1, 4, 7, 10, 13, 16-hexaazacyclooctadecane is an anion binding sometimes referred to as Hexacyclen or 18-aza crown-6 (Figure 2.5). Hexacyclen is an example of aza-crown ether (Austin and Rodgers, 2014). This compound has been proven to have a potent ability to form complexes and is highly selective for different inorganic anions, inorganic phosphate, AMP, ADP and ATP (El-Hashani *et al.*, 2007). The 18-aza crown-6 ring consists of nitrogen known to display electron-donor properties, favouring complexes with cations (El-Hashani *et al.*, 2007). Hexacyclen shares similar properties with known metal chelators such as the ethylenediaminetetraacetic acid (EDTA) macrocyclic chelator 1,4,7,10-tetraazacyclododecane-1,4,7,10-tetraacetic acid (DOTA), which has been previously exploited for its anti-cancer properties (Kahnt *et al.*, 2019). Hexacyclen has been reported to preferentially bind alkali and alkaline earth metal cations including tin (Sn^{2+}), cobalt (Co^{3+}) and mercury (Hg^{2+}), and transition metal cations such as copper (Cu^{2+}), Manganese (Mn^{2+}), cobalt (Co^{2+}), iron (Fe^{2+}), nickel (Ni^{2+}) and zinc (Zn^{2+}) (Austin and Rodgers, 2014).

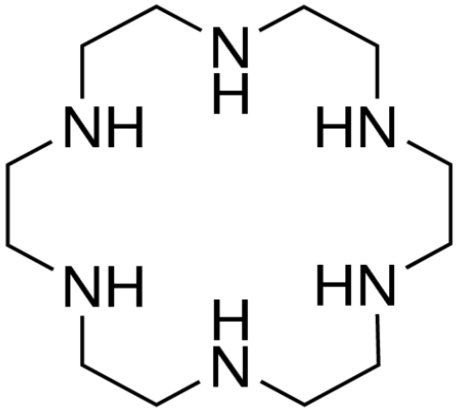

Figure 2.5: The structure of 1, 4, 7, 10, 13, 16-hexaazacyclooctadecane crown ether (El-Hashani et al., 2007, Austin and Rodgers, 2014).

The ability of crown ethers to cross the cell membrane during drug delivery has been investigated and it was found that they can easily penetrate the membrane due to their lipophilic properties (Chehardoli and Bahmani, 2019). Lipophilicity refers to the affinity of the drug toward a lipid setting which is important for penetration through the lipid membrane during drug delivery. The beneficial effect of using crown ethers as drug carriers is that they possess the capability of reducing the toxicity of the drugs (Chehardoli and Bahmani, 2019). Cytotoxic effects of 15-crown-5 and 18-crown-6 were investigated by Boojar and Goodarzi (2006) in which they investigated the role of the crown ether in oxidative stress within lung tissue (Boojar and Goodarzi, 2006b). It was revealed that these crown ethers enhance the activity of antioxidant molecules such as superoxide dismutase (SOD), catalase, and glutathione peroxidase (GPx-1) due to the induced production of ROS (Boojar and Goodarzi, 2006b). Furthermore, a study conducted by Wang *et al.* (2010) identified synthesized crown ether host-rotaxanes (CEHRs) derivatives as ionophores compounds that induced apoptosis without necrosis by enhancing Mg^{2+} and Ca^{2+} intracellular concentration in SKOV-3 cell line (Wang *et al.*, 2010).

Previous studies have shown the role of crown ethers in cellular processes such as oxidative stress and apoptosis may be due to their ability to interact with metal ions such as potassium (K^+), chloride (Cl^-) and calcium (Ca^{2+}) (Chehardoli and Bahmani, 2019). These ions are essential for cell proliferation and are considered critical regulators of apoptosis (Kunzelmann, 2005, Chehardoli and Bahmani, 2019). For the cell cycle to progress through the G1 phase, activation of K^+ channels are required for cells to proliferate, whereas apoptotic processes are

induced by changes in ionic strength due to K^+ efflux, Cl^- efflux and Ca^{2+} influx (Kralj *et al.*, 2008, Urrego *et al.*, 2014). It has been reported by most studies that K^+ efflux induces cell shrinkage and apoptosis by either plasma membrane potential or disrupting the mitochondria. At the same time, K^+ channel blockers hinder cell proliferation by arresting cells in the G1 phase (Litan and Langhans, 2015).

The organic tridentate ligand 1,4,7-tiazacyclononane (TACN) is also a member of aza-crown ethers with strong chelating abilities (Somboro *et al.*, 2019). The cytotoxic effect of TACN has been previously investigated and found not to induce oxidative stress and cell death in HepG2 and Hek293 cells (Mcoyi *et al.*, 2020, Tsotetsi *et al.*, 2020). Therefore, it is important to exploit the effect of other aza crown ethers such as Hexacyclen in cellular processes including inflammation, oxidative stress and mechanisms of cell death.

2.4 INFLAMMATION

Inflammation is a cellular process that involves the recruitment, activation and action of innate and adaptive immunity (Greten and Grivennikov, 2019). Inflammation plays an essential role in host defence against pathogens and is also involved in tissue repair, renewal and remodelling. Chronic inflammation has been linked to various chronic infections such as cancer (Greten and Grivennikov, 2019). Triggers of chronic inflammation include exposure to asbestos and silica, which have been linked to pneumonia and lung cancer; alcohol abuse, which has been linked to liver inflammation and cancer; and inflammatory bowel disease (IBD), which has been linked to the onset of colon cancer (Lin and Karin, 2007, Zhao *et al.*, 2021). The role of chronic inflammation in cancer is that it causes tumours by genetically altering normal cells to become malignant, promoting the growth of the altered cells and encouraging tumour progression by becoming increasingly aggressive (Taniguchi and Karin, 2018). The link between cancer and chronic inflammation in the promotion and progression of tumours is the continuous activation of the NF-κB-kinase/ NF-κB (IKK/NF-κB) signalling pathway. This is further connected to overexpression of Signal Transducer and Activator of Transcription-3 (STAT -3), which play an essential role in the activation of pro-inflammatory cytokines such as TNF-α, IL -1 and IL-6 (Ji *et al.*, 2019, Zhao *et al.*, 2021).

2.4.1 The nuclear factor-kappa B (NF-κB) signalling pathway

The NF-κB signalling pathway is a recognised key regulator of cellular responses in the innate and adaptive immune systems. It contributes to the pathogenesis of several diseases including cardiovascular disorders, diabetes and cancer (Mitchell *et al.*, 2016). The NF-κB protein contributes toward carcinogenesis by accelerating cell proliferation, inhibiting apoptosis, promoting the initiation and progression of tumours and stimulating angiogenesis as well as metastasis (Yu *et al.*, 2017). In cancer cells, the genes encoding the NF-κB transcription factors or genes that control the protein are mutated leading to its continuous activation (Yu *et al.*, 2017). In normal non-cancer cells, the activation of the NF-κB pathway is dependent on the degradation of the IκB(s) proteins, which are inhibitors of NFκB. The IκBs proteins are degraded due to phosphorylation through the IκB kinase (IKK) complex activated by cytokines like TNF and IL1, produced by tissue macrophages (Dorrington and Fraser, 2019). The NF-κB signalling pathway can be activated in one of two ways, namely, the canonical (classical) and non-canonical (alternative) pathways (Figure 2.6) (Liu *et al.*, 2017b).

2.4.1.1 Canonical pathway

The canonical signalling pathway (Figure 2.6) is rapidly activated by inflammatory stimuli including pro-inflammatory cytokines TNFα and IL1, pathogen-associated molecular patterns (PAMPs) and damage-associated molecular patterns (DAMPs). These molecules act through specific receptors such as tumour necrosis factor receptor (TNFR), interleukin-1 receptor (IL -1R), toll-like receptors (TLRs) and antigens (Taniguchi and Karin, 2018). The binding of inflammatory stimuli to their respective receptors activates the receptor to recruit and phosphorylate adaptation molecules called the IKK complex. The IKK complex consists of several subunits, namely the catalytic subunits IKKα (IKK1) and IKKβ (IKK2) and a regulatory subunit NF-κB essential modulator (NEMO) (IKKγ) (Yu *et al.*, 2017). The active IKK complex causes phosphorylation, ubiquitination and degradation of IκB proteins such as IκB-alpha (α), and subsequently, the IκB protein releases p50: RelA and p50:c-Rel dimers (Taniguchi and Karin, 2018). The p50:RelA and p50:c-Rel dimers translocate to the nucleus and activate the transcription of various target genes (Giuliani *et al.*, 2018). The canonical pathway is activated for innate immunity and is responsible for inhibiting apoptosis under most conditions in response to infections or exposure to proinflammatory cytokines (Yu *et al.*, 2020).

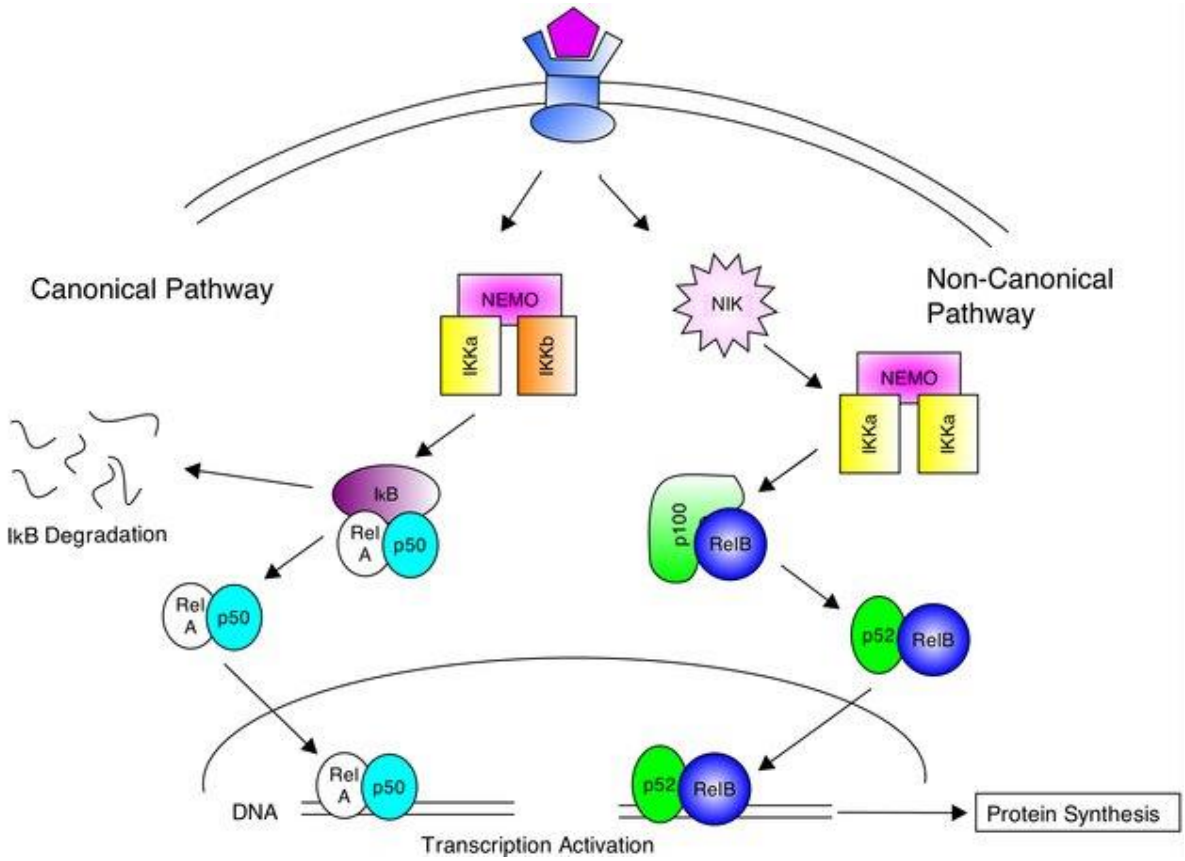

Figure 2.6: The canonical (classical) and noncanonical (alternative) pathways of NF-κB (Williams *et al.*, 2014).

2.4.1.2 The non-canonical pathway

The alternative or non-canonical pathway (Figure 2.6) is activated by another set of receptors, including nuclear factor kappa B receptor activator (RANK), B-cell activating factor receptor (BAFFR), TNFR2, lymphotoxin-β receptor (LTβR), CD40 and Fn14 (Taniguchi and Karin, 2018). The activation of these receptors induces the recruitment and activation of NF-κB inducing kinase (NIK), which in turn phosphorylates and activates mainly IKK1 (Yu *et al.*, 2020). The activation of NF-κB via the non-canonical pathway is therefore independent of the activity of IKK2 and NEMO (Liu *et al.*, 2017a). The active IKK1 causes the proteasome-dependent degradation of the RelB inhibitor NF-κB p100, resulting in the activation of the RelB/p52 complex that translocate and binds to DNA (Sun, 2017). The non-canonical NF-κB pathway is mainly activated to regulate the adaptive immune system (Hariharan *et al.*, 2021).

In lung, lymphoma, breast, and liver cancer, NF-κB persistence in the nucleus is reported where it controls the expression of several genes linked with proliferation, invasion, angiogenesis and

metastasis of cancer (Fan *et al.*, 2013). Furthermore, NF-κB promotes cell survival via its transcription regulation of anti-apoptotic genes, including Bcl-2 family members such as Bcl-2 and Bcl-xL, and inhibitor of apoptosis proteins like Ciap1, Ciap2, XIAP (Luo *et al.*, 2005, Fan *et al.*, 2013). Also, constitutive activation of NF-κB via both classical and alternative pathways further upregulates the production of major inflammatory factors, for example, IL-6, IL-1, IL-8 and TNFα (Fan *et al.*, 2013, Yu *et al.*, 2017). Notably, the NF-κB activity in tumours requires a constitutively activated STAT3, which is also reported to be upregulated in cancer (Yoon *et al.*, 2012).

2.4.2 Signal transducer and activator of the transcription (STAT) signalling pathway

The STAT3 protein is a member of the STAT transcription factor family along with STAT1, STAT2, STAT4, STAT5, STAT5B, and STAT6, which are involved in regulating various cellular signalling processes (Martincuks *et al.*, 2017). Generally, STAT3 is activated mainly by binding of IL-6 and IL-1β cytokines to gp130 and IL-6 receptors, which activates the Janus kinase (JAK) (Fan *et al.*, 2013, Lin *et al.*, 2020). Phosphorylated JAK recruits and activates STAT3 via phosphorylation at Tyr705 (Lin *et al.*, 2020). Dimers of phosphorylated STAT3 translocate to the nucleus to regulate several genes involved in cell proliferation, survival, invasion and metastasis (Egusquiaguirre *et al.*, 2018), as seen in Figure 2.7. The prolonged signalling by both the innate and adaptive systems can cause excess free radicals and depletion of antioxidant molecules, thus causing oxidative stress (Mittal *et al.*, 2013).

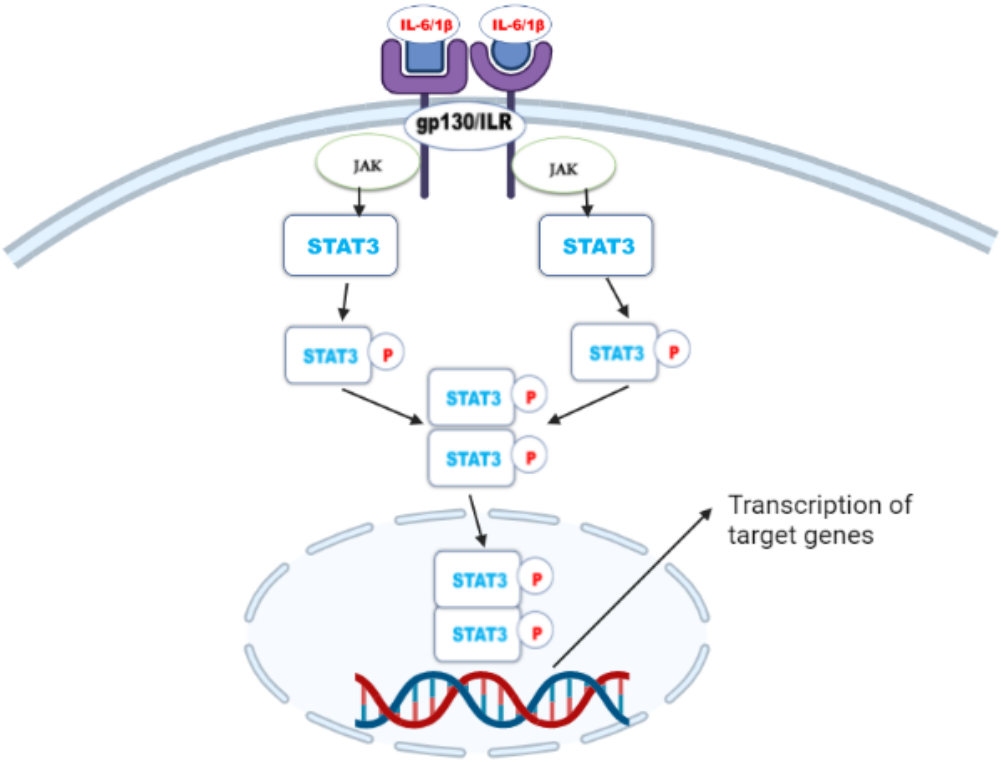

Figure 2.7: Activation of the extrinsic pathway of *a* STAT3 signalling pathway (prepared by author).

2.5 OXIDATIVE STRESS

Oxidative stress refers to the inequality of free radical and antioxidants molecules in the body that can lead to cellular damage (Sies, 2015). Free radicals contain an unpaired electron in the outer orbital; they are therefore highly reactive and can oxidize or reduce other atoms (Adwas *et al.*, 2019). Reactive oxygen species (ROS) are important free radicals derived from oxygen that are produced as a by-product of cellular metabolism, while reactive nitrogen species (RNS) are nitrogen-containing radicals derived from reaction with ROS. Thus, oxidative stress may be further defined as an imbalance between ROS and RNS, and the diminished ability of the host's antioxidant defence system (NavaneethaKrishnan *et al.*, 2019). Cellular antioxidants and free radical imbalances are strongly associated with cardiovascular diseases, Parkinson's disease, diabetes, Alzheimer's disease, arthritis, arteriosclerosis, cataracts, as well as cancers (Khan *et al.*, 2020).

The ROS molecules are generated from different sources (Figure 2.8) including exposure to UV light, pollution, cigarette smoking and consumption of processed and unprocessed foods, to name a few. Examples of ROS include superoxide anion ($O_2^{\bullet}$), hydrogen peroxide (H_2O_2),

hypochlorous acid (HOCl), hydroxyl radicals (•OH), hydrogen peroxide, and singlet oxygen (Adwas *et al.*, 2019). Examples of RNS include nitric oxide (NO) and peroxynitrite (•ONOO); •ONOO is formed when $O_2^{\bullet}$ reacts with NO (Figure 2.9), and is the source of other RNS (Lushchak, 2014). Free radicals are produced by the cell to act as secondary messengers in signalling cascades, which are essential for the normal physiological functions of the cell (Sies, 2015). The overproduction of ROS and RNS can cause damage to the biomolecules of the cell such as proteins, lipids, DNA and carbohydrates, ultimately resulting in the loss of cell integrity thereby triggering the onset of diseases (Figure 2.8, Figure 2.9) (Jat and Nahar, 2017).

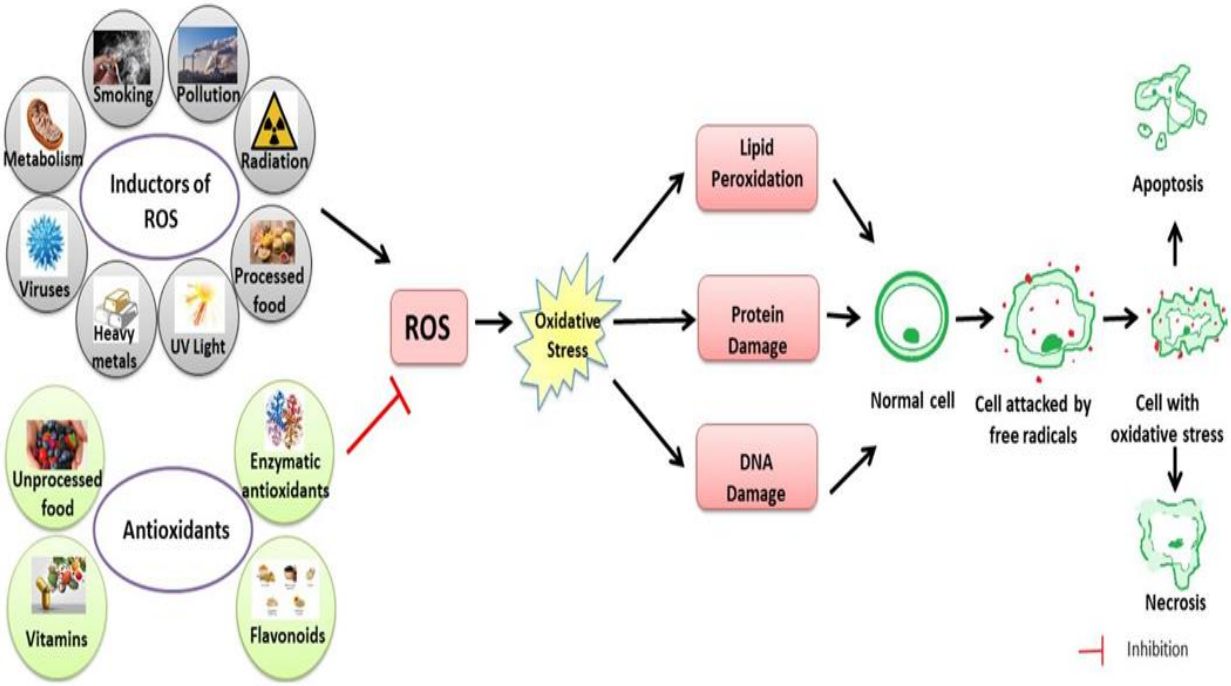

Figure 2 8: Sources of ROS and inhibition via antioxidant response, thus oxidative stress (Sharifi-Rad *et al*., 2020).

Intracellular balance mechanisms are mediated by antioxidants that prevent free radicals from damaging the cell by removing them (Adwas *et al.*, 2019). Antioxidants are classified into distinct groups, namely the neutralizing enzymes such glutathione peroxidase (GPx-1), superoxide dismutase (SOD) and catalase (CAT), and the non-enzymatic antioxidants like reduced glutathione (GSH), ascorbic acid (Vitamin C), alpha-tocopherol (Vitamin E), flavonoids and carotenoids (Dumanović *et al.*, 2021). The free radical, $O_2^{\bullet}$ is produced in the mitochondria through complexes I and III of the electron transport chain (Zhao *et al.*, 2019). It is converted by SOD into H_2O_2, which is then reduced to water in a reaction catalysed by GPx-1, using GSH as a source of electrons (Figure 2.9); GSH is oxidised to glutathione disulphide (GSSG) in this reaction and is replenished through the action of glutathione reductase

(Ighodaro and Akinloye, 2018). The H_2O_2 may also be converted to water and oxygen by CAT, or react with transition metals in the Fenton reaction to form the potent $^{\bullet}OH$ (Figure 2.9) (Dumanović *et al.*, 2021). The master transcription factor called the nuclear factor erythroid 2-(NFE2-) related factor 2 (Nrf2), also regulates oxidative stress by upregulating the expression of SOD, GSH, CAT, GPx-1, heme oxygenase-1 (HO-1, and peroxiredoxin (PRX) antioxidant enzymes (Khan *et al.*, 2020).

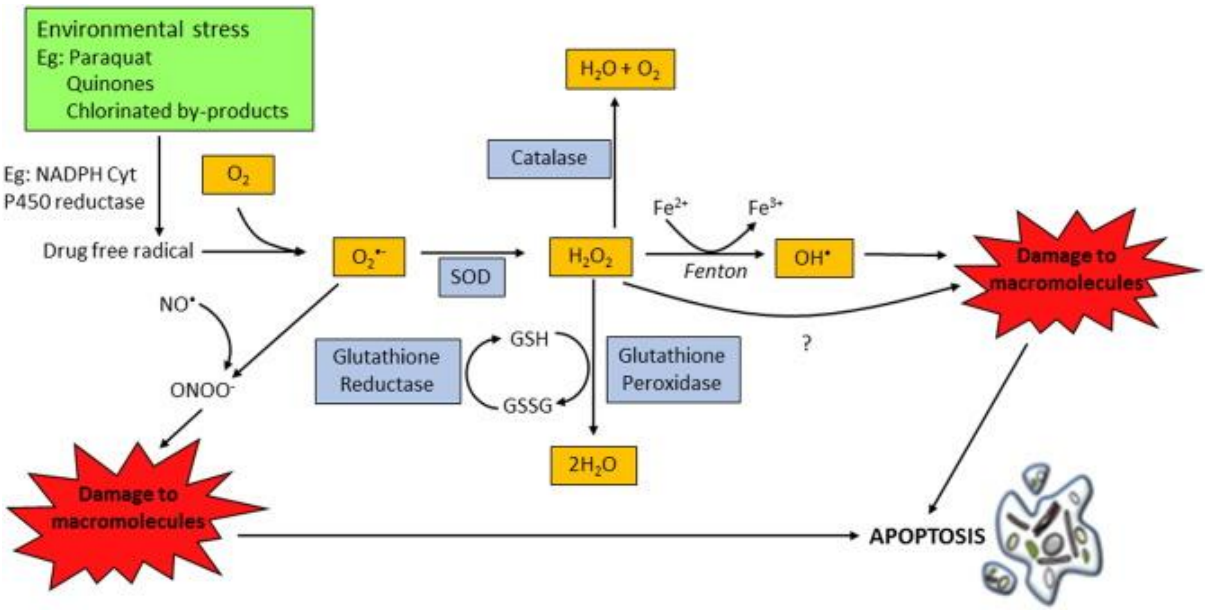

Figure 2.9: Detoxification of free radicals from different sources by antioxidant molecule (Redza-Dutordoir and Averill-Bates, 2016).

It has been reported that oxidative stress contributes to the initiation, promotion and progression stages of carcinogenesis (Gavet and Pines, 2010, Zahra *et al.*, 2021, Aggarwal *et al.*, 2019). In the initiation stage, structural alterations and gene mutations are introduced due to DNA damage caused by ROS (Aggarwal *et al.*, 2019). During the promotion stage, ROS causes cell-to-cell communication blockage, abnormal gene expression and modification of second-messenger systems, and cell proliferation is increased while apoptosis is decreased. Lastly, oxidative stress participates in the progression stage by adding further DNA alterations to the initiated cell population (Aggarwal *et al.*, 2019). Several studies have noted that increased ROS production enhances cell survival and proliferation (Arfin *et al.*, 2021, Aggarwal *et al.*, 2019, Zahra *et al.*, 2021).

2.6 CELL CYCLE CHECKPOINTS

The cell cycle is a highly coordinated process that plays a role in maintaining, retaining, and passing down genetic information from parent cells to daughter cells, in a very organised manner through DNA replication and cell division (Mens and Ghanbari, 2018). Somatic cells undergo two main phases during cell division: the interphase and mitotic phase (Otto and Sicinski, 2017). The interphase of the cell cycle consists of different subdivisions, including the G1/G0 phase, S-phase and G2-phase (Otto and Sicinski, 2017). The cell cycle is regulated by two groups of proteins: the cyclin-dependent kinases (CDKs) including CDK2, CDK4 and CDK6 that are expressed throughout the cycle and the cyclins such as A-, B-, D- and E-type cyclins which are synthesised and degraded during a specific time of the cycle as seen in Figure 2.10 (Visconti *et al.*, 2016). The binding of specific cyclins activates the CDKs, and their activity is inhibited by cycle inhibitory proteins called cyclin kinase inhibitors (CKIs) such as 15, p16, p18, p19, p21, p27 and p57 (Otto and Sicinski, 2017).

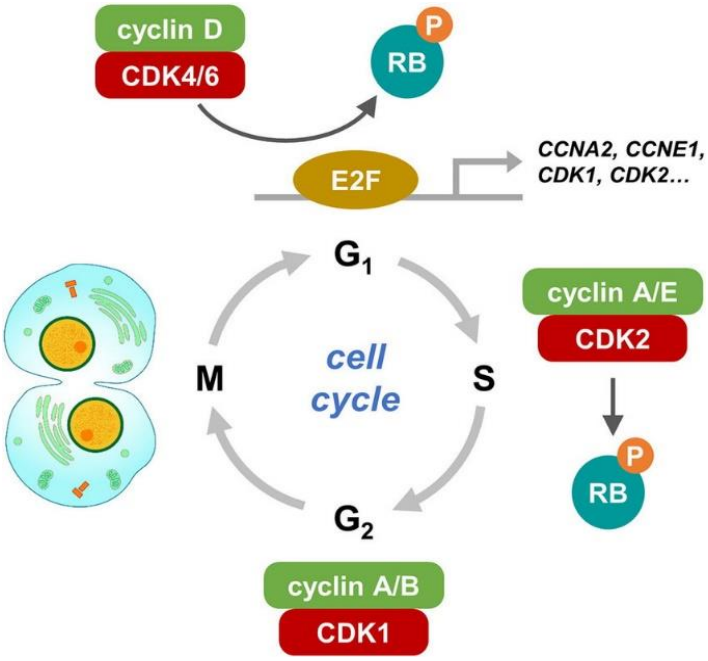

Figure 2.10: Cell cycle phases regulated by different cyclin-CDKs complexes (Mok *et al.*, 2018).

The cell cycle also contains several checkpoints. The role of checkpoints is to regulate the cell cycle by ensuring that the cell undergoes cell arrest, promoting repair and progression, and stimulating cell death if cell repair failed (Visconti *et al.*, 2016). Different cell cycle checkpoints include G1/S and G2/M checkpoints that are regulated by the tumour suppressor

proteins, retinoblastoma protein (pRb) and p53 (Figure 2.11) respectively (Visconti *et al.*, 2016, Liu *et al.*, 2019).

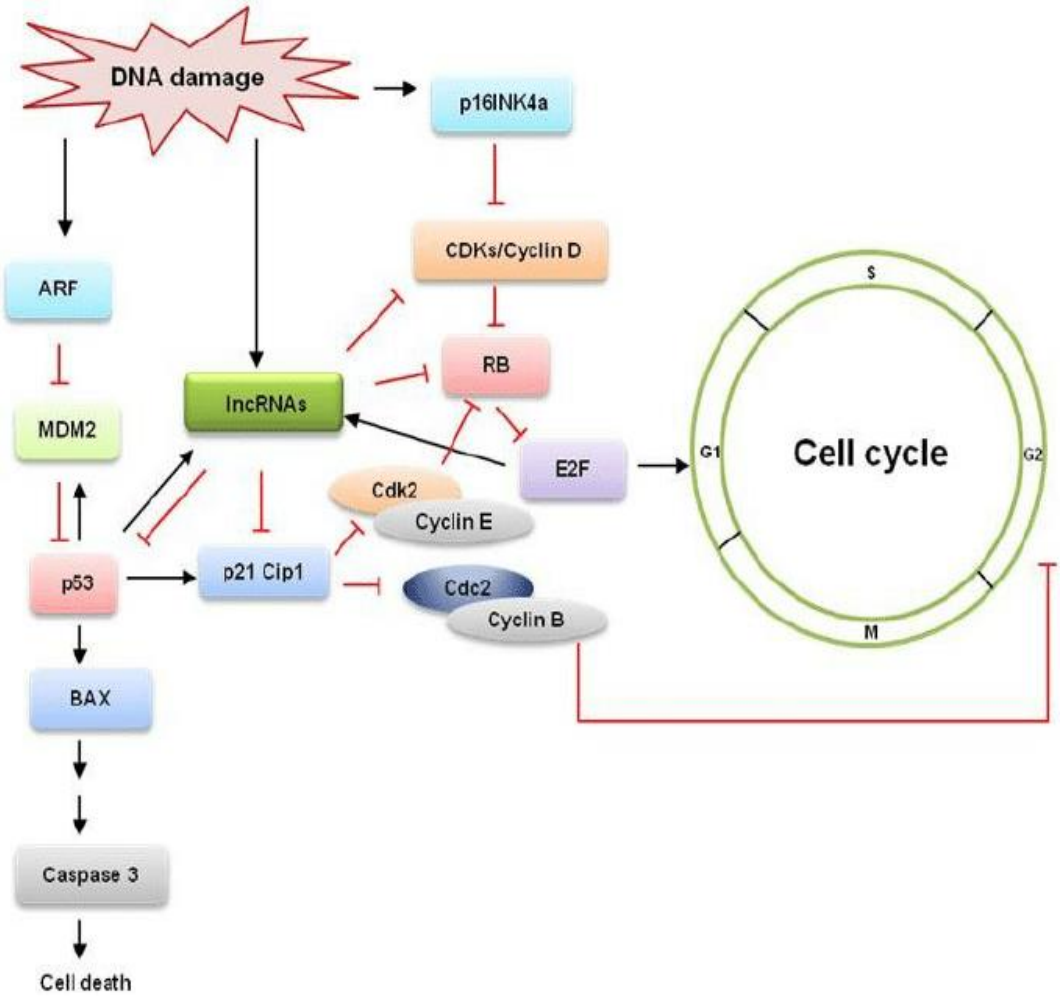

Figure 2.11: Different types of cell cycle regulatory proteins (Subramanian *et al.*, 2013).

The tumour suppressor p53 protein, essential for regulating the cell cycle, is known to prevent several diseases including cancer (Ebata *et al.*, 2016). The p53 protein was discovered in 1979 and has been recognised as the most critical tumour suppressor, which is referred to as an all-powerful guardian of the cell (Liu *et al.*, 2019). The p53 transcription factor is encoded by the *TP53* gene, which is mutated in more than 50% of human cancers (Ebata *et al.*, 2016). Activation of p53 is stimulated exogenously by ROS such as $O_2^{\bullet}$, H_2O_2 and $^{\bullet}OH$ that causes damage to proteins, lipids and DNA (Shi *et al.*, 2021). Activated p53 regulates stress signals such as telomere erosion, oncogene activation, hypoxia, and ribosomal stress. It also controls several cellular processes like apoptosis, cycle arrest, DNA repair, autophagy, ferroptosis or senescence to ensure cell survival or limit the malignant transformation of the cell (Liu *et al.*,

2019). In the cell cycle, p53 is activated in the G1 checkpoint in response to DNA damage (Figure 2.11) (Otto and Sicinski, 2017). Activated p53 initiates cell cycle arrest to facilitate DNA repair and survival by inducing the expression of the CDK inhibitor, p21CIP1, leading to inhibition of cyclin E-CDK2 complexes. The activity of p53 is negatively regulated by Mouse double minute 2 homolog (MDM2) protein, which maintains its stability by acting as an E3 ligase to ubiquitinate p53, thus degrading and inactivating it (Figure 2.11) (Hou *et al.*, 2019). However, when DNA damage occurs, the AFR tumour suppressor, also known as p14 in humans, is induced to negatively regulate MDM2 by sequestering it, therefore increasing the levels of p53 as seen in Figure 2.11 (Subramanian *et al.*, 2013). When the DNA repair mechanism fails, p53 triggers the cell to undergo cell death (Pfeffer and Singh, 2018).

2.7 CELL DEATH

Cells can die in various ways including autophagic cell death (ACD), necrosis and apoptosis (Figure 2.12) (Galluzzi *et al.*, 2018). Cell death by ACD occurs when the cytoplasmic organelles such as mitochondria or the endoplasmic reticulum are sequestrated into autophagosomes that fuse with the lysosome to form autolysosome (Green and Llambi, 2015). Cell death by autophagy is usually triggered by low ATP levels, nutrients and damaged organelles. Therefore, it is the way of cell survival under metabolic crisis (Green and Llambi, 2015). Necrosis is the type of cell death induced by cellular stressors such as irradiation, oxygen deprivation (hypoxia), ischemia (restricted blood supply), cytokines, pathogens, heat and toxins (Galluzzi *et al.*, 2018). Necrosis results in a loss of energy, swelling of the cell and damage to the plasma membrane. As a result, the components of the cytosol leak into the extracellular space, where they can cause inflammation, ultimately damaging surrounding tissue (Choi *et al.*, 2019). Apoptosis is the programmed form of cell death.

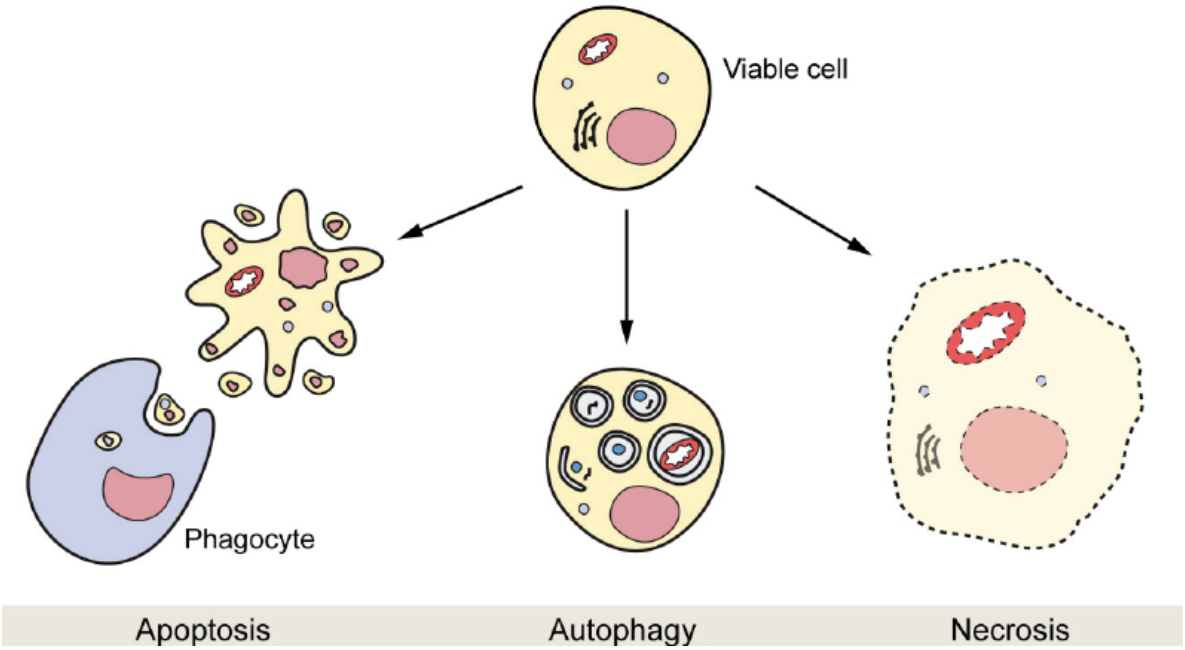

Figure 2.12: Different types of cell death namely apoptosis, autophagy and necrosis (Mizushima and Komatsu, 2011).

2.7.1 Apoptosis

Apoptosis is a form of cell death, also known as programmed cell death, characterised by a reduction in cell volume (pyknosis), fragmentation of the cell nucleus (karyorrhexis), chromatin condensation and distension of the plasma membrane, as well as the formation of intact small vesicles called apoptotic bodies (Kroemer *et al.*, 2009, Pfeffer and Singh, 2018). The term "apoptosis" was conceived by Kerr, Wyllie and Currie in 1972 to relate to this type of cell death with the "dropping off" leaves from trees in autumn (Kerr *et al.*, 1972). The process of apoptosis is initiated by both internal and external factors that lead to the activation of cysteine proteases proteins called caspases (Pfeffer and Singh, 2018). After that, the activated caspases cause the cleavage of crucial cellular protein, degradation of nuclear scaffold and cytoskeleton, and activate DNase that degrades nuclear DNA (Green and Llambi, 2015). There are two pathways of apoptosis, the intrinsic (mitochondrial) and extrinsic (receptor-dependent) pathways (Pfeffer and Singh, 2018).

2.7.1.1 Extrinsic pathway

The extrinsic signalling pathway (Figure 2.13) is triggered by extracellular signals such as tumour necrosis factor (TNF), Fas ligand (Fas-L), and TNF-related apoptosis-inducing ligand (TRAIL), which bind to tumour necrosis factor (TNF) gene superfamily receptors to induce

apoptosis (Zaman *et al.*, 2014). The binding of the signalling factors causes the recruitment of the adapter protein in the cytoplasm, such as the Fas-associated death domain (FADD) and the TNF receptor-associated death domain (TRADD), which have corresponding death domains to bind to the receptors (Pfeffer and Singh, 2018). The adaptor protein is then activated and associated with pro-caspase-8 and -10, forming a death-inducing signalling complex (DISC) in which pro-caspase-8 and 10 are activated to form caspase-8 and -10 (Green and Llambi, 2015). Activated initiator caspase-8 subsequently activates executor caspase-3/-7 (Figure 2.13) (Pfeffer and Singh, 2018). Activated caspase-8 also contributes to the intrinsic pathway by stimulating the cleavage of BID to tBid, which causes mitochondrial outer membrane permeabilization (MOMP) through the activation of Bax and Bak (Huang *et al.*, 2016).

2.7.1.2 Intrinsic pathway

The intrinsic mechanism of apoptosis (Figure 2.13) relies on the mitochondria and associated proteins. This process is triggered by internal stimuli such as free radicals, hyperthermia, toxins, viral infections, hypoxia and radiation that causes upregulated expression of oncogenes or damaged DNA in cells (Green and Llambi, 2015). The intrinsic pathway is regulated by the B-cell lymphoma protein 2 (Bcl-2) family proteins, both pro-apoptotic and anti-apoptotic members (Pfeffer and Singh, 2018). The pro-apoptotic Bcl-2 such as Bak and Bax are sequestered by anti-apoptotic proteins like Bcl-2, $BclX_L$, Bcl-W and Bcl-B, preventing them from inducing apoptosis (Goldar *et al.*, 2015). Pro-apoptotic proteins will be activated when p53-mediated repair of damaged DNA fails; in this event, p53 will cause the transcription of BH3-only Bcl-2 family proteins, Puma and Noxa (Pfeffer and Singh, 2018). Both Puma and Noxa bind and inhibit anti-apoptotic Bcl-2 proteins, thus releasing Bax and Bak. Homo- or heterodimerisation of Bax and Bak, and their insertion into the outer mitochondrial membrane induces MOMP (Pfeffer and Singh, 2018).

The induction of MOMP facilitates the release of cytochrome c, second mitochondria-derived activator of caspase/direct inhibitor of apoptosis-binding protein with low pI (Smac/DIABLO), serine protease HtrA2/Omi, apoptosis inducing factor (AIF) and endonuclease G and from the mitochondrial intermembrane space (Green and Llambi, 2015). The release of cytochrome c recruits apoptotic protease-activating factor-1 (Apaf-1), dATP and procaspase- 9, forming an apoptosome in which pro-caspase-9 is activated to caspase-9 (Lopez and Tait, 2015). The activated caspase-9 activates the executor caspase-3/7 (Pfeffer and Singh, 2018). Apoptosis

induced by Smac/DIABLO and Omi disrupts the activity of inhibitors of apoptosis protein (IAP), while AIF and endonuclease G play a role is the condensation of chromatin, thus causing DNA fragmentation (Kalkavan and Green, 2018).

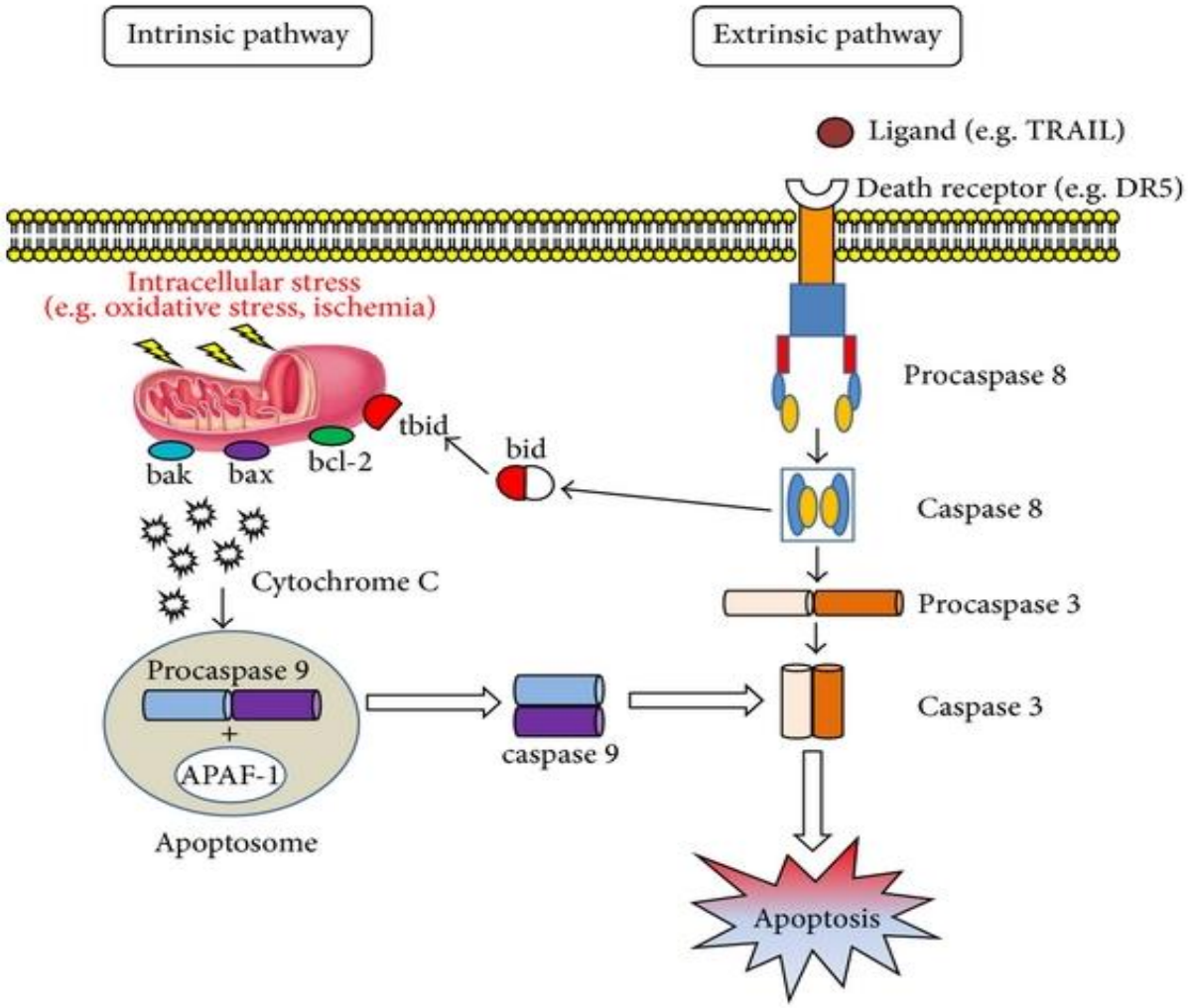

Figure 2.13: The extrinsic and extrinsic pathways of apoptosis (Loreto *et al.*, 2014).

Caspase 3/7 triggers the morphological changes associated with apoptosis. A cell that has undergone apoptosis is indicated by the flipping of the phosphatidylserine from the cytoplasmic side or in the inner plasma membrane to the exterior of the membrane bilayer (Kupcho *et al.*, 2019).

CHAPTER 3 : MATERIALS AND METHODS

3.1 MATERIALS

The Hek293 and Caco2 cells were acquired from Highveld Biological (Johannesburg, South Africa (SA)). Hexacyclen was purchased from Sigma Aldrich (Johannesburg, SA). Cell culture reagents and plasticware were obtained from Whitehead Scientific (Johannesburg, SA). The western blot reagents were purchased from Bio-Rad (Hercules, CA, USA), whilst all of the antibodies and Promega products were purchased from Cell Signalling Technology (CST) (Anatech (Johannesburg, SA). Unless stated otherwise, all other reagents were purchased from Merck (Darmstadt, Germany).

3.2 CELL CULTURE

The Hek293 and Caco2 cells were cultured (37^{o}C, 5% CO_2) in 25cm^2 flasks and reconstituted in a complete culture medium (CCM) containing Dulbecco's Modified Eagle Medium (DMED), supplemented with 10% foetal calf serum, 1% L-glutamine and 1% penicillin-streptomycin-fungizone. Cell growth was consistently monitored and CCM was changed when needed. The Caco2 cells were washed with 0.1 molar (M) phosphate-buffered saline (PBS). The Caco2 cells were trypsinised with 1ml trypsin at approximately 80% confluent, while Hek293 cells were detached by moderate agitation. Cells were counted using the trypan blue exclusion method.

3.3 PREPARATION OF THE TREATMENT

A stock solution of Hexacylen [3870 micromolar (µM)] was prepared by dissolving 5mg in 5ml of CCM. The treatment medium was diluted with CCM to obtain the treatment concentrations used in this study.

3.4 3-(4,5-DIMETHYLTHIAZOL-2-YL)-2,5-DIPHENYLTETRAZOLIUM BROMIDE (MTT) ASSAY

3.4.1 Principle

The colorimeter MTT assay was performed to determine cell viability and cytotoxicity. The principle of this assay is based on the reduction of a yellow water-soluble MTT salt to produce a purple formazan product (Bahuguna *et al.*, 2017) (Figure 3.1). This metabolic activity is due

to NAD(P)H-dependent mitochondrial dehydrogenase enzymes that reduce NAD(P)H to NAD^+/$NADP^+$ in viable cells. The formazan produced is solubilised with an organic solvent like dimethyl sulfoxide (DMSO). The intensity of formazan colour, quantified by measuring the optical density using a plate reader at a wavelength of 570 nanometres (nm) and 690nm, is directly proportional to the number of viable cells hence illustrating cell viability (Bahuguna *et al.*, 2017).

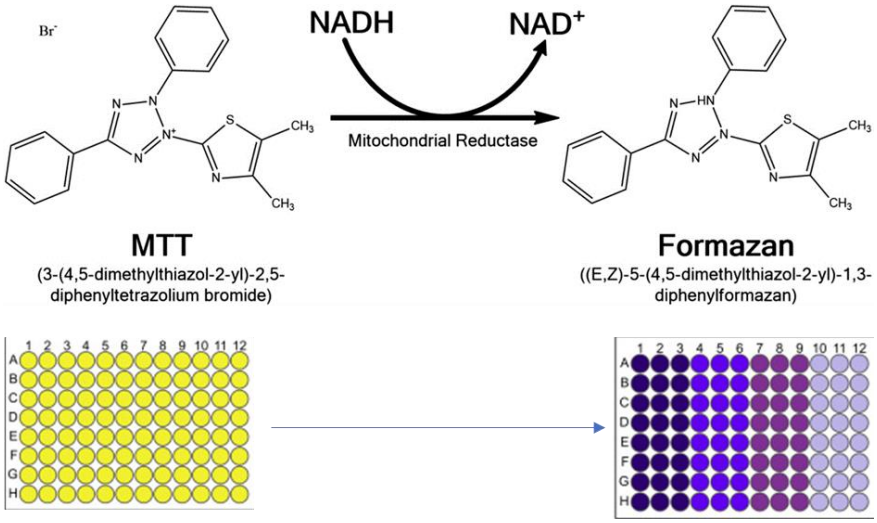

Figure 3.1: The reaction showing the reduction of MTT to formazan crystals [Adapted from *(Kamiloglu et al.*, 2020)].

3.4.2 Protocol

The MTT assay was conducted to determine the cytotoxicity and half-maximal inhibitory concentration (IC_{50}) of Hexacyclen in Hek293 and Caco2 cells. The suspension of Hek293 and Caco2 cells were seeded into a 96-well microtiter plate at a concentration of 15,000 cells/well (200µl/well) in triplicate, and cells were allowed to attach overnight (37^{o}C, 5% CO_2). Cells were then treated with different concentrations of Hexacyclen [Hek293 (0-500µM) and Caco2 (0-50µM)] and incubated for 48 hours (37^{o}C, 5% CO_2). After incubation, sample treatments were removed and replaced with 20µl of 5mg/ml MTT salt solution (in 0.1M PBS) and 100µl of CCM, then incubated for 4 hours (37^{o}C, 5% CO_2). The MTT salt solution was discarded after incubation and 100µl of DMSO was added to each well and incubated for 1 hour to solubilise formazan crystals (37^{o}C, 5% CO_2). The absorbance was measured using a SPECTROstar® Nano microplate reader (BMG LABTECH, Ortenberg, Germany) at 570nm

with a reference wavelength of 690nm. Cell viability percentage, relative to the control was calculated using the absorbance values:

$$\% \text{ cell viability} = \frac{average\ absorbance\ of\ treated\ cells}{average\ absorbance\ o\ f\ control\ cells} \text{ x } 100$$

GraphPad Prism v5.0 software (GraphPad Software Inc., La Jolla, California, USA) was used to construct a concentration-response curve to determine the concentration of Hexacyclen that produced half of the maximum inhibition (IC_{50}); the concentration that produced 20% inhibition (IC_{20}) was extrapolated from the curve. The IC_{50} and IC_{20} [Hek293 (138 and 6 µM), and Caco2 (5 and 1.2 µM)] were used to treat cells in subsequent assays (48 hours, 37ºC, 5% CO_2), while untreated cells were immersed in only CCM to serve as the control. The treatment medium was retained to quantify lactate dehydrogenase (LDH), malondialdehyde (MDA) and nitrites/nitrates concentration. The treated cells were washed 3x 0.1M PBS, then trypsinised and counted for luminometry and protein isolation.

3.5 ATP QUANTIFICATION ASSAY

3.5.1 Principle

Intracellular adenosine triphosphate (ATP) is required by metabolic active cells for life, as functional energy. It is produced via the electron transport chain (ETC) during oxidative phosphorylation and at the substrate level by tricarboxylic acid cycle (TCA) or the Krebs cycle (Zhao *et al.*, 2019). The ATP assay was used as a viable cell biomarker because when a cell is damaged, it loses membrane integrity and the ability to synthesize ATP. The ATPases quickly deplete the stores of ATP in the cytoplasm (Kamiloglu *et al.*, 2020). The ATP detection reagent contains a detergent to lyse the cells, ATPase inhibitors to stabilize the ATP released from the lysed cells, luciferin as a substrate and the stable form of luciferase enzyme to catalyse the reaction that generates photons of light (Figure 3.2) (Sanna *et al.*, 2018). The luminescent signal produced is directly proportional to the concentration of ATP present in the cell (Kamiloglu *et al.*, 2020).

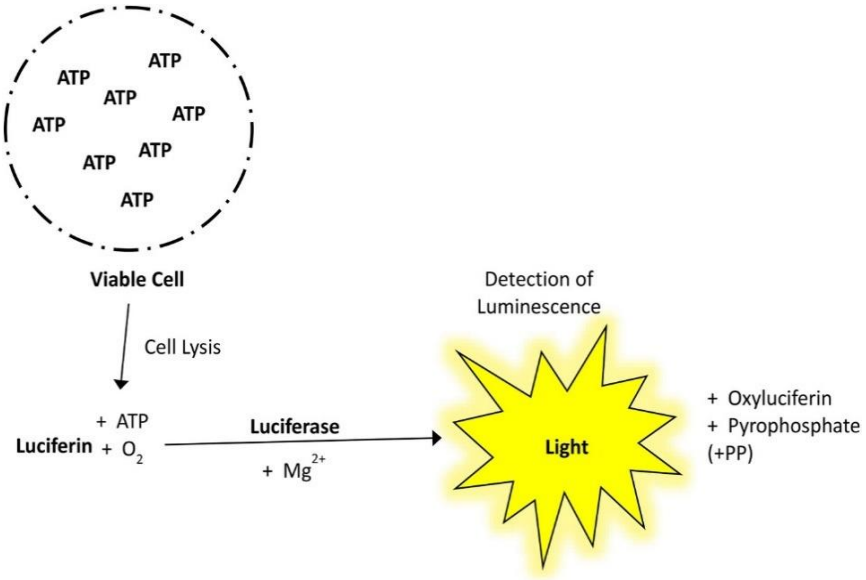

Figure 3.2: The schematic representation of ATP assay principle in the reaction catalysed by luciferase enzyme (Kamiloglu *et al*., 2020).

3.5.2 Protocol

Intracellular ATP levels were quantified using the Promega CellTiter-Glo® assay (#G7570, Anatech, Johannesburg, South Africa). The reagents were prepared according to the manufacturer's instructions. Cell suspension of Hek293 and Caco2 cells were seeded into a white opaque 96-well luminometer plate at a concentration of 20,000 cells/well (200µl/well) in triplicate and incubated overnight (37ºC, 5% CO_2). After incubation, the cell culture medium was removed and cells were treated with the respective concentration of Hexacyclen treatment solution (control, IC_{20}, $IC_{50;}$ 200µL), then incubated for 48 hours (37ºC, 5% CO_2). Thereafter, sample treatment was removed and 50µl of 0.1M PBS and 25µl of the ATP reagent was added to each well. Incubation in dark for 30 minutes at room temperature (RT) allowed the luciferin-luciferase reaction to occur, thus producing a luminescent signal proportional to the levels of intracellular ATP. Luminescence was quantified using the Modulus™ microplate luminometer (Winooski, USA) and the data generated was expressed as relative light units (RLU).

3.6 JC-10 MITOCHONDRIAL MEMBRANE POTENTIAL ASSAY

3.6.1 Principle

The mitochondrial membrane potential (ΔΨM) was used as an indicator for the function of the mitochondria. The mitochondrion is referred to as a powerhouse of the cells where cellular energy in the form of ATP is produced through the electron transport chain (Sakamuru *et al.*, 2016). Therefore, the ΔΨM is used as an indicator of healthy functioning cells. The ΔΨM assay

is based on the cationic, lipophilic JC-10/JC-1 dye, which concentrates in the mitochondrial matrix in cells with a polarized mitochondrial membrane, forming red fluorescent aggregates that can be detected at 540/590nm (Sivandzade *et al.*, 2019). However, in necrotic and apoptotic cells the ΔΨM collapse causes JC-10/JC-1 to diffuse out of mitochondria and return to its monomeric form that fluoresces green; monomers are detected at 490/525nm (Figure 3.3). The ratio of the red/green fluorescence intensity indicates ΔΨM.

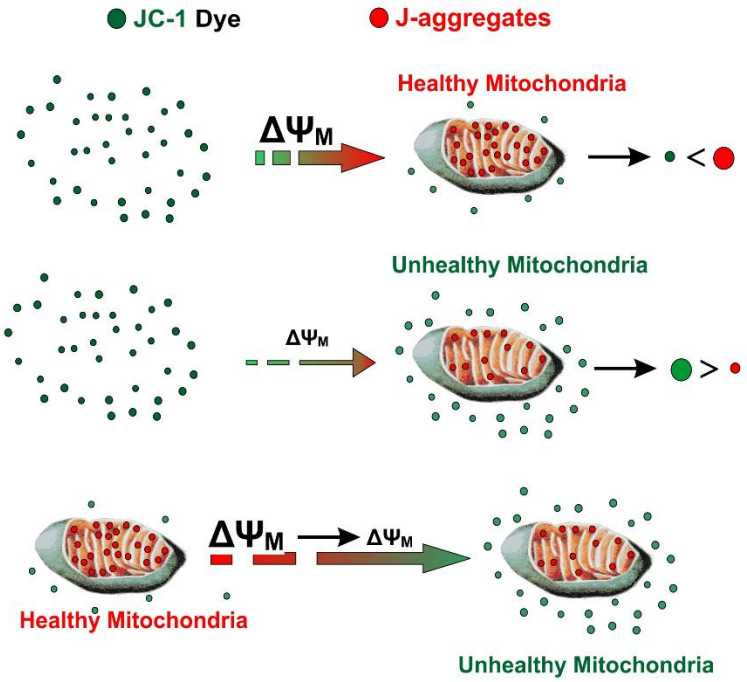

Figure 3.3: Schematic representation of the principle of JC-10 mitochondrial membrane potential assay (Sivandzade *et al*., 2019).

3.6.2 Protocol

The ΔΨM, a key indicator of appropriate mitochondria functioning, was quantified using JC-10 dye (MAK159, Sigma, Johannesburg, South Africa). The cell suspensions of Hek293 and Caco2 cells were seeded into a white opaque 96-well luminometer plate (20,000 cells/well (200µl/well) in triplicate and incubated overnight (37ºC, 5% CO_2). After incubation, the medium was removed and cells were treated with the respective concentrations of Hexacyclen treatment solution (control, IC_{20}, IC_{50}; 200µL/well), then incubated for 48 hours (37ºC, 5% CO_2). Afterwards, sample treatments were removed and 50µl of 0.1M PBS was added to each well. In addition, 25µl of JC-10 reagent was prepared according to the manufacturer's guidelines and subsequently added to each well. The plate was incubated in the dark for 30 minutes at RT, then fluorescence was measured at 540/590nm and 490/525nm respectively,

using a Modulus™ microplate luminometer (Turner Bio-systems, Sunnyvale, California, USA). The data was obtained as relative fluorescence units (RFU) and was expressed as red/green fluorescence intensity.

3.7 THIOBARBITURIC ACID REACTIVE SUBSTANCES (TBARS) ASSAY

3.7.1 Principle

The TBARS assay was used as an indicator of oxidative stress by measuring the lipid peroxidation end-product malondialdehyde (MDA) (Ghani *et al.*, 2017). Lipid peroxidation is the attack of lipids containing carbon-carbon double bond(s), especially polyunsaturated fatty acids, by free radicals thereby removing hydrogen to form a lipid radical in the initiation stage. Subsequent reaction of a lipid radical with oxygen during the progression stage produces a peroxyl radical, which abstracts a hydrogen from another lipid molecule generating a new lipid radical that continues the chain reaction and a lipid hydroperoxide. The reaction is terminated by antioxidants that donate their electrons to the lipid radicals resulting in the formation of non-radical molecules. Malondialdehyde (MDA) is produced as a by-product of lipid peroxidation and is used as an indirect marker of oxidative stress (Alché, 2019). The MDA reacts with thiobarbituric acid-butylated hydroxytoluene (TBA-BHT) in the presence of heat and acid to produce a coloured MDA-2TBA end-product that absorbs light at 530-540 nm (Figure 3.4), BHT prevents the oxidation of lipids during the reaction (Labudda, 2013). The intensity of the colour at 532 nm corresponds to the level of lipid peroxidation in the sample (Ghani *et al.*, 2017).

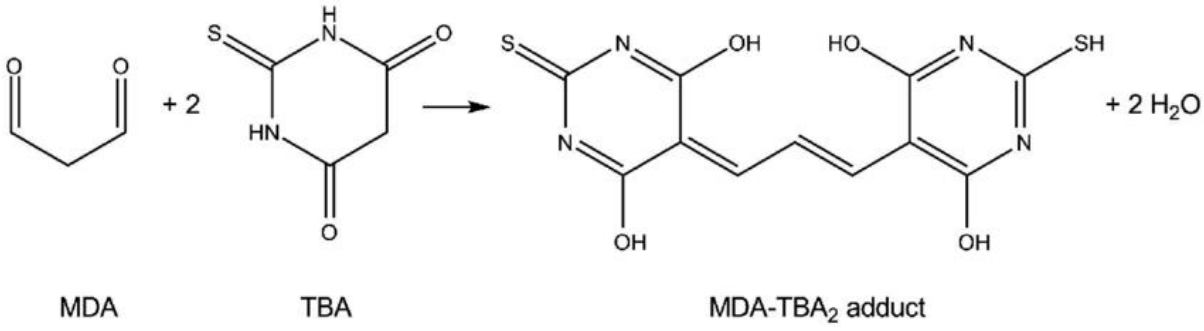

Figure 3.4: The reaction of malondialdehyde (MDA) with two molecules of thiobarbituric acid (TBA) to form an MDA-TBA adduct (Labudda, 2013).

3.7.2 Protocol

Five labelled test tubes for each cell line (Hek293 and Caco2) were prepared (control, IC_{20}, IC_{50}, positive and negative controls). The treated and untreated supernatant samples (200µl), as well as positive (199µl of CCM and 1µl of MDA) and negative (200µl of CCM) controls were added to their respective labelled test tubes, followed by the addition of 200µl of 7% phosphoric acid (H_3PO_4) to each sample. Thereafter, 400µl of TBA/BHT solution was added into each tube containing the sample except the negative control test tube; 3mM HCl (200µl) was added to the negative control, which served as the blank. All tubes were briefly vortexed and the pH was acidified in all test tubes by adding 200µl of 1M HCl. All test tubes were boiled at 100^{o}C for 15 minutes in a hot water bath. Afterwards, test tubes were removed and allowed to cool to RT. Butanol (1500µl) was added to each tube and vortexed for 30 seconds. Samples were placed aside to allow the separation of the mixture into two distinct layers. Then, 500µl of the upper butanol layer was pipetted into a microcentrifuge tube. Samples (100µl) were pipetted into a 96-well plate, in triplicate. The absorbance was measured using a SPECTROstar® Nano microplate reader (BMG LABTECH, Ortenberg, Germany) at 532nm with a reference wavelength of 600nm. The absorbance readings were used to calculate MDA levels by dividing the absorbance with the absorption coefficient [156 millimolar (mM^{-1})] to generate the mean MDA concentration (µM).

$$[\text{MDA}] = \frac{sample\ absorbance}{156mM^{-1}} \text{ x1000}$$

3.8 NITRIC OXIDE SYNTHASE (NOS) ASSAY

3.8.1 Principle

The NOS assay was used to determine nitric oxide concentrations based on the enzymatic conversion of nitrate to nitrite by nitrate reductase (Antoniou *et al.*, 2018). The reaction is facilitated by vanadium chloride (VCl_3), followed by colorimetric detection of nitrite as an azo dye product of the Griess reaction, which is based on the two-step diazotization reaction. In this reaction, acidified NO_2 produces a nitrosating agent that reacts with sulfanilic acid to produce the diazonium ion (Figure 3.5). This ion is then coupled to N-(1-naphthyl) ethylenediamine (NEDD) to form the chromophoric azo-derivative, which absorbs light at 540-570 nm (Böhmer *et al.*, 2014).

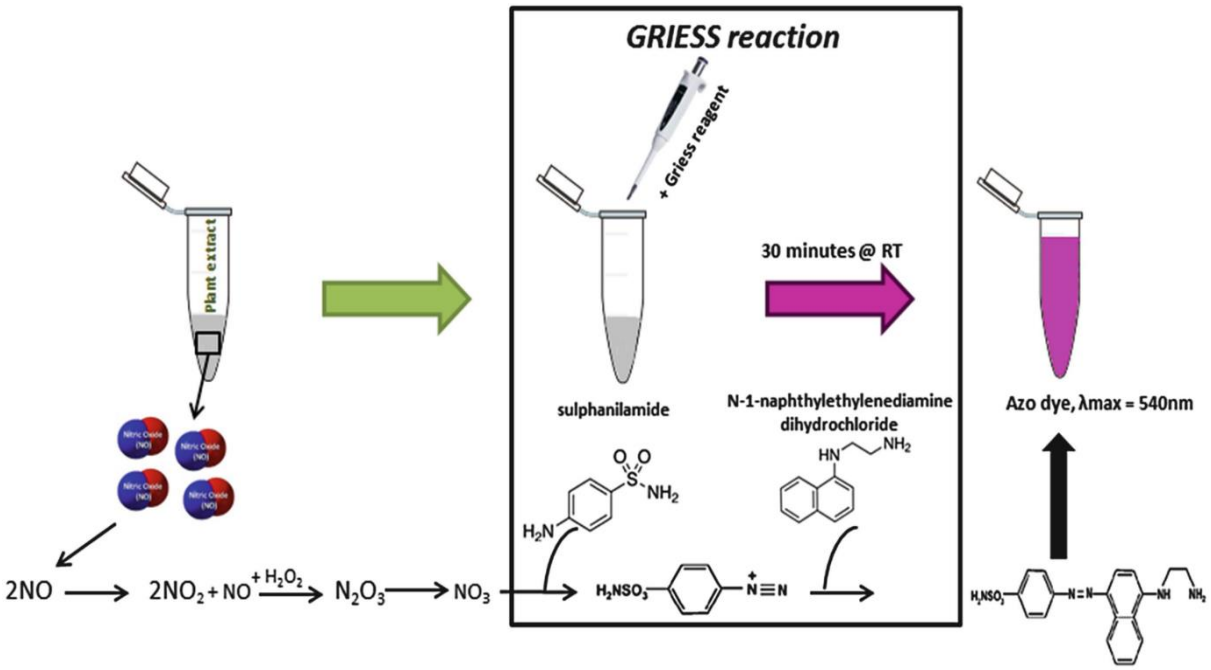

Figure 3.4: The principle of nitric oxide synthase assay based on Griess Reaction (Antoniou *et al.*, 2018).

3.8.2 Protocol

Sodium nitrate standards (0-200µM) were prepared and 50µl of each concentration was aliquoted into a 96-well microtiter plate in triplicate. The treated and untreated supernatant samples (50µl) of each cell line were also added into separate wells of the 96-well plate in triplicate. Thereafter, 50µl VCl_3, 25µl SULF and 50µl of NEDD were added sequentially to each well and the plate was incubated in the dark for 45 minutes (37ºC, 5% CO_2). After incubation, the absorbance was measured using a SPECTROstar® Nano microplate reader (BMG LABTECH, Ortenberg, Germany) at 540nm with a reference wavelength of 690nm. The average absorbances of sodium nitrate were used to prepare a standard curve, and the extrapolated equation was used to determine the nitrate and nitrite concentrations (µM) of treated and untreated samples.

3.9 GLUTATHIONE ASSAY

3.9.1 Principle

Reduced glutathione (GSH) is an important intracellular antioxidant that serves as a co-factor for glutathione peroxidase and glutathione-S-transferase (GST). The quantity of GSH thus

provides an indication of oxidative stress in cells (Matuz-Mares *et al.*, 2021). The GSH assay (Figure 3.6) relies on the conversion of a luciferin derivative into luciferin in a reaction catalysed by GST in the presence of GSH. A luciferin detection reagent couples the reaction with luciferase and ATP producing a luminescent signal that is proportional to the amount of GSH (Salbitani *et al.*, 2017).

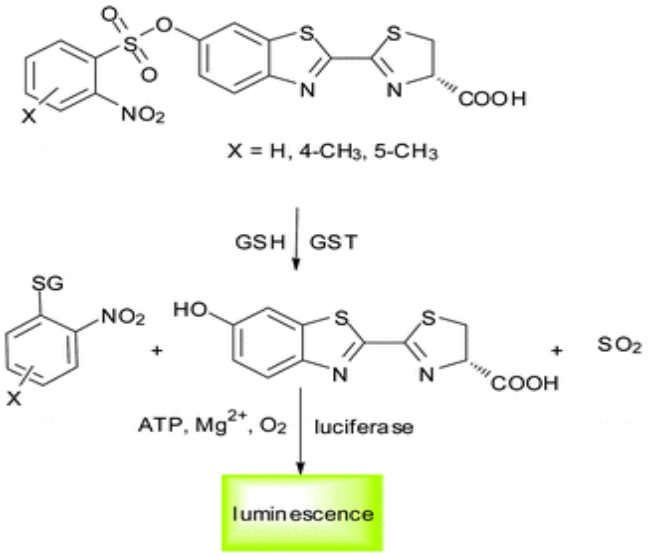

Figure 3.5: The schematic representation of glutathione (GSH) assay principle (Li *et al.*, 2013).

3.9.2 Protocol

Intracellular GSH levels were quantified using the GSH-Glo™ assay (Cat. #V6911/2). The Hek293 and Caco2 cells were seeded into a white opaque 96-well luminometer plate (20,000 cells/well cells, 200µl/well), in triplicate and incubated overnight (37°C, 5% CO_2). After incubation, the medium was removed and cells were treated with respective Hexacyclen concentrations (control, IC_{20}, IC_{50}; 200µl), then incubated for 48 hours (37°C, 5% CO_2). Thereafter, treatment medium was removed and 50µl of 0.1M PBS was added to each well. Afterwards, GSH-Glo™ reagent was prepared according to the manufacturer's guidelines and 25µl added to each well. The plate was incubated in dark for 30 minutes at RT, then the luminometric detection reagent (12.5µl) was added. After 15 minutes, luminescence was measured using a Modulus™ microplate luminometer (Turner Bio-systems, Sunnyvale, California, USA). The obtained data was expressed as mean RLU.

3.10 ANNEXIN V ASSAY

3.10.1 Principle

The Annexin V assay allows for differentiation between apoptotic and necrotic cells. Viable cells consist of an asymmetrical plasma membrane, which is lost during apoptosis. Phosphatidylserine is an integral component of the plasma membrane that is used as a biomarker to detect early apoptosis since it flips from the inside surface to the exterior (Kupcho *et al.*, 2019). The apoptotic cells are detected by labelled Annexin V, which binds specifically to exposed charged head groups of phosphatidylserine through a Ca^{2+} dependent process (Figure 3.7) and emits a luminescent signal that is proportional to phosphatidylserine exposure (Demchenko, 2012). Propidium iodide or an analogous fluorescent DNA-binding probe is used in conjunction with labelled Annexin V. Propidium iodide is a vital dye that will only enter cells due to loss of membrane integrity and is thus a marker of necrosis; necrotic cells are permeable while viable/apoptotic cells are not permeable (Crowley *et al.*, 2016).

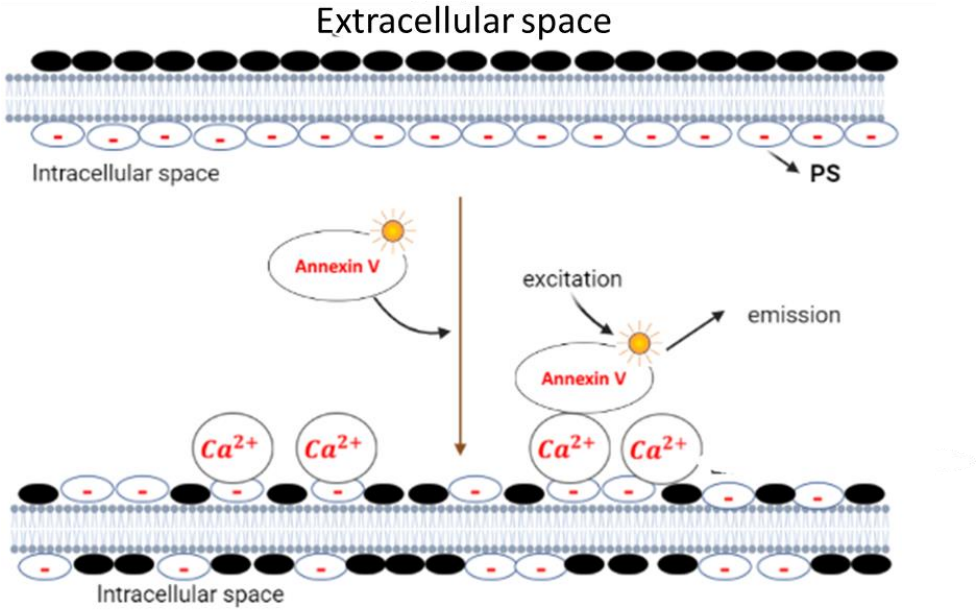

Figure 3.6: Schematic representation of changes in the plasma membrane during early events of apoptosis (prepared by author).

3.10.2 Protocol

The presence of apoptosis was detected using the Annexin V apoptosis and necrosis assay. The Hek293 and Caco2 cell suspensions were seeded into a white opaque 96-well luminometer

plate at a concentration of 20,000 cells/well (200µl/well) in triplicate and incubated overnight (37°C, 5% CO_2). After removing the culture medium, 200µl of Hexacyclen treatments solution was added to the respective wells (control, $IC_{20,}$ IC_{50}). The plate was incubated for 48 hours (37°C, 5% CO_2), then the treatment medium was replaced with 50µl of 0.1M PBS. The RealTime-Glo™ Annexin V Apoptosis and Necrosis Assay reagent (Cat. #JA1011) was prepared according to the manufacturer's guidelines and 25µl was added to the sample wells. After 30 minutes incubation (dark, RT), the luminescent and fluorescent signal was detected using the Modulus™ microplate luminometer (Turner Bio-systems, Sunnyvale, California, USA) and the results were expressed as mean RLU and RFU respectively.

3.11 LDH ASSAY

3.11.1 Principle

The LDH assay was used to determine levels of damage to the cell membrane. The LDH is a stable cytoplasmic enzyme that is released when cells undergo cellular damage due to the loss of membrane integrity (Kamiloglu *et al.*, 2020). This assay is driven by the LDH enzyme, which catalyses the conversion of lactate to pyruvate, while oxidizing reduced nicotinamide adenine dinucleotide (NADH) to produce NAD^+ as seen in Figure 3.8 (Forest *et al.*, 2015). In this reaction, NADH reduces the yellow tetrazolium (iodonitrotetrazolium or 2-(4-iodophenyl) -3-(4-nitrophenyl) -5-phenyl-2H-tetrazolium, INT) salt into a water-soluble red formazan dye. Formazan is measured at 490/600nm and is directly proportional to the level of damage present within a given sample (Kamiloglu *et al.*, 2020).

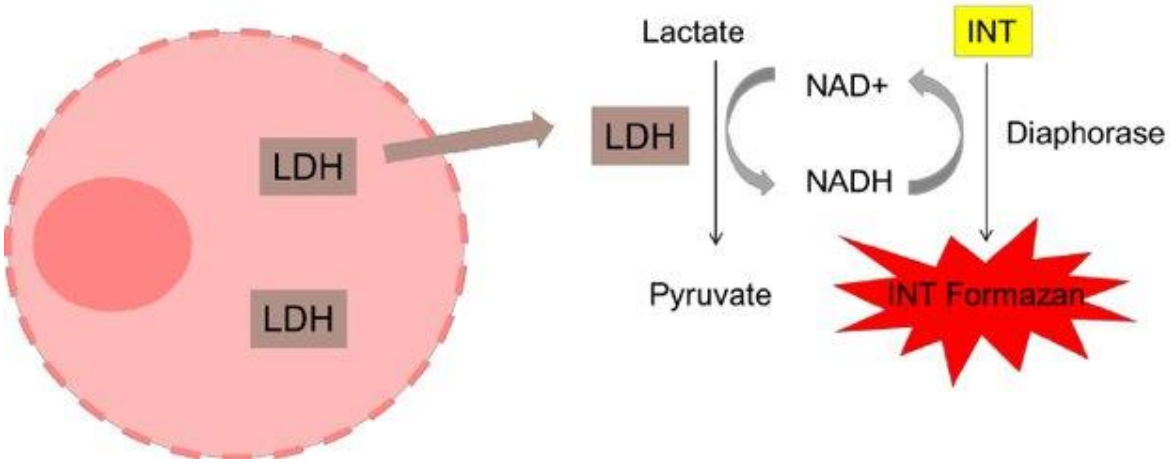

Figure 3.7: The Schematic representation of the principle of the LDH assay catalysed by lactate dehydrogenase converting lactate to pyruvate (Forest *et al.*, 2015).

3.11.2 Protocol

The levels of damage to the cell membrane were determined by measuring the extracellular LDH levels using a Cytotoxicity Detection Kit (#0474926001, Roche, Mannheim, Germany). The treated and untreated supernatant samples (50µl) of each cell line (Hek293 and Caco2) were added into a 96-well microtiter plate, in triplicate. The substrate mixture (25µl) comprising of dye solution (INT/sodium lactate) and catalyst (diaphorase/NADþ) was added into each well with the sample and the plate was incubated (in the dark, RT, 30 minutes). Stop solution (12.5µl/well) was added into all wells containing samples and the absorbance was measured at 490nm with a reference wavelength of 600nm, using a SPECTROstar® Nano microplate reader (BMG LABTECH, Ortenberg, Germany). The results obtained were represented as mean optical density (OD).

3.12 CASPASE ACTIVATION

3.12.1 Principle

The activity of caspases 8, -9 and -3/7 was assessed using the Promega caspase-glo® assay. Caspases are a family of cysteine proteases that play an important role during apoptosis to proteolytically disassemble most cellular structures such as the cytoskeleton and cell junctions (Pfeffer and Singh, 2018). The caspase activity assays contain cell lysis and an aminoluciferin-DEVD substrate that is cleaved by the respective caspase to release aminoluciferin. The released animoluciferin reacts with luciferase in the presence of ATP, magnesium ions (Mg^{2+}) and O_2 to generate light that is quantified by the luminometer (Scabini *et al.*, 2011) (Figure 3.9). The amount of light produced is proportional to the active caspases in the sample.

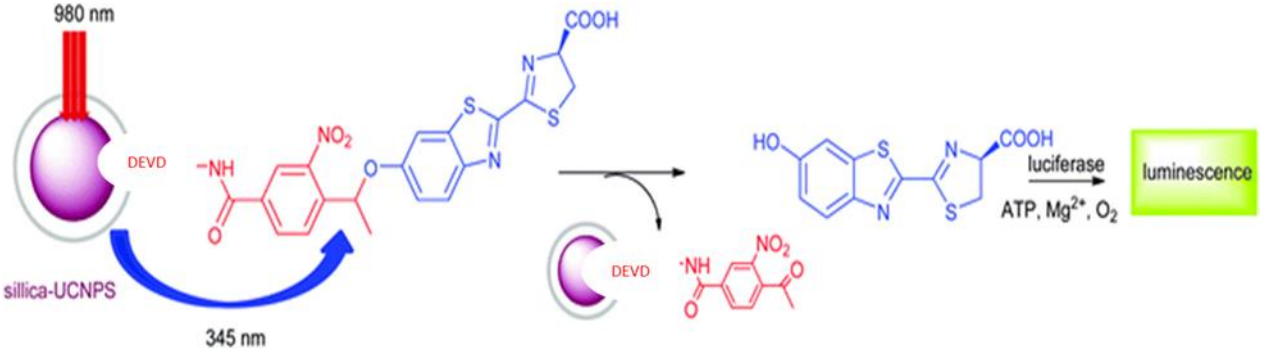

Figure 3.8: An example of the principle of caspase activity assay catalysed by caspases (Li *et al.*, 2013).

3.12.1 Protocol

The activity of caspases 8, -9 and -3/7 were assessed using Promega caspase-Glo® assays. The Hek293 and Caco2 cell suspensions were seeded into a white opaque 96-well luminometer plate at a concentration of 20,000 cells/well (200µl/well) in triplicate and incubate overnight (37ºC, 5% CO_2). Following incubation, 200µl of Hexacyclen treatment solution was added after removing the culture medium (control, IC_{20}, IC_{50}), then incubated for 48 hours (37ºC, 5% CO_2). Thereafter, sample treatment medium was removed and 50µl of 0.1M PBS was added to each well. The Caspase-Glo®-3/7, -8 and -9 reagents [#G8090, #G8200 and #G8210 respectively, Promega (Madison, Wisconsin, USA)] were prepared according to the manufacturer's instructions, and the caspase reagent (25µl) was added into the relevant treatment wells. The plate was then incubated (dark, 30 minutes, RT). Luminescence was detected using the Modulus™ microplate luminometer (Winooski, USA) and the data obtained was expressed as mean RLU.

3.13 WESTERN BLOTTING

3.13.1 Principle

The western blotting assay was used for the detection and characterization of proteins. Firstly, proteins of interest are extracted from a homogenous sample, then quantified and standardised (Mohammad, 2016). The proteins are separated according to their molecular size in a polyacrylamide gel applying an electrophoretic current. The separated proteins are transferred to a high-affinity membrane. Subsequently, membranes are blocked to reduce non-specific binding, and precise proteins are detected using primary antibodies. Secondary antibodies are linked to a label that can be detected with a chemiluminescent substrate to develop a signal, which is theoretically proportional to the degree of antigen/antibody binding (Figure 3.10). Finally, the resultant bands are analysed by applying densitometry software (Bass *et al.*, 2017).

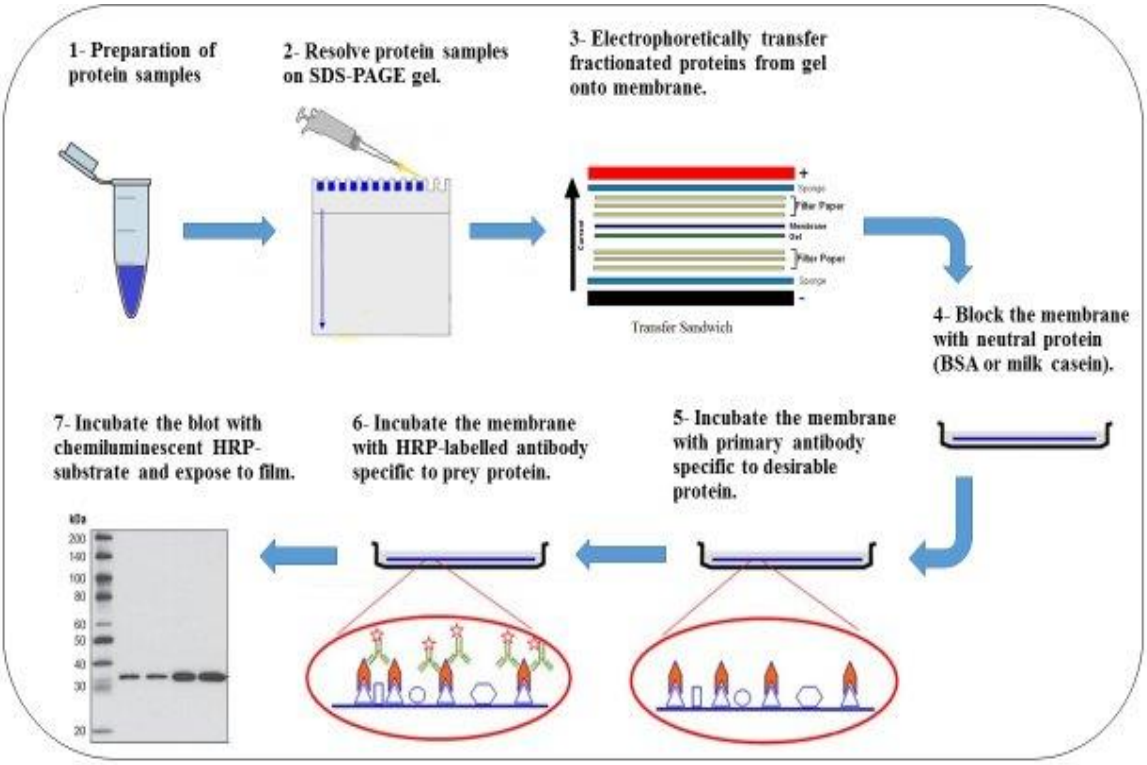

Figure 3.9: Western blotting procedure (Mohammad, 2016).

3.13.2 Protocol

Western blotting was used to detect and quantify the expression of proteins in a homogenous sample. Following treatment, the crude protein was isolated from treated and untreated cells using Cytobuster™ reagent (Novagen, San Diego, CA, USA) supplemented with protease and phosphatase inhibitor [(Roche (Germany), 05892791001 and 04906837001 respectively]. The cytobuster reagent (400µl) was added to the treated and untreated flasks, which were then placed on ice for 15 minutes and scraped. The cell lysate was collected into a microcentrifuge tube and placed on ice for a further 10 minutes, then centrifuged at 10,000×g, 4^{o}C for 5 minutes. The supernatants containing the crude protein were removed and subsequently quantified using the bicinchoninic acid (BCA) assay.

Using a 96-well microtiter plate, 25µl of the crude protein and bovine serum albumin (BSA) standards (0, 0.2, 0.4, 0.6, 0.8 and 1mg/ml) were added, in triplicate. The BCA solution (4µl $CuSO_4$ and 198µl BCA) was prepared and 200µl was added to each of the sample and standard wells. The plate was then incubated at 37^{o}C for 30 minutes and absorbance was measured at 562nm using a SPECTROstar® Nano microplate reader (BMG LABTECH, Ortenberg, Germany). A standard curve was constructed using the mean absorbances of the standards and

the protein concentration of each sample was calculated using the extrapolated equation. The protein samples were standardised to 1mg/ml, and Laemmli buffer [de-ionised water (dH_2O), 0.5M Tris-HCl (pH 6.8), glycerol, 10% of sodium dodecyl sulfate (SDS), β-mercaptoethanol, 1% bromophenol blue] was added to each sample in a 1:4 ratio. The samples were then boiled at 100^oC for 5 minutes, placed at RT to cool down and stored at -80^oC until use.

The standardised samples (25µl) were loaded into prepared polyacrylamide gels. The gels comprised a lower 10% resolving gel layer and an upper 4% stacking gel layer [10% resolving gel: dH_2O, 1.5M Tris-HCl (pH 8.8), 10% (w/v) SDS, 30% Acrylamide/Bis, 10% ammonium persulfate (APS) and tetramethyl ethylenediamine (TEMED) and 4% stacking gel: dH_2O, 0.5M Tris-HCl (pH 6.8), 10% (w/v) SDS, 30% Acrylamide/bis, 10% APS and TEMED]. The gels were submerged in 1x running (electrode) buffer [dH_2O, Tris, glycine, pH 8.3, 4^oC) and subjected to an electric field for 90 minutes at 150V using a Bio-Rad compact power supply.

Once the electrophoresis was completed, the gels were placed into a cold transfer buffer (dH_2O, Tris, glycine, methanol, pH 8.3) for 10 minutes. Then, proteins were electro-transferred onto a nitrocellulose membrane using the Transblot®Turbo™ Transfer system (Bio-Rad, California, USA). The transfer method involves assembling of the sandwich using the electrophoresed polyacrylamide gel, nitrocellulose membrane and fibre pads in a cassette, removal of air bubbles, submerged in transfer buffer, drainage of excess buffer and applying external electric current (25V, 2.5mA, 30 minutes). Following transfer, the nitrocellulose membranes were blocked for 2 hours at RT with 2% BSA in Tris-buffered saline [TTBS; 150mM sodium chloride (NaCl), potassium chloride (KCl), 25mM Tris; pH7.5) containing 0.05% Tween20]. Blocking solution was then removed and the membrane was probed for 1 hour on the shaker (RT) with primary antibodies [SOD2 (13141), GPx1 (3286), iNOS (13120), CAT (12980), p-p53 (48818), Bcl-2 (15071), Bax (5023), HSP70 (46477), PARP1 (9542), cPARP1 (9541), NF-κB p65 (8242), STAT3 (4904), and pSTAT3 (9145)] at 1:1000 dilution in 2% BSA/TTBS. The membranes were then incubated overnight at 4^oC, to allow the binding of the primary antibody to the specific targeted protein.

The next day, the membranes were equilibrated to RT for 1 hour, and primary antibodies were then removed and washed five times with TTBS (10 minutes per wash). Following the wash, membranes were incubated with 5ml of secondary antibody conjugated to horse-radish peroxidase (HRP) [anti-rabbit IgG, 7074 (SOD2, catalase, iNOS, GPx1, Bax, PARP1,

cPARP1, NF-κB p65, STAT3, and pSTAT3) or anti-mouse IgG, 7076 (p-p53, Bcl-2, HSP70)] in a 1:2500 dilution in 2% BSA/TTBS for 2 hours on the shaker (RT) and incubated overnight at 4^{o}C. The secondary antibody was removed and the membranes were rinsed five times with TTBS (10 minutes per wash). Images of the nitrocellulose membranes were viewed using the Clarity Western ECL Substrate (catalogue no. 1705061, Bio-Rad) and captured using the Chemidoc™ Imaging System and Bio-Rad imaging system (Bio-Rad, California, USA).

Membranes were then quenched using 5% hydrogen peroxide (H_2O_2) (37^{o}C, 30 minutes), rinsed twice with TTBS and blocked in 2% BSA in TTBS (1 hour) before being probed for beta (β)-actin (A0bD12141, Sigma) (1 hour, RT), a house-keeping protein that is used to normalise protein expression. The nitrocellulose membranes were washed three times with TTBS (10 minutes per wash) and viewed. Images were captured using the Chemidoc™ Imaging System and Bio-Rad imaging system (Bio-Rad, California, USA) and were analysed by measuring the band intensity of each protein and the bands were normalised against β-actin. Data was presented as mean relative band density (RBD).

3.14 DATA ANALYSIS

All statistical analyses were carried out using GraphPad Prism V5 (GraphPad Software Inc., La Jolla, USA). For all experiments three replicates were used, and experiments were repeated to ensure reproducibility. Data was expressed as mean ± standard deviation. One-way analysis of variance with a Tukey's post-test and an unpaired students *t*-test with Welch's correction was used to determine statistically significant differences ($p < 0.05$) between the treatments and the control.

CHAPTER 4 : RESULTS

4.1 CELL VIABILITY AND METABOLIC ACTIVITY

4.1.1 Cytotoxic response

The toxicity of Hexacyclen was measured in Hek293 and Caco2 cells using the MTT assay (Figure 4.1). The dose-response curve revealed a decrease in cell viability with increasing Hexacyclen concentration (0-500µM) in Hek293 cells (Figure 4.1A). Similarly, cell viability decreased in Caco2 cells for Hexacyclen treatments (0-50µM, Figure 4.1B). The inhibitory concentrations that resulted in 50% and 20% (IC_{50} and IC_{20}) cell death was 138µM and 6µM respectively for Hek293 cells, and 5µM and 1.2µM in Caco2 cells, respectively. The recorded IC_{50} and IC_{20} concentrations were used in all subsequent assays.

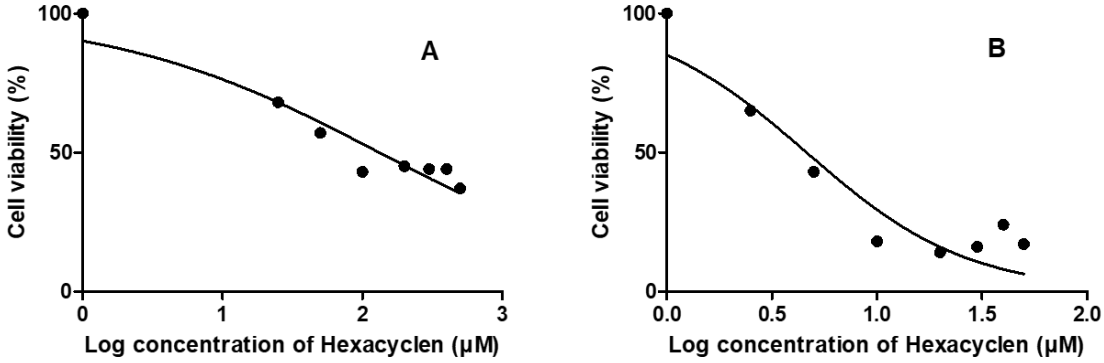

Figure 4.1: A dose-dependent curve showing a decline in cell viability in Hek293 (**A**) and Caco2 (**B**) cells after 48 hours of treatment with a varying concentration range of Hexacyclen.

4.1.2 ATP production

The luminometric CellTiter-Glo® quantified intracellular concentrations of ATP in Hek293 and Caco2 cells. The ATP levels in Hek293 cells (Figure 4.2A) were decreased to 0.66-fold and 0.50-fold for IC_{20} (11470000± 88190 RLU ; p = 0.0032) and IC_{50} (8631000±65940; p = 0.0014) respectively, in relation to the control (17270000±318000 RLU). In Caco2 cells, the ATP concentration decreased from 2133000±274500 RLU in the control to 1883000±85980 RLU in IC_{20}-treated cells. A decrease to 0.39-fold of the control was observed in IC_{50}-treated Caco2 cells (821700±193600 RLU) (Figure 4.2B).

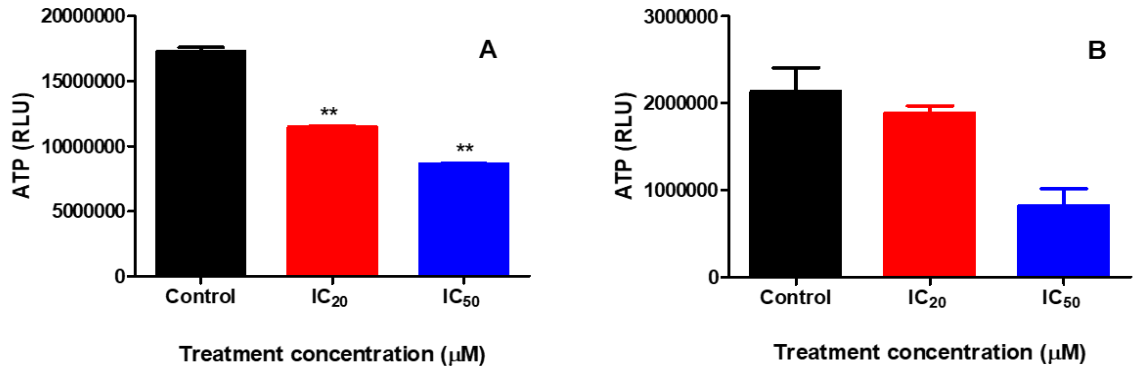

Figure 4.2: (A) A significant decrease ATP concentration in Hek293 cells treated with IC_{20} and IC_{50} (**p = 0.0032, **p = 0.0014; using the unpaired t-test with Welch's correction). **(B)** A non-significant decrease in ATP concentration was detected in Caco2 cells.

4.1.3 JC-10 Mitochondrial Membrane Potential Assay

The ΔΨM changes in Hek293 and Caco2 cells were detected using the JC-10 dye. The ΔΨM of Hek293 cells was decreased by the IC_{20} (0.05283±0.0009528 RLU; p = 0.0166) and IC_{50} (0.04533±0.0007219 RLU; p = 0.0012) treatments to 0.89- and 0.77-fold in relation to the control (0.0591±0.0008660 RLU), respectively (Figure 4.3A). The IC_{20} (0.06257±0.001848 RLU) and IC_{50} (0.06187±0.0002603 RLU) Hexacyclen treatments did not significantly decrease the ΔΨM of Caco2 cells relative to the untreated control (0.0656±0.0001732 RLU); ΔΨM decreased to 0.95-fold and 0.94-fold of the control respectively (Figure 4.3B).

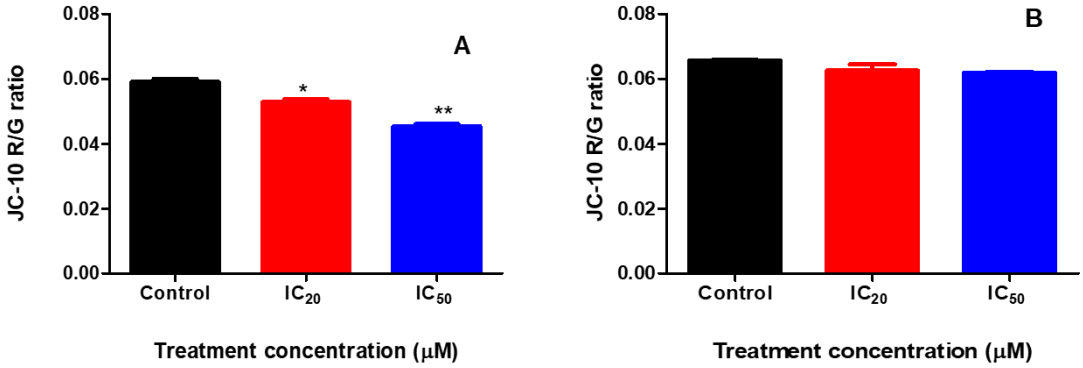

Figure 4.3: (A) The ΔΨM was significantly decreased in Hek293 cells (*p = 0.0166, **p = 0.0012, using the unpaired t-test with Welch's correction) after 48-hour exposure. **(B)** The IC_{20} and IC_{50} treatments maintained ΔΨM of Caco2 cells similar to the control.

4.2 OXIDATIVE STRESS

4.2.1 Production of RNS

The presence of RNS was identified by indirect measurement of nitrate and nitrite levels to quantify nitric oxide using the NOS assay. When related to control (4.457±0.1883 µM), the extracellular levels of RNS in Hek293 cells were elevated non-significantly to 1.07-fold of the control by the IC_{20} treatment (4.783±0.0000001947 µM; p = 0.2254), while RNS were increased significantly to 1.29-fold by IC_{50} treatment (5.761±0.06276 µM; p = 0.0224) (Figure 4.4A). The RNS were minimally increased in Caco2 cells from the control (3.696± 0.2510µM) to 4.022±0.06276 µM (p = 0.3347) and 4.565±0.2510 µM (p = 0.0917), representing 1.09-fold and 1.24-fold increases for the IC_{20} and IC_{50} treatments, respectively (Figure 4.4B).

Western blotting was used to determine the effects of Hexacyclen on protein expression of iNOS. The IC_{20} (0.6646±0.04136 RBD, p = 0.3900) and IC_{50} (0.8187±0.1103 RBD, p = 0.2121) treatments induced non-significant 1.11 and 1.37-fold increase in protein expression of iNOS in comparison to the control (0.5990±0.05076 RBD) in Hek293 cells (Figure 4.4C). The recorded protein expression of iNOS in the control Caco2 cells was 0.6119±0.03405 RBD. The IC_{20} treatment non-significantly increased iNOS expression by 1.17-fold to 0.7164±0.03713 RBD (p = 0.1296), while the IC_{50} caused a significant 1.62-fold increase to 0.9897±0.01525 RBD (p = 0.0096) in Hexacyclen-treated Caco2 cells (Figure 4.3D).

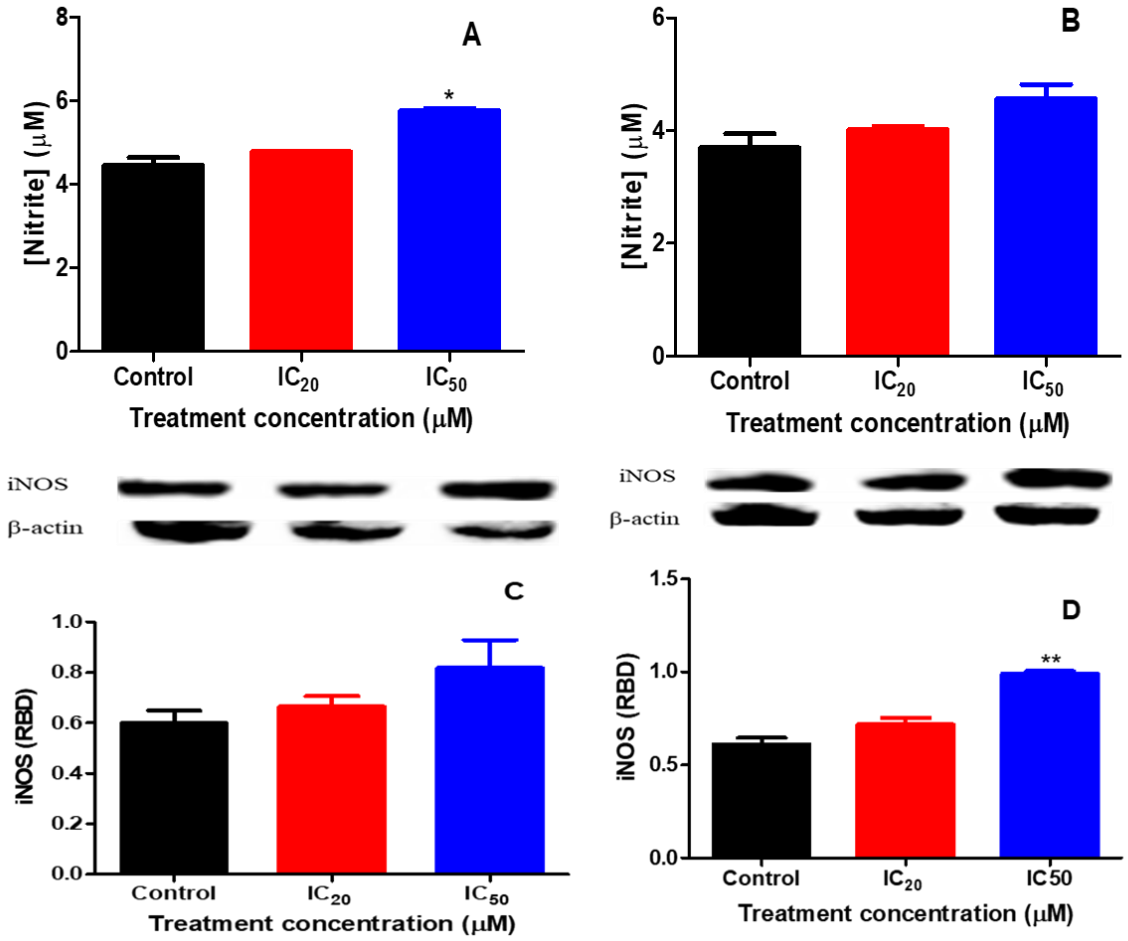

Figure 4.4: The IC_{20} induced a non-significant increase while the IC_{50} caused a significant elevation in RNS **(A)**, whereas iNOS expression was increased non-significantly for both t reatments in Hek293 cells **(C)**. The RNS were non-significantly increased **(B)**, while iNOS expression was upregulated significantly by the IC_{50} in Caco2 treated cells **(D)** (**p* = 0.0224, ***p* = 0.2121, using the unpaired *t*-test with Welch's correction).

4.2.2 ROS and the antioxidant response

4.2.2.1 The MDA levels and SOD2 expression

The MDA levels were measured to quantify ROS as an indicator of lipid peroxidation using the TBARS assay. Hexacyclen induced a non-significant reduction of ROS in Hek293 cells to 0.78-fold (0.1058±0.003205, *p* = 0.1562) and 0.81-fold (0.1047±0.004274 µM; *p* = 0.1548) of the control (0.1261 ± 0.008547 µM) for the IC_{20} and IC_{50} respectively (Figure 4.5A). Slight 1.11- and 1.05-fold increase in ROS was triggered by the IC_{20} (0.1111±0.007704 µM; *p* =

0.3450) and IC_{50} (0.1090±0.003701 µM; p = 0.2952) Hexacyclen treatments in relation to the control (0.1004±0.005653 µM) as observed in Caco2 cells after 48 hour (Figure 4.5B).

Protein expression of SOD2 was significantly upregulated in Hek293 cells from 1.831±0.03548 RBD in the control to 2.988±0.05259 µM (1.63-fold, p = 0.0004) and 4.648±0.2788 µM (2.54-fold, p = 0.0098) for the IC_{20} and IC_{50} Hexacyclen treatments respectively (Figure 4.5C). Meanwhile, minimal increase in SOD2 protein expression to 1.04-fold and 1.11-fold of the control (2.755±0.08766 RBD) was noted for the IC_{20} (2.860±0.01316 RBD; p = 0.3574) and IC_{50} (3.063±0.07069 RBD; p = 0.0716) Hexacyclen treatments in Caco2 cells (Figure 4.5D).

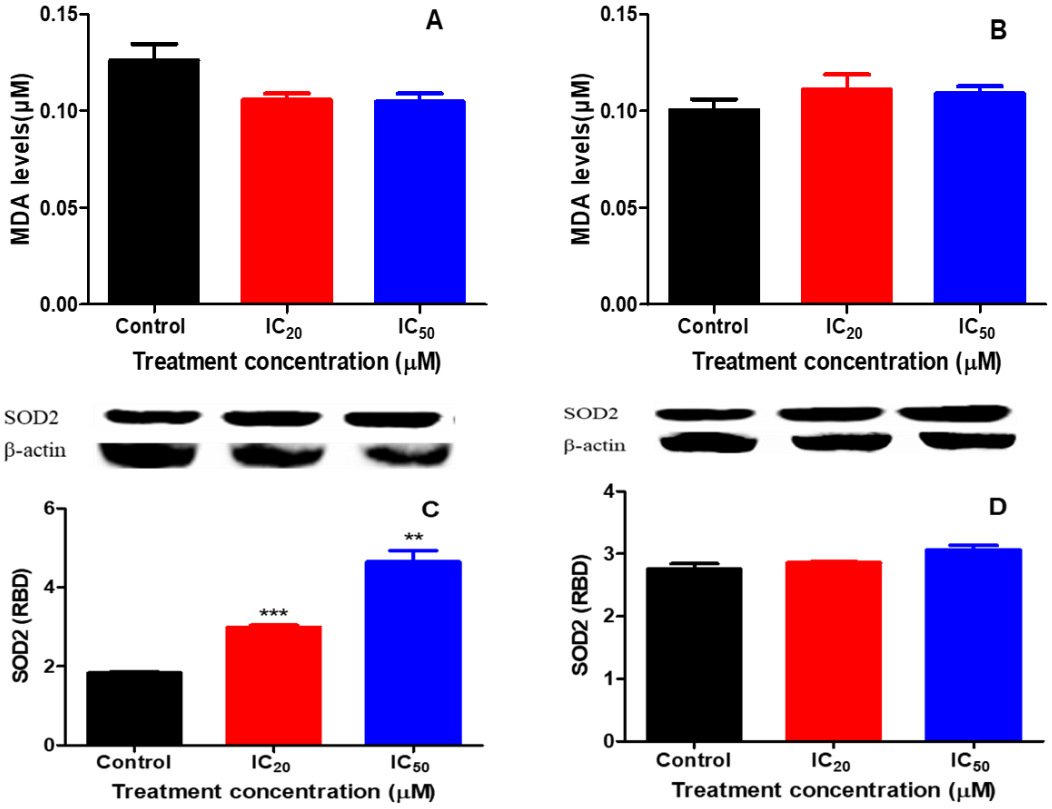

Figure 4.5: The MDA levels were non-significantly decreased in Hek293 cells **(A)**, but slightly increased in Caco2 cells (**B**). Protein expression of SOD2 was significantly upregulated in Hek293 cells (**p < 0.005, using the unpaired t-test with Welch's correction) (**C**) and non-significantly increased in Caco2 cells following a 48-hour treatment (**D**).

4.2.2.2 GSH and GPx-1 antioxidants

The GSH levels were quantified to measure the antioxidant response to the presence of oxidative stress. In Hek293 cells, the quantity of GSH was increased by the IC_{20} and IC_{50}

treatment concentrations to 96160±10860 RLU (p = 0.5714) and 128000±4467 RLU (p = 0.0129), representing a 1.08- and 1.44-fold change respectively, when compared to the untreated control (88870±308.6 RLU) (Figure 4.6A). In the IC_{20} treatment, Caco2 cells increased GSH levels 1.11-fold to 237700±10960 RLU (p = 0.1801), whereas a significant 3.39-fold increase in GSH was noted for the IC_{50} treatment (729800±42440 RLU, p = 0.0067) compared to the control (215000±2087 RLU) (Figure 4.6B).

A significant 2.83- and 4.46-fold elevation in GPx-1 protein expression was induced in Hek293 cells by the IC_{20} (1.665±0.05984 RBD, p = 0.0016) and IC_{50} (2.628±0.1621 RBD, p = 0.0077) Hexacyclen treatment, when compared to the control (0.5887±0.07808 RBD) (Figure 4.6C). However, the IC_{20} (2.476±0.08291 RBD, p = 0.0718) induced a non-significant 1.16-fold upregulation of GPx-1 protein expression in Caco2 cells, while the IC_{50} (2.886±0.1592 RBD, p = 0.0268) triggered a significant 1.35-fold increase from 2.139±0.09118 RBD in the control (Figure 4.6D).

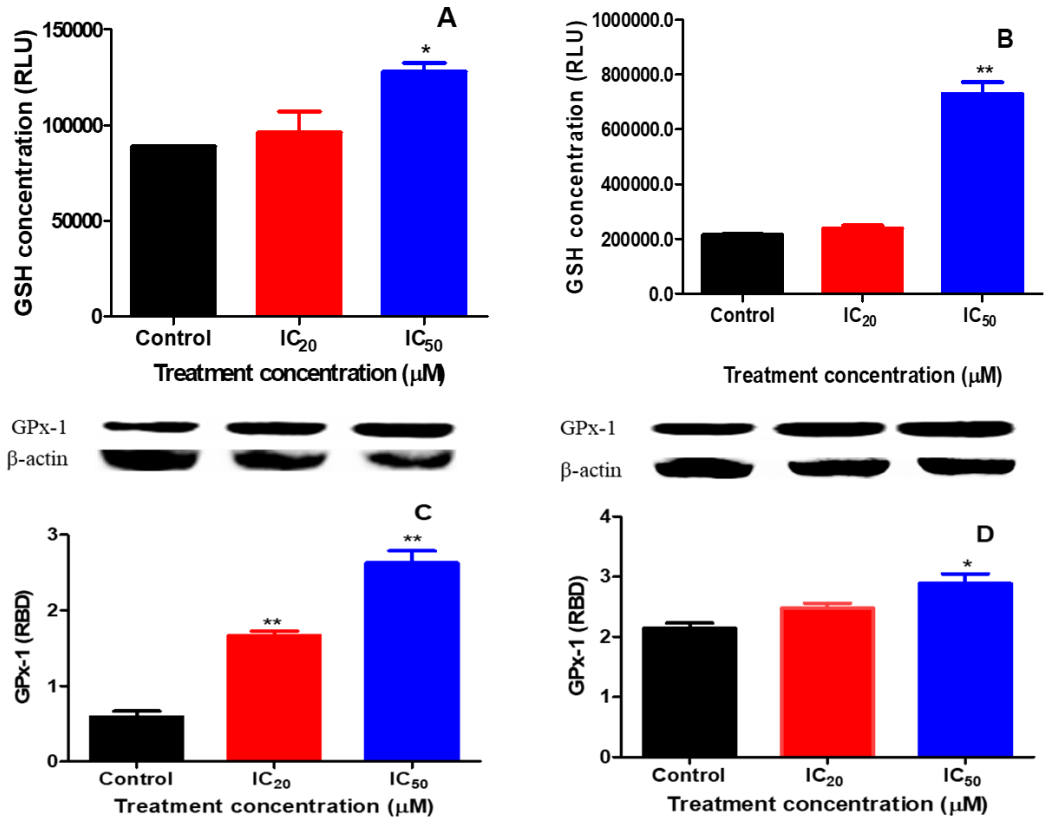

Figure 4.6: (A) The GSH levels were increased by the IC_{20} and IC_{50} treatments in Hek293 cells (**p* = 0.0129). **(B)** The IC_{20} induced a non-significant increase, while the IC_{50} caused a significant elevation in GSH levels in Caco2 cells (***p* = 0.0129). **(C)** The GPx-1 expression was significantly increased by both treatments in Hek293 cells (***p* = 0.0016 and ***p* = 0.0077 for the IC_{20} and IC_{50} respectively) after 48-hour exposure. **(D)** An IC_{20} treatment non-significantly increased GPx-1 activity in Caco2 cells, while the IC_{50} produced a significant increase (**p* = 0.0567). *, ** - unpaired *t*-test with Welch's correction.

4.2.2.3 Catalase activity

In Hek293 cells, catalase protein expression in the IC_{20} (1.366±0.07263 RBD; *p* = 0.8862) was similar to the control (1.338±0.1616 RBD), but decreased non-significantly to 0.64-fold of the control for the IC_{50} treatment (0.8552±0.1264 RBD; *p* = 0.1002) (Figure 4.7A). Hexacyclen downregulated catalase protein expression by 0.59-fold (0.6326±0.08384 RBD; *p* = 0.0742) and 0.46-fold (0.4888±0.04085 RBD; *p* = 0.0567) for the IC_{20} and IC_{50} respectively, compared to the control (1.068±0.1381 RBD) (Figure 4.7B).

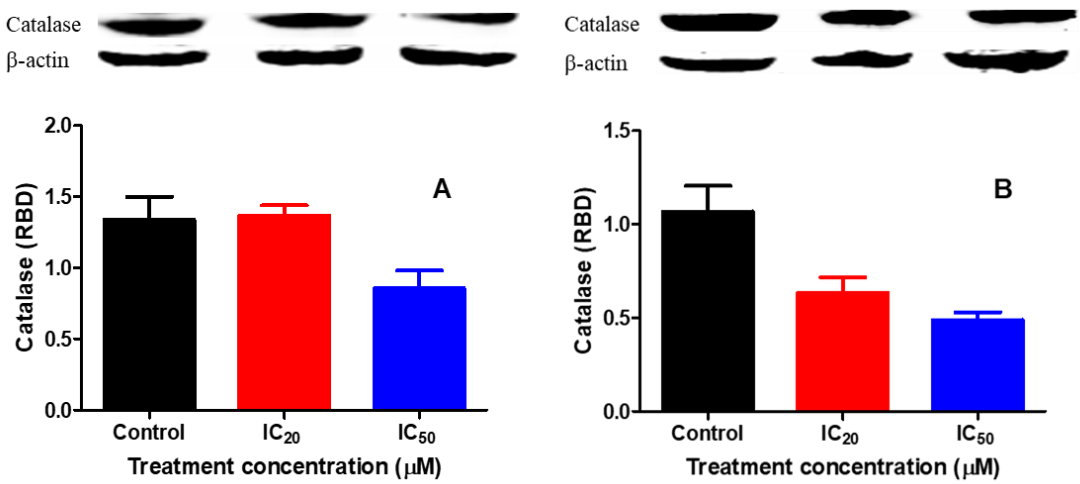

Figure 4.7: (**A**) While catalase the same in IC_{20} treated Hek293 cells, it was non-significantly decreased by the IC_{50} treatment in comparison to the untreated control. (**B**) Catalase was non-significantly downregulated in Caco2 cells.

4.3 CELL DEATH

4.3.1 Initiation of apoptosis

4.3.1.1 Initiator caspases

The initiation of apoptosis through the extrinsic (caspase-8 activity) and intrinsic (caspase-9 activity) pathways was assessed. Following treatment, the activity of caspase-8 in Hek293 cells was significantly reduced to 0.67-fold and 0.48-fold in the IC_{20} (5683000±15460 RLU; p = 0.0129) and IC_{50} treatments (4090000±297800 RLU; p = 0.0021) respectively, in comparison to the control (8459000±317800 RLU) (Figure 4.8A). In contrast, the IC_{20} and IC_{50} Hexacyclen treatments caused a significant 1.25-fold and 1.34-fold elevation to 3739000±108100 RLU (p = 0.0213) and 3971000±76440 RLU (p = 0.0070) respectively, compared to 2974000±34570 RLU in the Caco2 control cells (Figure 4.8B). Results indicated a slight 1.09-fold increase in caspase 9 activity induced by IC_{20} (8419000±411800 RLU; p = 0.2345) and a significant 1.16-fold increase induced by IC_{50} (8923000±17400 RLU; $p < 0.0001$) Hexacyclen treatment in comparison to the control (7725000±15430 RLU) in Hek293 cells (Figure 4.8C). Furthermore, caspase 9 activity was elevated 1.53-fold and 1.19-fold by IC_{20} (7229000±1141000; p = 0.3538) and IC_{50} (5638000±40240 RLU; p = 0.5453) treatments respectively, compared to the control (4711000±1069000 RLU) in Caco2 cells (Figure 4.8D).

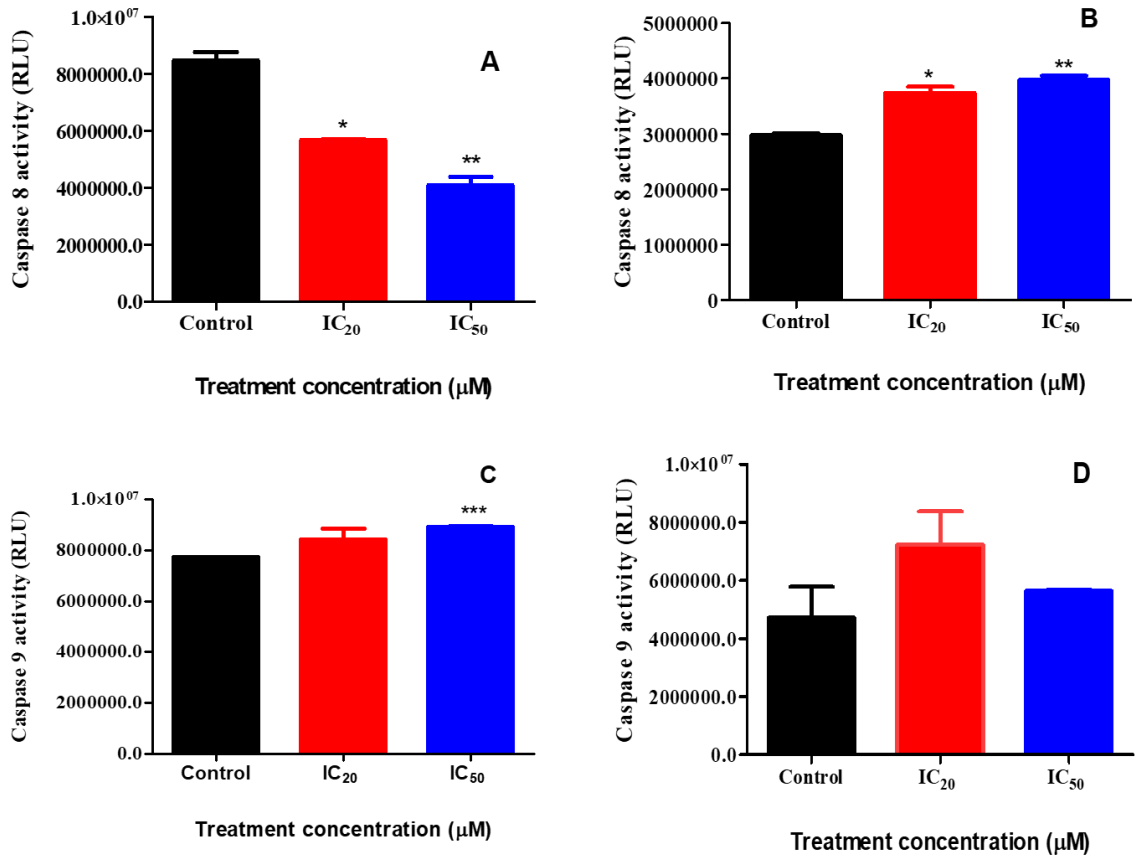

Figure 4.8: The activity of caspase 8 was significantly reduced in Hek293 for the IC_{20} (*p = 0.0129) and IC_{50} (**p = 0.0021) Hexacyclen treatments (**A**), while it was significantly increased in Caco2 cells (*p = 0.0213; **p = 0.0070) (**B**) after 48-hours of treatment. Hexacyclen treatment slightly increased the activity of caspase-9 in Hek293 cells (IC_{50}, ***p < 0.0001) (**C**). Furthermore, caspase 9 activity was elevated non-significantly by IC_{20} and IC_{50} treatments in Caco2 cells exposed to Hexacyclen for 48-hours (**D**). *, ** - unpaired *t*-test with Welch's correction).

4.3.1.2 p-p53 pro-apoptotic protein

Western blotting was used to determine the effects of Hexacyclen on protein expression of p-p53. Figure 4.9A shows that the p-p53 protein expression in Hek293 cells was similar to the control at the IC_{20} (2.450±0.07415 RBD vs. control: 2.523±0.04203 RBD, p = 0.4588), but a significant decrease to 0.48-fold of the control was observed at the IC_{50} (1.223±0.1598 RBD, p = 0.0158). Similarly, no effect was induced by Hexacyclen in the IC_{20}-treated Caco2 cells (2.183±0.03289 RBD vs. control: 2.107±0.1831 RBD, p = 0.7209) treatment, while the IC_{50} significantly reduced the activity of p-p53 to 0.37-fold (0.7834±0.07255 RBD, p = 0.0214) compared to control Caco2 cells (Figure 4.9B).

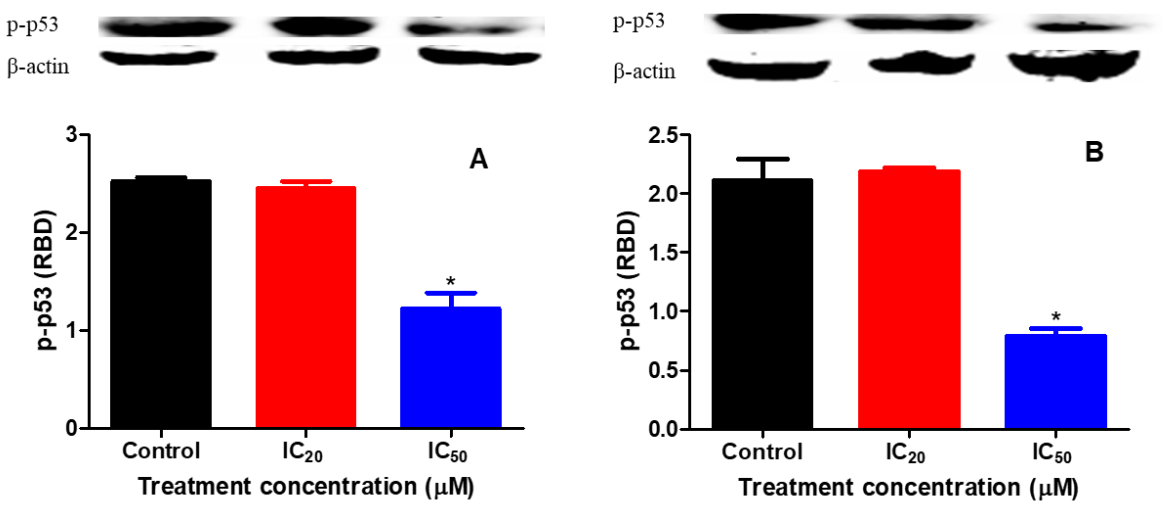

Figure 4.9: (**A**) Hexacyclen induced a non-significant decrease in p-p53 expression of Hek293 cells at the IC_{20}, and a significant downregulation at the IC_{50} (**p* = 0.0158). (**B**) No effect was detected for the IC_{20} treatment, while the IC_{50} significantly reduced the activity of p-p53 in Caco2 cells (**p* = 0.0214). * - unpaired *t*-test with Welch's correction.

4.3.1.3 Bcl-2 and HSP70 anti-apoptotic proteins

Western blotting was used to measure the expression of Bcl-2 and HSP70 anti-apoptotic proteins. Both treatments significantly downregulated Bcl-2 protein expression in Hek293 (Figure 4.10A) and Caco2 cells (Figure 4.10B). In Hek293 cells, the Bcl-2 protein expression was downregulated to 0.71-fold (1.658±0.08550 RBD, p = 0.0151) and 0.73-fold (1.709±0.09449 RBD, p = 0.0211) of control levels (2.332±0.1031 RBD) respectively. Similarly, Bcl-2 was decreased from 2.438±0.09669 RBD in the control to 1.596±0.05695 RBD (0.67-fold, p = 0.0049) and 1.629±0.05906 RBD (0.65-fold, p = 0.0057) in Caco2 cells.

Furthermore, the activity of HSP70 protein was also decreased by both treatments in Hek293 (Figure 4.10C) and Caco2 (Figure 4.10D) cells respectively. A non-significant decrease to 0.78-fold (1.242±0.02898 RBD; p = 0.0575) and 0.79-fold (1.265±0.06860 RBD; p = 0.0551) for observed for IC_{20}- and IC_{50}-treated Hek293 cells, in relation to the control (1.597 ± 0.08425 RBD). When compared to the control (1.287±0.02898 RBD), significant reduction in HSP70 protein expression to 0.79-fold (1.010±0.01584 RBD; p = 0.0036) and 0.71-fold

(0.9100±0.006852 RBD; p = 0.0062) was detected in Caco2 cells for the IC_{20} and IC_{50} treatments respectively.

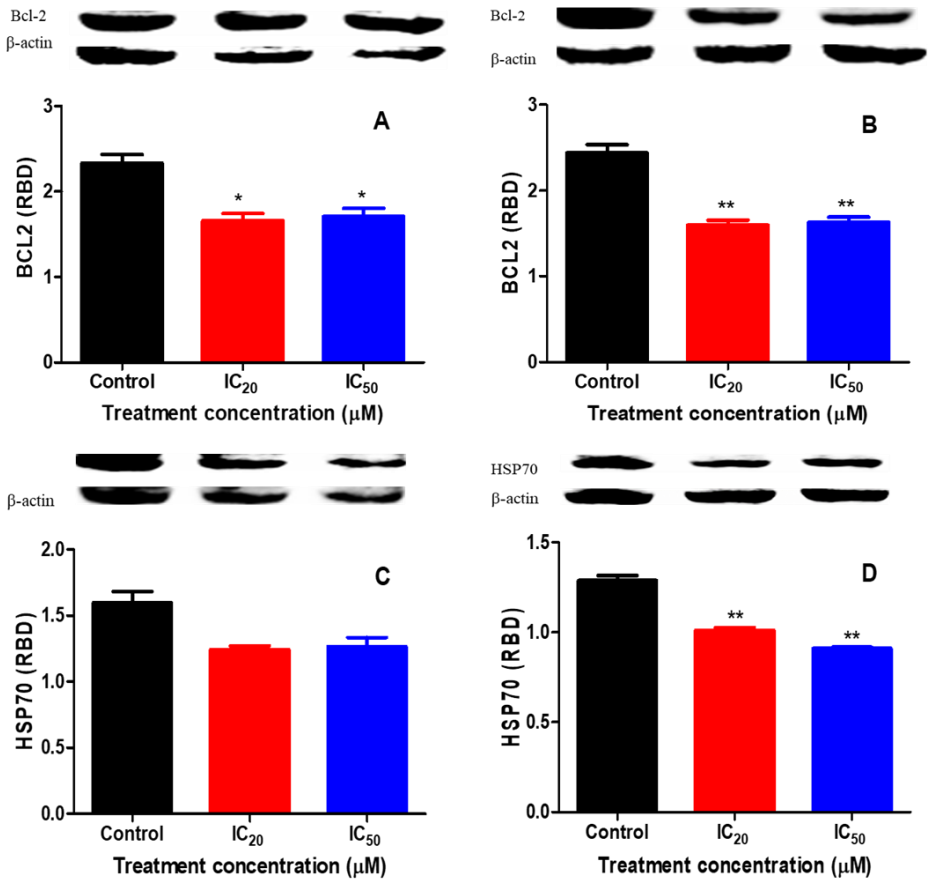

Figure 4.10: Bcl-2 expression was downregulated significantly was in both Hek293 and Caco2 cells (*p = 0.0151 and *p = 0.0211, and **p = 0.0049 and **p = 0.0057, respectively) (**A** and **B**). The activity of HSP70 protein non-significantly decreased in Hek293 cells, whereas it was significantly reduced in Caco2 cells (**p = 0.0575; **p = 0.0551) (**C** and **D**). *, ** - unpaired *t*-test with Welch's correction.

4.3.2 Execution of apoptosis

4.3.2.1 Caspase activation

The execution of apoptosis was assessed by quantifying the activity of the executor caspase 3/7. Caspase 3/7 activity was increased to 1.15- and 3.64-fold in treated Hek293cells at IC_{20} (1649000±31920 RLU; p = 0.1784) and IC_{50} (5209000±176700 RLU; p = 0.0003) respectively, in relation to the control (1430000±102600 RLU) (Figure 4.11A). Moreover, the IC_{20} resulted in a significant increase to 1.49-fold (2183000±138300 RLU; p = 0.0414) and the IC_{50} to 1.66-

fold (2445000±104100 RLU; p = 0.0038) in comparison to the control Caco2 cells (1469000±57830 RLU) (Figure 4.11B).

Protein expression of PARP and cleaved PARP were analysed to determine the PARP/cPARP ratio; similar PARP/cPARP ratio was detected for IC_{20}-treated Hek293 (1.674±0.06152 RBD, p = 0.9830) and Caco2 (0.6574±0.008394 RBD, p = 0.7887) cells compared to their respective controls (1.677±0.07006 and 0.6625±0.01549 RBD, respectively). However, the IC_{50} caused a significant decrease to 0.19-fold of the control in the PARP/cPARP ratio in Hek293 cells (0.3257±0.03742, p = 0.0374), and to 0.67-fold of the control in Caco2 cells (0.4448±0.01486 RBD, p = 0.0020) (Figure 4.11C and D).

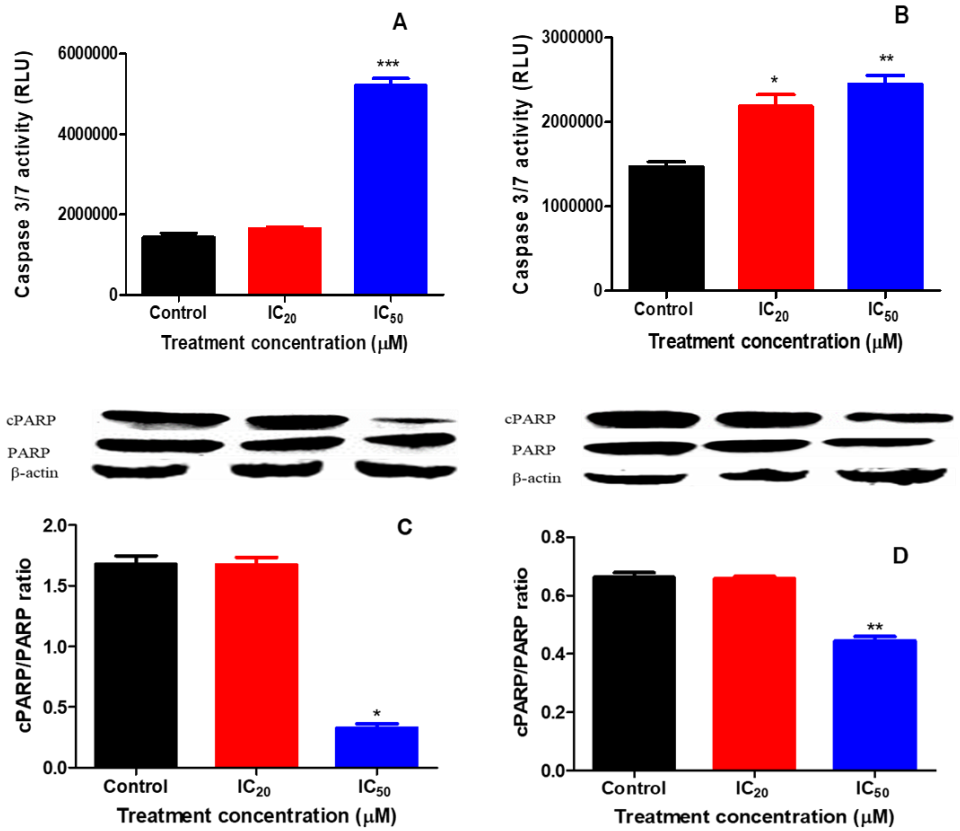

Figure 4.11: (**A**) Caspase 3/7 activity in Hek293 cells was increased non-significantly by the IC_{20} treatment and significantly increased by the IC_{50} treatment (***p = 0.0003). Furthermore, the treatments significantly increased the activity of caspase 3/7 in Caco2 cells after 48-hour exposure (*p = 0.0414; **p = 0.0038) (**B**). No effect was induced by the IC_{20} in both cell lines, while the IC_{50} significantly reduced the cPARP/PARP ratio in treated Hek293 and Caco2 cells (**C** and **D**) (*p = 0.0374, **p = 0.0020). *, ** - unpaired t-test with Welch's correction.

4.3.2.2 Apoptosis markers

The annexin V assay detected PS externalisation as an early apoptosis marker. The externalised PS was similar to the control for the IC_{20} (482000±26440, p = 0.9768), and significantly elevated 4.51-fold for the IC_{50} (2143000±77380, p = 0.0177) when compared to the control (475100±210900 RLU) in Hek293 cells (Figure 4.12A). However, the IC_{20} and IC_{50} treatments non-significantly increased PS from 27830±3930 RLU in the control to 28980±374.0 (1.04-fold, p = 0.7969) and 39080±4195 (1.40-fold, p = 0.1452) respectively in Caco2 cells (Figure 4.12B).

The LDH assay was used to determine possible membrane damage by measuring the extracellular LDH leakage from the cytoplasm. The IC_{20} and IC_{50} Hexacyclen treatments significantly increased the extracellular levels of LDH in Hek293 cells from 0.0890±0.005196 OD in the control to 0.1230±0.002887 OD (1.38-fold, p = 0.0106) and 0.3270±0.03349 OD (3.67-fold, p = 0.0197), respectively (Figure 4.12C). The IC_{20} treatment non-significantly decreased the extracellular levels of LDH to 0.81-fold (0.1767±0.005487 OD, p = 0.1228) compared to the control (0.2187±0.01530 OD), in contrast to the IC_{50} treatment that non-significantly increased extracellular LDH to 1.23-fold (0.2687±0.01588 OD, p = 0.1082) in comparison to the control Caco2 cells (Figure 4.12D).

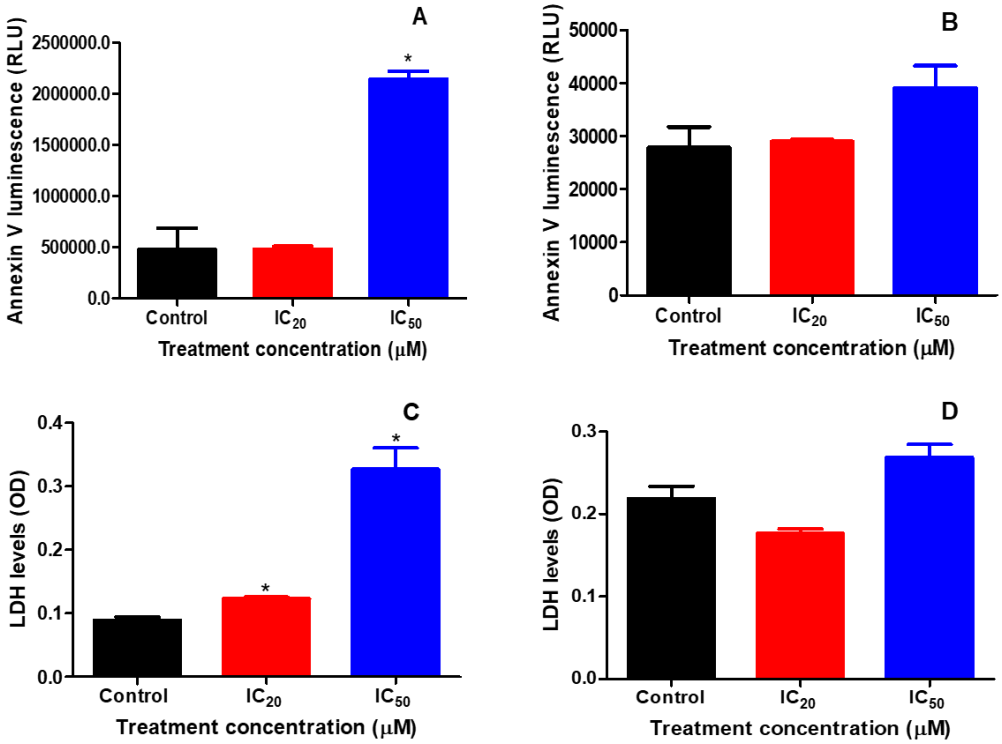

Figure 4.12: The externalised phosphatidylserine was non-significantly increased by the IC_{20} and significantly increased by the IC_{50} Hexacyclen treatment in Hek293 cells (*p = 0.0177) **(A)**, whereas it was non-significantly increased in Caco2 cells after 48-hours of exposure **(B)**. The extracellular levels of LDH were significantly increased after IC_{20} and IC_{50} Hexacyclen treatment of Hek293 cells (*p < 0.05) **(C)**, while a non-significant decrease and non-significant increase was observed for the IC_{20}- and IC_{50}-treated Caco2 cells **(D)**. * - unpaired *t*-test with Welch's correction.

4.4 INFLAMMATION

The expression of NF-κB, STAT3 and p-STAT3 proteins, which are involved in cell survival pathways, was determined by the western blotting. In Figure 4.13A, the protein expression of NF-κB was minimally decreased to 0.91-fold of the control at the IC_{20} (0.7317±0.01755 RBD, p = 0.3013) in Hek293 cells after 48hrs exposure to Hexacyclen, while a significant decrease from 0.7998±0.04607 RBD in the control to 0.3147 ± 0.03430 RBD (0.39-fold, p = 0.0035) was induced by the IC_{50} treatment. In Caco2 cells, a significant decrease to 0.39- and 0.55-fold was induced by the IC_{20} (0.1750±0.008183 RBD; p = 0.0351) and IC_{50} (0.2466±0.03631 RBD; p = 0.0497) respectively, compared to the control (0.4490±0.05206 RBD) (Figure 4.13B).

When compared to the control (0.2120±0.02027), the p-STAT3/STAT3 ratio was significantly decreased at the IC_{20} (0.1054±0.01602, p = 0.0258) and IC_{50} (0.03587±0.004986, p = 0.0137),

representing a 0.50- and 0.17-fold decrease, respectively (Figure 4.13C). However, p-STAT3/STAT3 ratio in Caco2 cells was decreased to 0.86- and 0.38-fold at IC_{20} (0.1176±0.01080, p = 0.6158) and IC_{50} (0.05180±0.004760, p = 0.0307) respectively (Figure 4.13D).

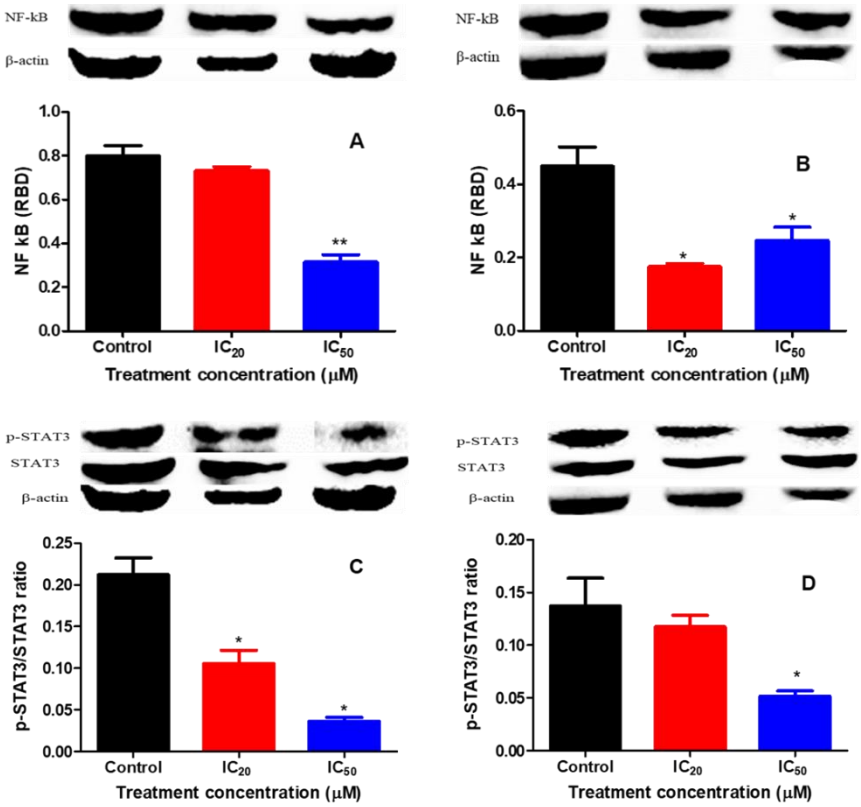

Figure 4.13: (A) A non-significant (IC_{20}) and significant (IC_{50}, **p = 0.0035) decrease in NF-κB activity was observed in Hek293 cells. **(B)** There was a significant decrease in NF-κB detected in Caco2 cells for the IC_{20} and IC_{50} Hexacyclen treatments after 48-hours of exposure (*p = 0.0351 and *p = 0.0497 respectively). **(C)** The p-STAT3/STAT3 ratio was significantly decreased in Hek293 cells (*p = 0.0258, *p = 0.0137). **(D)** Hexacyclen slightly decreased the p-STAT3/STAT3 ratio at the IC_{20}, but significant reduction was observed for IC_{50}-treated Caco2 cells (*p = 0.0307). *, ** - unpaired t-test with Welch's correction).

CHAPTER 5 : DISCUSSION

Cancer is fast becoming a global healthcare and economic burden, affecting both developing and first-world countries. Hepatocellular carcinoma (HCC) and colorectal cancers (CRC) are major contributors to the incidence and mortality rate of cancer (Sung *et al.*, 2021). Current cancer therapeutics such as chemotherapeutic drugs, surgery and radiation have gained a negative reputation due to their excessive cost, limited accessibility and invasiveness (Heidari-Soreshjani *et al.*, 2017, Barnett and Cummings, 2018). It has also been noted that anticancer drugs cause nephrotoxicity, which contributes to approximately 60% of acute renal injuries. Therefore, it is important to study the effect of anticancer drugs in normal kidney cells. Recent studies have shown interest in anticancer drugs that inhibit pathways that drive the onset and development of carcinogenesis, including anticancer agents that are considered potent metal ion chelators (Gaur *et al.*, 2018, Kontoghiorghes and Kontoghiorghe, 2020). One such cancer therapeutic drug is Hexacyclen, a nitrogen-electron donor that favours the formation of complexes with cations and can bind the different metal and transition metal cations (El-Hashani *et al.*, 2007, Austin and Rodgers, 2014). To date, this is the first study to investigate the biochemical effects underlying the mechanism of Hexacyclen on human -derived colorectal adenocarcinoma cells (Caco2) and normal embryonic kidney cells (Hek293) after 48-hour exposure.

In this study, the MTT assay assessed the cell viability of metabolically active cells exposed to Hexacyclen. Hexacyclen induced a dose-dependent decline in cell viability in both cell lines (Figure 4.1A and B), indicating that the reduction of the MTT salt by succinate dehydrogenase (SDH) was decreased (Bahuguna *et al.*, 2017). The enzyme SDH contributes to the electron transport chain (ETC) by transferring electrons from $FADH_2$ to complex III while catalysing the oxidation of succinate to fumarate (Huang and Millar, 2013, Zhao *et al.*, 2019, Moosavi *et al.*, 2020). The enzyme SDH has iron-sulfur centres and inhibition of SDH by Fe^{2+}chelation has been reported in other studies (Kim and Moon, 2012, Kontoghiorghes and Kontoghiorghe, 2020). Thus, Hexacyclen-induced inhibition of SDH via chelation may be the possible cause of reduced cell viability. Interestingly, 18-crown-6, an analogue of Hexacyclen, demonstrated a similar cytotoxic effect against the WI38 cells, where a dose-dependent reduction in cell viability was observed (Boojar and Goodarzi, 2006a). Furthermore, Hexacyclen homologue

1,4,7-Triazacyclononane (TACN) triggered a decline in cell viability in HepG2 and Hek293 cells (Mcoyi *et al.*, 2020, Tsotetsi *et al.*, 2020).

The possible inhibition of SDH by Hexacyclen could disrupt ATP production, thus impacting the ability of cells to carry out vital cellular processes necessary for survival. The results from this study showed that both the IC_{20} and IC_{50} (Figure 4.2A and B) had considerably lower intracellular levels of ATP after being treated with Hexacyclen. It is well established that two components, the proton gradient and mitochondrial membrane potential ($\Delta\Psi M$), are essential for ATP synthesis through oxidative phosphorylation (OXPHOS) in the mitochondria (Zhao *et al.*, 2019). The proton gradient is generated by the transfer of electrons from NADH to complexes I, III and IV of the ETC (Zhao *et al.*, 2019). Subsequently, ATP is produced when adenosine diphosphate (ADP) is phosphorylated by ATP synthetase at complex V (Vakifahmetoglu-Norberg *et al.*, 2017). Enzymes catalysing complexes I, III and IV contain iron-sulphur (Fe-S) clusters. Since Hexacyclen is a Fe^{2+} chelator, it likely chelated Fe^{2+} in these complexes (I, III, IV) leading to impaired proton gradient formation by the ETC and resulting in reduced ATP production (El-Hashani *et al.*, 2007). These findings are consistent with the study carried out by Zhang (2019), who reported that chelating Fe^{2+} from complex I with deferoxamine (DFO), a known hexadentate iron chelator, suppressed the ETC of osteoclast precursors *in vitro* (Zhang *et al.*, 2019).

Overall, the depletion of the ATP (Figure 4.2) is consistent with the dying of cells observed (Figure 4.1), thus validating the disturbance in the appropriate functioning of mitochondria, the cellular organelle responsible for ATP production. Indeed, decreased ATP production is associated with reduced $\Delta\Psi M$; the $\Delta\Psi M$ is produced by the proton pumps of complexes I, III and IV which also contribute to the production of ATP (Zorova *et al.*, 2018). With the exception of the Caco2 IC_{20} treatment, this study showed that the $\Delta\Psi M$ was significantly reduced by the Hexacyclen treatments (Figure 4.3A and B), indicating that the ETC was hampered, resulting in proton gradient disruption and electron leakage (Adwas *et al.*, 2019).

Disruption of the ETC and the leakage of electrons at complex I and complex III form superoxide ($O_2^{\bullet}$), the first ROS formed via oxygen reduction (Adwas *et al.*, 2019). Under normal circumstances, the ROS are formed to act as secondary messengers in signalling cascades, which is vital for the normal physiological functions of the cell (Sies, 2015). The $O_2^{\bullet}$ produced by mitochondria is transformed into hydrogen peroxide (H_2O_2) by SOD2 (Ighodaro

and Akinloye, 2018). In this study, upregulated protein expression of SOD2 in Hek293 and Caco2 cells (Figure 4.5C and D) may be attributed to increased $O_2^{\bullet}$. Similar induction of SOD2 was induced in HepG2 cells by the metal chelator TACN (Mcoyi *et al.*, 2020). The consequent increase in H_2O_2 in the presence of increased SOD2 is toxic to somatic cells and leads to the formation of hydroxyl radicals ($^{\bullet}OH$) via the Fenton reaction. The $^{\bullet}OH$ can oxidise biomolecules including the membrane, proteins and DNA and cause oxidative stress (Jat and Nahar, 2017).

Excess $O_2^{\bullet}$ may also contribute to reactive nitrogen species (RNS) formation by reacting with nitric oxide (NO) to produce peroxynitrite ($ONOO^-$). In this study, NO concentration was increased in both Hek293 and Caco2 cells (Figure 4.4A and B). The NO is produced by inducible NOS (iNOS) in the presence of L-arginine, O_2 and NADPH as co-substrate (Förstermann and Sessa, 2012). Thus, NO elevation is due to increased protein expression of iNOS in both Hek239 and Caco2 cells (Figure 4.4C and D). The enzyme iNOS is a heme-Fe^{3+} protein with N-terminal oxygenase and C-terminal reductase, with a flavin mononucleotide (FMN) binding subdomain (Cinelli *et al.*, 2020). The FMN domain contributes to the conversion of heme iron from iron (III) to iron (II), thus recruiting and activating molecular oxygen to form a Fe^{3+}-NO complex (Campbell *et al.*, 2014, Cinelli *et al.*, 2020). Moreover, it is reported that iron (III) prefers reacting with oxygen rather than nitrogen (Sánchez *et al.*, 2017). Since Hexacyclen is a nitrogen compound, it is possible that Fe^{3+} chelation in iNOS was not supported. In addition, Hexacyclen is a chelator of divalent metal cations (Varadwaj *et al.*, 2011). Therefore, increased NO (Figure 4.4A and B) and $O_2^{\bullet}$ triggered an increase in $ONOO^-$ (Pfeffer and Singh, 2018). The resultant nitrosative stress is associated with damage of biomolecules including protein oxidation, protein nitration, enzyme inactivation and lipid peroxidation (Radi, 2018, Ighodaro and Akinloye, 2018, Sharifi-Rad *et al.*, 2020).

Lipid peroxidation is one of the most severe side effects of ROS- and RNS-induced cellular damage but can also be induced by RNS. Malondialdehyde (MDA), the by-product of lipid peroxidation, is a well-known indicator of oxidative stress (Alché, 2019). The results of this study indicated that Hexacyclen reduced the MDA levels in Hek293 cells (Figure 4.5A), while MDA levels were not significantly increased in Caco2 cells (Figure 4.5B). The reduction in MDA in Hek293 cells implies that the Fenton reaction was inhibited by Hexacyclen Fe^{2+} chelation. Furthermore, the presence of ROS stimulated antioxidant molecules to prevent cellular damage by detoxifying free radicals (Adwas *et al.*, 2019). Indeed, the H_2O_2 may be

eliminated by the antioxidant enzyme glutathione peroxidase (GPx-1) to H_2O (Ighodaro and Akinloye, 2018, Adwas *et al.*, 2019). Thus, the enhanced activity of GPx-1 (Figure 4.6C and D) in both Hek293 and Caco2 cells contributed to H_2O_2 removal. It is interesting to note that the GPx1 response in Caco2 cells was not as significant as in Hek293 cells (Figure 4.6C and D), and this limited antioxidant response by GPx-1 may account for the differences in MDA levels observed (Figure 4.5A and B).

Another crucial antioxidant is glutathione (GSH) which is used in the reaction catalysed by GPx-1 and is transformed into oxidised glutathione (GSSG) (Adwas *et al.*, 2019). This study showed that Hexacyclen IC_{20} and IC_{50} treatments increased intracellular GSH concentrations in Hek293 cells and Caco2 cells (Figure 4.6A and B). The data suggest that GSH is possibly replenished by glutathione reductase in the presence of NADPH and is thus available to prevent the accumulation of ROS (Figure 4.5B). Alternatively, GPx-1, GSH and SOD2 increases are associated with a transcription factor Nrf2 which is upregulated by oxidative stress to activate the transcription of antioxidants (Khan *et al.*, 2020). Additionally, catalase, a porphyrin heme (iron) containing protein, detoxifies H_2O_2 to O_2 and H_2O (Ighodaro and Akinloye, 2018). It was shown in this study that the downregulation of catalase expression for both IC_{20} and IC_{50} treatments may be attributed to Hexacyclen-Fe^{2+} chelation in Hek293 and Caco2 cells (Figure 4.7A and B). Similarly, TACN downregulated catalase while SOD2, GPx-1 and GSH concentrations were elevated in HepG2 cells (Mcoyi *et al.*, 2020). Furthermore, the study by Boojar and Goodarzi (2006) revealed that 15-crown-5 and 18-crown-6 ether indeed enhanced the activity of SOD2, catalase and GPx-1 antioxidant molecules due to the induced production of ROS within lung tissue (Boojar and Goodarzi, 2006a).

Research shows that ROS, particularly H_2O_2, contributes to NF-κB activation (Lingappan, 2018). Since ROS were not upregulated in this study (Figure 4.5A, B), this could be linked to reduced expression of NF-κB in Hek293 (Figure 4.13A) and Caco2 (Figure 4.13B) cells. NF-κB persistence in the nucleus is reported where it controls the expression of the number of genes linked with proliferation, invasion, angiogenesis and metastasis (Fan *et al.*, 2013). Also, NF-κB promotes cell survival via transcriptional regulation of anti-apoptotic genes, including Bcl-2 and XIAP (Luo *et al.*, 2005, Fan *et al.*, 2013). The decrease in NF-κB could also have contributed to the downregulation of the Bcl-2 protein observed in this study (Figure 4.10A and B). Contrastingly, TACN upregulated NF-κB expression in Hek293 cells, but this was associated with inhibition of apoptosis (Tsotetsi *et al.*, 2020).

Among other functions, NF-κB upregulates the production of major inflammatory factors, such as IL-6 and IL-1β cytokine that activates the STAT3 signalling pathway (Fan *et al.*, 2013). It was therefore not surprising that the protein expression of STAT3 was concurrently decreased in Hek293 and Caco2 cells (Appendix 7). Furthermore, STAT3 was not activated via phosphorylation by JNK2 at Tyr705 (Appendix 7) with a consequently decreased ratio of p-STAT3/STAT3 in both cell lines (Figure 4.13C and D); this phosphorylation is crucial for STAT3 dimerization, nuclear translocation and DNA binding (Lin *et al.*, 2020, Tolomeo and Cascio, 2021). This trend of reduced expression of STAT3, pSTAT3 and p-STAT3/STAT3 has been observed in pancreatic cancer (PANC-1 and MIAPaCa-2) and prostate cancer (DU145) cell lines in response to di-2- pyridylketone-4,4-dimethyl-3-thiosemicarbazone (Dp44mT) and di-2-pyridylketone 4- cyclohexyl-4-methyl-3-thiosemicarbazone (DpC) metal chelators (Lui *et al.*, 2015). Interestingly, p-STAT3 recruits and activates another STAT3 to form a dimer that translocates to the nucleus to control the expression of many genes that inhibit apoptosis including Bcl-xL, survivin and IAPs (Yu *et al.*, 2009, Tolomeo and Cascio, 2021). Therefore, a decrease in active p-STAT3 implies that fewer anti-apoptotic proteins were transcribed. Moreover, NF-κB activity in tumours requires a constitutively activated STAT3 (Yoon *et al.*, 2012), thus a decrease in STAT3 expression may also have resulted in the downregulation of NF-κB (Figure 4.13A and B), and therefore apoptosis was favoured.

Free radicals (ROS and RNS) and oxidative stress are known to activate p53 in physiological settings to aid cell cycle arrest and promote DNA repair and survival (Redza-Dutordoir and Averill-Bates, 2016). The phosphorylated p53 (p-p53) is a stable and active form involved in downstream processes (Phatak and Muller, 2015). Proper functioning and stable p53 require the binding of Zn^{2+} metal ions (Phatak and Muller, 2015). Likely, Zn^{2+} chelation by Hexacyclen could have caused the downregulation of p53 expression (Figure 4.9A and B). Similarly, a decrease in p53 was induced by Di(2-picolyl) amine (DPA) metal chelator in Hek293 cells (Satyo *et al.*, 2020). Nevertheless, when the DNA repair mechanism fails, p53 causes apoptosis by initiating the transcription of pro-apoptosis proteins such as Noxa and Puma; these pro-apoptotic proteins function to inhibit anti-apoptotic proteins like Bcl-2 that obstruct apoptosis (Pfeffer and Singh, 2018, Redza-Dutordoir and Averill-Bates, 2016). In this study, the downregulation of Bcl-2 protein expression (Figure 4.10A and B) implies that its inhibition by pro-apoptotic protein may have occurred. The Bcl-2 protein usually prevents apoptosis via heterodimer formation with Bax and Bak; therefore, downregulation of Bcl-2 suggests an

increase in Bax protein expression (Redza-Dutordoir and Averill-Bates, 2016). Indeed, Hexacyclen downregulation of Bcl-2 prompted significantly increased Bax protein expression in Hek293 cells (Appendix 4). Reduced HSP70 protein expression ensured Bax function was not inhibited since Bax's ability to initiate apoptosis in human cancer cells also requires dimerization and translocation to the mitochondria, which is blocked by HSP70 (Yang *et al.*, 2012, Wang *et al.*, 2014). In this study, Bax-induced MOMP was not impeded due to decreased HSP70 (Figure 4.10C and D). Furthermore, Hexacyclen-induced Zn^{2+} chelation facilitated Bax activation, since Zn^{2+} is an inhibitor of Bax (Ganju and Eastman, 2003, Austin and Rodgers, 2014). This is plausible since Bax upregulation in HCT116 colon cancer cells by N,N,N′,N′-tetrakis(2-pyridinylmethyl)-1,2-ethanediamine (TPEN) metal chelator induced cell death (Fatfat *et al.*, 2014). Activated Bax, together with Bak, causes mitochondria outer membrane permeabilization (MOMP), leading to the release of pro-apoptotic proteins including Smac/Diablo, cytochrome c, endoG and apoptosis-inducing factor (AIF) to the cytosol (Pfeffer and Singh, 2018). In this study, the released cytochrome c recruited procaspase-9 and Apaf-1 to form the apoptosome in the presence of dATP (Lopez and Tait, 2015). Inhibition of apoptosome formation by HSP70 binding to Apaf-1 could not occur due to a decrease in HSP70 (Figure 4.10C and D) and procaspase-9 was cleaved to active caspase-9 (Figure 4.8C and D) (Li *et al.*, 2000, Beere *et al.*, 2000, Wang *et al.*, 2014). This is indicative of increased apoptosis initiation via the mitochondria-dependent apoptotic pathway. Following activation, caspase-9 induces proteolytic cleavage to activate the executor caspase-3/7 (Pfeffer and Singh, 2018).

Elevated caspase 3/7 activity in both cell lines (Figure 4.11A and B) was accomplished via the intrinsic pathway for both cell lines (Figure 4.8C and D) and the extrinsic pathway of apoptosis facilitated by active caspase-8 (Figure 4.8B) for Caco-2 cells. Execution of apoptosis is mediated by active caspase 3/7 through cleavage of CAD, causing DNA fragmentation and/or activating proteins or endonucleases, which degrades nuclear materials and cytoskeleton protein (Pfeffer and Singh, 2018). Caspase-3/7 is also responsible for the cleavage of an ATP-dependent Zn-finger endonuclease called Poly (ADP-ribose) polymerase 1 (PARP-1), which functions to recognize DNA strands breaks and repair the damage (Mashimo *et al.*, 2021). This study indicated that PARP-1 expression was decreased in Hek293 and Caco2 cells (Appendix 6), which may be attributed to Zn-finger chelation by Hexacyclen that results in inactive PARP-1. Similarly, Zn^{2+} chelation from PARP-1 by TPEN and arsenite inhibited its activity in the human keratinocyte cell line (HaCaT) (Sun *et al.*, 2014). Cleavage of PARP-1 by caspase-3/7

forms 89 and 24 kDa fragments, which were decreased in this study (Appendix 6) (Sun *et al.*, 2014). Accordingly, the cleaved PARP-1 to PARP-1 (cPARP/PARP-1) was significantly reduced in Hek293 and Caco2 cells (Figure 4.11C and D). Nevertheless, apoptosis could still proceed due to AIF and endonuclease G released following MOMP and was confirmed by the externalisation of PS and LDH markers of apoptosis. Externalisation of PS was also increased (Figure 4.12A and B) in response to caspase 3/7 (Figure 4.11A, B), suggesting that Hexacyclen induced apoptosis in Hek293 and Caco2 cells since flipping of PS from the inside plasma membrane to the outside surface is used as an early marker of apoptosis (Lee *et al.*, 2013). Increased LDH levels (Figure 4.12C and D), a stable cytoplasmic enzyme, also indicate apoptosis since LDH is rapidly released when cells undergo cellular damage due to the loss of membrane integrity (Kumar *et al.*, 2018, Kamiloglu *et al.*, 2020). This agrees with the cell viability decline reported prior and confirms the type of cell death.

CHAPTER 6 : CONCLUSION

Hexacyclen is a potent metal ion chelator and is considered an anticancer agent. However, the cytotoxic effect of Hexacyclen on CRC and human kidney cells has not been determined. Hence, biochemical effects of Hexacyclen in Caco2 and Hek293 cells were investigated following a 48-hour exposure.

A summary of the results is presented in Figure 6.1. The ROS production induced upon treatment with IC_{20} and IC_{50} was associated with decreased cell viability, mitochondrial membrane potential and ATP. However, upregulation of antioxidants molecules including SOD2, GPx and GSH eliminate ROS, thus ameliorate oxidative stress. The study revealed that RNS increased upon exposure to Hexacyclen as shown by NO and iNOS elevation, leading to cell death. Apoptosis was a mechanism of cell death as shown by increases in Bax, Caspase-9, -3/7, externalised phosphatidylserine and LDH. Apoptosis was mediated mainly by intrinsic pathway in Hek293 cells, while both pathways facilitated apoptosis in Caco2 cells Furthermore, NF-κB / cell survival pathway was reduced, allowing a decrease in anti-apoptosis proteins such as Bcl-2, alternately favouring the intrinsic apoptotic pathway. Hexacyclen induced similar biochemical effect in Caco2 and Hek293 cells. This implies that there is a possibility of Hexacyclen inducing nephrotoxicity if used *in vivo.* However, Caco2 cells were sensitive at low concentration of Hexacyclen, hence, it can be used to help in the development of new promising therapeutic treatments for CRC without stimulating kidney toxicity.

There is a need to investigate the mechanism that led to NF-κB and STAT3 signalling pathways decrease including the initiator cytokines such as TNFα, IL-6 and IL-1β. Also, the cytotoxicity of Hexacyclen in other cell lines including in human hepatocellular carcinoma cells and *in-vivo* studies must be conducted.

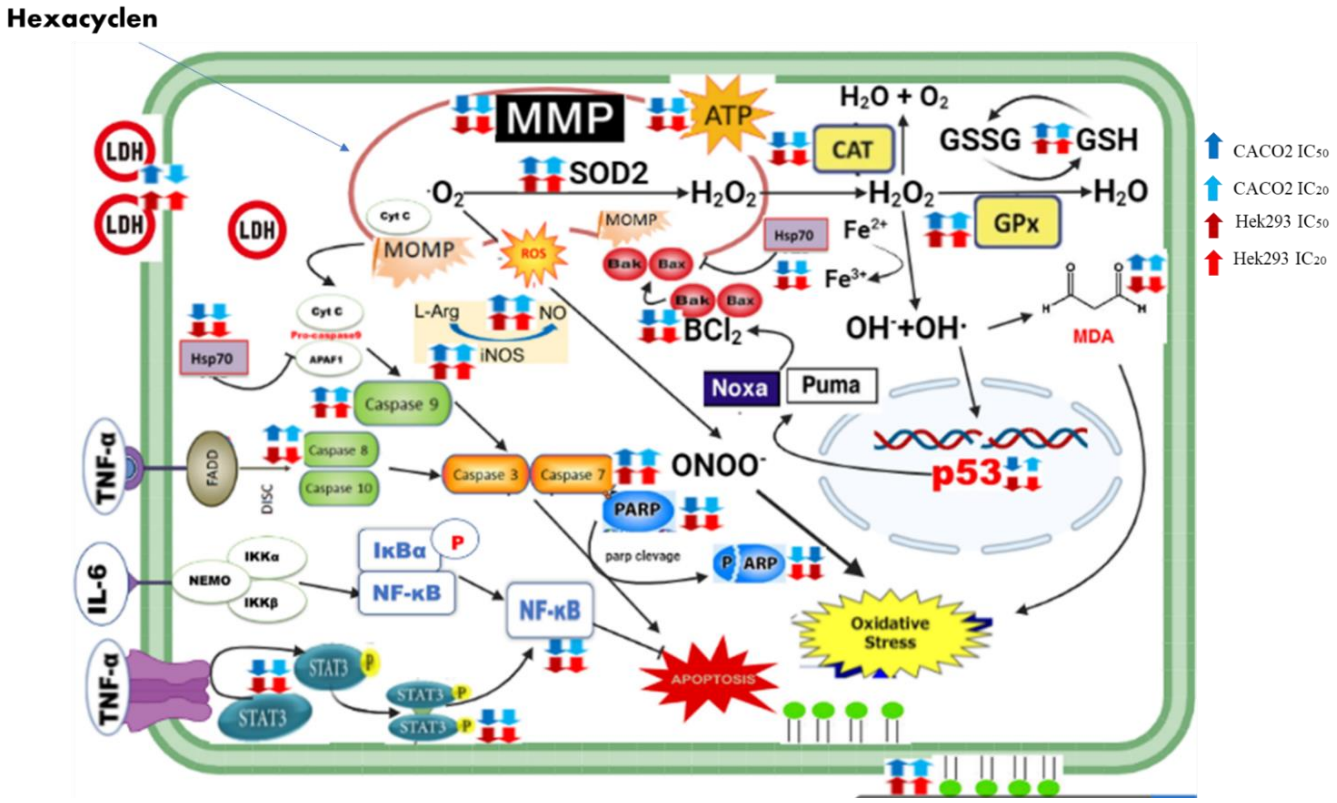

Figure 6.1: Schematic overview of the biochemical effects of Hexacyclen on cell viability, metabolic activity, oxidative stress, apoptosis and inflammation on human colorectal adenocarcinoma cells (Caco2) and normal embryonic kidney cells (Hek293) over 48-hour acute exposure. (Prepared by Author).

REFERENCES

Abancens M, Bustos V, Harvey H, McBryan J, Harvey BJ. Sexual Dimorphism in Colon Cancer. Front Oncol. 2020 Dec 9;10:607909. doi: 10.3389/fonc.2020.607909. PMID: 33363037; PMCID: PMC7759153.

ADWAS, A. A., IBRAHIMELSAYED, A. S., AZAB, A. E. & QUWAYDIR, F. A. 2019. Oxidative stress and antioxidant mechanisms in human body. *Journal of Applied Biotechnology & Bioengineering,* 6**,** 43–47.

AGGARWAL, V., TULI, H. S., VAROL, A., THAKRAL, F., YERER, M. B., SAK, K., VAROL, M., JAIN, A., KHAN, M. A. & SETHI, G. 2019. Role of Reactive Oxygen Species in Cancer Progression: Molecular Mechanisms and Recent Advancements. *Biomolecules,* 9**,** 735.

AGHABOZORGI, A. S., EBRAHIMI, R., BAHIRAEE, A., TEHRANI, S. S., NABIZADEH, F., SETAYESH, L., JAFARZADEH-ESFEHANI, R., FERNS, G. A., AVAN, A. & RASHIDI, Z. 2020. The genetic factors associated with Wnt signaling pathway in colorectal cancer. *Life Sciences,* 256**,** 118006.

AL-NAIMI, M. S., RASHEED, H. A., HUSSIEN, N. R., AL-KURAISHY, H. M. & AL-GAREEB, A. I. 2019. Nephrotoxicity: Role and significance of renal biomarkers in the early detection of acute renal injury. *J Adv Pharm Technol Res,* 10**,** 95-99.

ALCHÉ, J. D. D. 2019. A concise appraisal of lipid oxidation and lipoxidation in higher plants. *Redox Biology,* 23**,** 101136.

ANTONIOU, C., SAVVIDES, A., GEORGIADOU, E. C. & FOTOPOULOS, V. 2018. Spectrophotometric Quantification of Reactive Oxygen, Nitrogen and Sulfur Species in Plant Samples. *In:* ALCÁZAR, R. & TIBURCIO, A. F. (eds.) *Polyamines: Methods and Protocols.* New York, NY: Springer New York.

ARFIN, S., JHA, N. K., JHA, S. K., KESARI, K. K., RUOKOLAINEN, J., ROYCHOUDHURY, S., RATHI, B. & KUMAR, D. 2021. Oxidative Stress in Cancer Cell Metabolism. *Antioxidants (Basel, Switzerland),* 10**,** 642.

AUBREY, B. J., KELLY, G. L., JANIC, A., HEROLD, M. J. & STRASSER, A. 2018. How does p53 induce apoptosis and how does this relate to p53-mediated tumour suppression? *Cell Death & Differentiation,* 25**,** 104-113.

AUSTIN, C. A. & RODGERS, M. T. 2014. Alkali metal cation-hexacyclen complexes: effects of alkali metal cation size on the structure and binding energy. *J Phys Chem A,* 118**,** 5488-5500.

BADER, N. & BUKHZAM, A. 2014. Crown Ethers: Their Complexes and Analytical Applications. *Journal of Applicable Chemistry,* 3**,** 237-244.

BAHUGUNA, A., KHAN, I., BAJPAI, V. & KANG, S. 2017. MTT assay to evaluate the cytotoxic potential of a drug. *Bangladesh Journal of Pharmacology,* 12**,** 8-2017.

BARNETT, L. M. A. & CUMMINGS, B. S. 2018. Nephrotoxicity and Renal Pathophysiology: A Contemporary Perspective. *Toxicol Sci,* 164**,** 379-390.

BASS, J. J., WILKINSON, D. J., RANKIN, D., PHILLIPS, B. E., SZEWCZYK, N. J., SMITH, K. & ATHERTON, P. J. 2017. An overview of technical considerations for Western blotting applications to physiological research. *Scandinavian journal of medicine & science in sports,* 27**,** 4-25.

BAUDINO, T. A. 2015. Targeted Cancer Therapy: The Next Generation of Cancer Treatment. *Curr Drug Discov Technol,* 12**,** 3-20.

BAUR, F., NIETZER, S. L., KUNZ, M., SAAL, F., JEROMIN, J., MATSCHOS, S., LINNEBACHER, M., WALLES, H., DANDEKAR, T. & DANDEKAR, G. 2019. Connecting Cancer Pathways to Tumor Engines: A Stratification Tool for Colorectal Cancer Combining Human In Vitro Tissue Models with Boolean In Silico Models. *Cancers (Basel),* 12.

BEERE, H. M., WOLF, B. B., CAIN, K., MOSSER, D. D., MAHBOUBI, A., KUWANA, T., TAILOR, P., MORIMOTO, R. I., COHEN, G. M. & GREEN, D. R. 2000. Heat-shock protein 70 inhibits apoptosis by preventing recruitment of procaspase-9 to the Apaf-1 apoptosome. *Nat Cell Biol,* 2**,** 469-475.

BÖHMER, A., GAMBARYAN, S., FLENTJE, M., JORDAN, J. & TSIKAS, D. 2014. [Ureido-^{15}N]citrulline UPLC-MS/MS nitric oxide synthase (NOS) activity assay: development, validation, and applications to assess NOS uncoupling and human platelets NOS activity. *J Chromatogr B Analyt Technol Biomed Life Sci,* 965**,** 173-182.

BOOJAR, M. M. A. & GOODARZI, F. 2006a. Cytotoxicity and the levels of oxidative stress parameters in WI38 cells following 2 macrocyclic crown ethers treatment. *Clinica Chimica Acta,* 364**,** 321-327.

BOOJAR, M. M. A. & GOODARZI, F. 2006b. Oxidative response of rat lung tissue after crown ethers exposure and the effects of alpha-tocopherol treatment. *Clinica Chimica Acta,* 370**,** 158-164.

BRAY, F., FERLAY, J., SOERJOMATARAM, I., SIEGEL, R. L., TORRE, L. A. & JEMAL, A. 2018. Global cancer statistics 2018: GLOBOCAN estimates of incidence and mortality worldwide for 36 cancers in 185 countries. *CA Cancer J Clin,* 68**,** 394-424.

BRITANNICA 2018. The Editors of Encyclopaedia. "colon". *In:* BRITANNICA, E. (ed.).

CAMPBELL, M. G., SMITH, B. C., POTTER, C. S., CARRAGHER, B. & MARLETTA, M. A. 2014. Molecular architecture of mammalian nitric oxide synthases. *Proceedings of the National Academy of Sciences of the United States of America,* 111**,** E3614-E3623.

CHEHARDOLI, G. & BAHMANI, A. 2019. The role of crown ethers in drug delivery. *Supramolecular Chemistry,* 31**,** 221-238.

CHOI, M. E., PRICE, D. R., RYTER, S. W. & CHOI, A. M. K. 2019. Necroptosis: a crucial pathogenic mediator of human disease. *JCI Insight,* 4.

CINELLI, M. A., DO, H. T., MILEY, G. P. & SILVERMAN, R. B. 2020. Inducible nitric oxide synthase: Regulation, structure, and inhibition. *Med Res Rev,* 40**,** 158-189.

CROWLEY, L. C., MARFELL, B. J., SCOTT, A. P. & WATERHOUSE, N. J. 2016. Quantitation of Apoptosis and Necrosis by Annexin V Binding, Propidium Iodide Uptake, and Flow Cytometry. *Cold Spring Harb Protoc,* 2016.

DEMCHENKO, A. P. 2012. The change of cellular membranes on apoptosis: fluorescence detection. *Exp Oncol,* 34**,** 263-268.

DORRINGTON, M. G. & FRASER, I. D. C. 2019. NF-κB Signaling in Macrophages: Dynamics, Crosstalk, and Signal Integration. *Frontiers in Immunology,* 10.

DUMANOVIĆ, J., NEPOVIMOVA, E., NATIĆ, M., KUČA, K. & JAĆEVIĆ, V. 2021. The Significance of Reactive Oxygen Species and Antioxidant Defense System in Plants: A Concise Overview. *Frontiers in Plant Science,* 11.

EBATA, T., HIRATA, H. & KAWAUCHI, K. 2016. Functions of the Tumor Suppressors p53 and Rb in Actin Cytoskeleton Remodeling. *BioMed Research International,* 2016**,** 9231057.

EGUSQUIAGUIRRE, S. P., YEH, J. E., WALKER, S. R., LIU, S. & FRANK, D. A. 2018. The STAT3 Target Gene TNFRSF1A Modulates the NF-κB Pathway in Breast Cancer Cells. *Neoplasia,* 20**,** 489-498.

EL-HASHANI, A., TOUTIANOUSH, A. & TIEKE, B. 2007. Layer-by-Layer Assembled Membranes of Protonated 18-Azacrown-6 and Polyvinylsulfate and Their Application for Highly Efficient Anion Separation. *The Journal of Physical Chemistry B,* 111**,** 8582-8588.

FAN, Y., MAO, R. & YANG, J. 2013. NF-κB and STAT3 signaling pathways collaboratively link inflammation to cancer. *Protein Cell,* 4**,** 176-185.

FATFAT, M., ABOU MERHI, R., RAHAL, O., STOYANOVSKY, D., ZAKI, A., HAIDAR, H., KAGAN, V., GALI-MUHTASIB, H. & MACHACA, K. 2014. Copper chelation selectively kills colon cancer cells through redox cycling and generation of reactive oxygen species. *BMC Cancer,* 14**,** 527.

FOREST, V., FIGAROL, A., BOUDARD, D., COTTIER, M., GROSSEAU, P. & POURCHEZ, J. 2015. Adsorption of Lactate Dehydrogenase Enzyme on Carbon Nanotubes: How to Get Accurate Results for the Cytotoxicity of These Nanomaterials. *Langmuir : the ACS journal of surfaces and colloids,* 31.

FÖRSTERMANN, U. & SESSA, W. C. 2012. Nitric oxide synthases: regulation and function. *European heart journal,* 33**,** 829-837d.

GALLUZZI, L., VITALE, I., AARONSON, S. A., ABRAMS, J. M., ADAM, D., AGOSTINIS, P., ALNEMRI, E. S., ALTUCCI, L., AMELIO, I., ANDREWS, D. W., ANNICCHIARICO-PETRUZZELLI, M., ANTONOV, A.

V., ARAMA, E., BAEHRECKE, E. H., BARLEV, N. A., BAZAN, N. G., BERNASSOLA, F., BERTRAND, M. J. M., BIANCHI, K., BLAGOSKLONNY, M. V., BLOMGREN, K., BORNER, C., BOYA, P., BRENNER, C., CAMPANELLA, M., CANDI, E., CARMONA-GUTIERREZ, D., CECCONI, F., CHAN, F. K., CHANDEL, N. S., CHENG, E. H., CHIPUK, J. E., CIDLOWSKI, J. A., CIECHANOVER, A., COHEN, G. M., CONRAD, M., CUBILLOS-RUIZ, J. R., CZABOTAR, P. E., D'ANGIOLELLA, V., DAWSON, T. M., DAWSON, V. L., DE LAURENZI, V., DE MARIA, R., DEBATIN, K. M., DEBERARDINIS, R. J., DESHMUKH, M., DI DANIELE, N., DI VIRGILIO, F., DIXIT, V. M., DIXON, S. J., DUCKETT, C. S., DYNLACHT, B. D., EL-DEIRY, W. S., ELROD, J. W., FIMIA, G. M., FULDA, S., GARCÍA-SÁEZ, A. J., GARG, A. D., GARRIDO, C., GAVATHIOTIS, E., GOLSTEIN, P., GOTTLIEB, E., GREEN, D. R., GREENE, L. A., GRONEMEYER, H., GROSS, A., HAJNOCZKY, G., HARDWICK, J. M., HARRIS, I. S., HENGARTNER, M. O., HETZ, C., ICHIJO, H., JÄÄTTELÄ, M., JOSEPH, B., JOST, P. J., JUIN, P. P., KAISER, W. J., KARIN, M., KAUFMANN, T., KEPP, O., KIMCHI, A., KITSIS, R. N., KLIONSKY, D. J., KNIGHT, R. A., KUMAR, S., LEE, S. W., LEMASTERS, J. J., LEVINE, B., LINKERMANN, A., LIPTON, S. A., LOCKSHIN, R. A., LÓPEZ-OTÍN, C., LOWE, S. W., LUEDDE, T., LUGLI, E., MACFARLANE, M., MADEO, F., MALEWICZ, M., MALORNI, W., MANIC, G. 2018. Molecular mechanisms of cell death: recommendations of the Nomenclature Committee on Cell Death 2018. *Cell Death Differ,* 25**,** 486-541.

GANJU, N. & EASTMAN, A. 2003. Zinc inhibits Bax and Bak activation and cytochrome c release induced by chemical inducers of apoptosis but not by death-receptor-initiated pathways. *Cell Death Differ,* 10**,** 652-661.

GAUR, K., VÁZQUEZ-SALGADO, A. M., DURAN-CAMACHO, G., DOMINGUEZ-MARTINEZ, I., BENJAMÍN-RIVERA, J. A., FERNÁNDEZ-VEGA, L., SARABIA, L. C., GARCÍA, A. C., PÉREZ-DELIZ, F., MÉNDEZ ROMÁN, J. A., VEGA-CARTAGENA, M., LOZA-ROSAS, S. A., ACEVEDO, X. R. & TINOCO, A. D. 2018. Iron and Copper Intracellular Chelation as an Anticancer Drug Strategy. *Inorganics (Basel),* 6.

GAVET, O. & PINES, J. 2010. Progressive activation of cyclinB1–Cdk1 coordinates entry to mitosis. *Dev. Cell* 18**,** 533–543

GHANI, M. A., BARRIL, C., BEDGOOD, D. R., JR. & PRENZLER, P. D. 2017. Measurement of antioxidant activity with the thiobarbituric acid reactive substances assay. *Food Chem,* 230**,** 195-207.

GIULIANI, C., BUCCI, I. & NAPOLITANO, G. 2018. The Role of the Transcription Factor Nuclear Factor-kappa B in Thyroid Autoimmunity and Cancer. *Frontiers in Endocrinology,* 9.

GOLDAR, S., KHANIANI, M. S., DERAKHSHAN, S. M. & BARADARAN, B. 2015. Molecular mechanisms of apoptosis and roles in cancer development and treatment. *Asian Pac J Cancer Prev,* 16**,** 2129-2144.

GRAHAM, A., ADELOYE, D., GRANT, L., THEODORATOU, E. & CAMPBELL, H. 2012. Estimating the incidence of colorectal cancer in Sub-Saharan Africa: A systematic analysis. *J Glob Health,* 2**,** 020404.

GREEN, D. R. & LLAMBI, F. 2015. Cell Death Signaling. *Cold Spring Harb Perspect Biol,* 7.

GRETEN, F. R. & GRIVENNIKOV, S. I. 2019. Inflammation and Cancer: Triggers, Mechanisms, and Consequences. *Immunity,* 51**,** 27-41.

HARIHARAN, A., HAKEEM, A. R., RADHAKRISHNAN, S., REDDY, M. S. & RELA, M. 2021. The Role and Therapeutic Potential of NF-kappa-B Pathway in Severe COVID-19 Patients. *Inflammopharmacology,* 29**,** 91-100.

HAUSMAN, D. M. 2019. What Is Cancer? *Perspect Biol Med,* 62**,** 778-784.

HAYES, J. D., DINKOVA-KOSTOVA, A. T. & TEW, K. D. 2020. Oxidative Stress in Cancer. *Cancer Cell,* 38**,** 167-197.

HEIDARI-SORESHJANI, S., ASADI-SAMANI, M., YANG, Q. & SAEEDI-BOROUJENI, A. 2017. Phytotherapy of nephrotoxicity-induced by cancer drugs: an updated review. *J Nephropathol,* 6**,** 254-263.

HOU, H., SUN, D. & ZHANG, X. 2019. The role of MDM2 amplification and overexpression in therapeutic resistance of malignant tumors. *Cancer Cell International,* 19**,** 216.

HUANG, K., ZHANG, J., O'NEILL, K. L., GURUMURTHY, C. B., QUADROS, R. M., TU, Y. & LUO, X. 2016. Cleavage by Caspase 8 and Mitochondrial Membrane Association Activate the BH3-only Protein Bid during TRAIL-induced Apoptosis. *J Biol Chem,* 291**,** 11843-11851.

HUANG, S. & MILLAR, A. H. 2013. Succinate dehydrogenase: the complex roles of a simple enzyme. *Curr Opin Plant Biol,* 16**,** 344-349.

IGHODARO, O. M. & AKINLOYE, O. A. 2018. First line defence antioxidants-superoxide dismutase (SOD), catalase (CAT) and glutathione peroxidase (GPX): Their fundamental role in the entire antioxidant defence grid. *Alexandria Journal of Medicine,* 54**,** 287-293.

IQBAL, T., ARSHAD, N., HASHIM, J., ALI, S. A., ZEHRA, B., AHMAD, M. S., HASSAN, N., ULLAH, A., HAMID, S. Z. & ISAAC, I. O. 2022. Natural products based crown ethers: synthesis and their anticancer potential. *Journal of Asian Natural Products Research,* 24**,** 268-277.

JAT, D. & NAHAR, M. 2017. Oxidative stress and antioxidants : an overview. *IJARR,* 2**,** 110-119.

JI, Z., HE, L., REGEV, A. & STRUHL, K. 2019. Inflammatory regulatory network mediated by the joint action of NF-kB, STAT3, and AP-1 factors is involved in many human cancers. *Proc Natl Acad Sci U S A,* 116**,** 9453-9462.

JIA, J. B., LALL, C., TIRKES, T., GULATI, R., LAMBA, R. & GOODWIN, S. C. 2015. Chemotherapy-related complications in the kidneys and collecting system: an imaging perspective. *Insights Imaging,* 6**,** 479-487.

KAHNT, M., HOENKE, S., FISCHER, L., AL-HARRASI, A. & CSUK, R. 2019. Synthesis and Cytotoxicity Evaluation of DOTA-Conjugates of Ursolic Acid. *Molecules,* 24.

KALKAVAN, H. & GREEN, D. R. 2018. MOMP, cell suicide as a BCL-2 family business. *Cell Death Differ,* 25**,** 46-55.

KAMILOGLU, S., SARI, G., OZDAL, T. & CAPANOGLU, E. 2020. Guidelines for cell viability assays. *Food Frontiers,* 1**,** 332-349.

KERR, J., WYLLIE, A. & CURRIE, A. 1972. Apoptosis: a basic biological phenomenon with wide-ranging implications in tissue kinetics. *British Journal of Cancer,* 26**,** 239–235.

KHAN, M. M., KIM, Y. K., BILKIS, T., SUH, J. W., LEE, D. Y. & YOO, J. C. 2020. Reduction of Oxidative Stress through Activating the Nrf2 mediated HO-1 Antioxidant Efficacy Signaling Pathway by MS15, an Antimicrobial Peptide from Bacillus velezensis. *Antioxidants (Basel),* 9.

KIM, S. Y. & MOON, A. 2012. Drug-induced nephrotoxicity and its biomarkers. *Biomol Ther (Seoul),* 20**,** 268-272.

KONTOGHIORGHES, G. J. 2020. Advances on Chelation and Chelator Metal Complexes in Medicine. *International journal of molecular sciences,* 21.

KONTOGHIORGHES, G. J. & KONTOGHIORGHE, C. N. 2020. Iron and Chelation in Biochemistry and Medicine: New Approaches to Controlling Iron Metabolism and Treating Related Diseases. *Cells,* 9**,** 1456.

KRALJ, M., TUSEK-BOZIĆ, L. & FRKANEC, L. 2008. Biomedical potentials of crown ethers: prospective antitumor agents. *ChemMedChem,* 3**,** 1478-1492.

KROEMER, G., GALLUZZI, L., VANDENABEELE, P., ABRAMS, J., ALNEMRI, E. S., BAEHRECKE, E. H., BLAGOSKLONNY, M. V., EL-DEIRY, W. S., GOLSTEIN, P., GREEN, D. R., HENGARTNER, M., KNIGHT, R. A., KUMAR, S., LIPTON, S. A., MALORNI, W., NUÑEZ, G., PETER, M. E., TSCHOPP, J., YUAN, J., PIACENTINI, M., ZHIVOTOVSKY, B. & MELINO, G. 2009. Classification of cell death: recommendations of the Nomenclature Committee on Cell Death 2009. *Cell Death Differ,* 16**,** 3-11.

KUIPERS, E., GRADY, W., LIEBERMAN, D., SEUFFERLEIN, T., SUNG, J., BOELENS, P., CORNELIS, J., VELDE, V. & WATANABE, T. 2015. Colorectal cancer. *Nature Reviews Disease Primers,* ePub ahead of print.

KUMAR, P., NAGARAJAN, A. & UCHIL, P. D. 2018. Analysis of Cell Viability by the Lactate Dehydrogenase Assay. *Cold Spring Harb Protoc,* 2018.

KUNZELMANN, K. 2005. Ion Channels and Cancer. *The Journal of Membrane Biology,* 205**,** 159.

KUPCHO, K., SHULTZ, J., HURST, R., HARTNETT, J., ZHOU, W., MACHLEIDT, T., GRAILER, J., WORZELLA, T., RISS, T., LAZAR, D., CALI, J. J. & NILES, A. 2019. A real-time, bioluminescent annexin V assay for the assessment of apoptosis. *Apoptosis,* 24**,** 184-197.

LABUDDA, M. 2013. Lipid peroxidation as a biochemical marker for oxidative stress during drought. An effective tool for plant breeding. *E-wydawnictwo***,** 1-12.

LAMEIRE, N. 2014. Nephrotoxicity of recent anti-cancer agents. *Clin Kidney J,* 7**,** 11-22.

LEE, S. H., MENG, X. W., FLATTEN, K. S., LOEGERING, D. A. & KAUFMANN, S. H. 2013. Phosphatidylserine exposure during apoptosis reflects bidirectional trafficking between plasma membrane and cytoplasm. *Cell death and differentiation,* 20**,** 64-76.

LI, C. Y., LEE, J. S., KO, Y. G., KIM, J. I. & SEO, J. S. 2000. Heat shock protein 70 inhibits apoptosis downstream of cytochrome c release and upstream of caspase-3 activation. *J Biol Chem,* 275**,** 25665-25671.

LI, J., CHEN, L., DU, L. & LI, M. 2013. Cage the firefly luciferin! – a strategy for developing bioluminescent probes. *Chemical Society Reviews,* 42**,** 662-676.

LIN, W. W. & KARIN, M. 2007. A cytokine-mediated link between innate immunity, inflammation, and cancer. *J Clin Invest,* 117**,** 1175-1183.

LIN, Y., HE, Z., YE, J., LIU, Z., SHE, X., GAO, X. & LIANG, R. 2020. Progress in Understanding the IL-6/STAT3 Pathway in Colorectal Cancer. *OncoTargets and therapy,* 13**,** 13023-13032.

LINGAPPAN, K. 2018. NF-κB in Oxidative Stress. *Curr Opin Toxicol,* 7**,** 81-86.

LITAN, A. & LANGHANS, S. A. 2015. Cancer as a channelopathy: ion channels and pumps in tumor development and progression. *Frontiers in Cellular Neuroscience,* 9.

LIU, T., ZHANG, L., JOO, D. & SUN, S.-C. 2017a. NF-κB signaling in inflammation. *Signal Transduction and Targeted Therapy,* 2**,** 17023.

LIU, T., ZHANG, L., JOO, D. & SUN, S. C. 2017b. NF-κB signaling in inflammation. *Signal Transduct Target Ther,* 2**,** 17023-.

LIU, Y., TAVANA, O. & GU, W. 2019. p53 modifications: exquisite decorations of the powerful guardian. *J Mol Cell Biol,* 11**,** 564-577.

LOPEZ, J. & TAIT, S. W. 2015. Mitochondrial apoptosis: killing cancer using the enemy within. *Br J Cancer,* 112**,** 957-962.

LORETO, C., LA ROCCA, G., ANZALONE, R., CALTABIANO, R., VESPASIANI, G., CASTORINA, S., RALPH, D. J., CELLEK, S., MUSUMECI, G., GIUNTA, S., DJINOVIC, R., BASIC, D. & SANSALONE, S. 2014. The Role of Intrinsic Pathway in Apoptosis Activation and Progression in Peyronie's Disease. *BioMed Research International,* 2014**,** 616149.

LUI, G. Y., KOVACEVIC, Z., S, V. M., KALINOWSKI, D. S., MERLOT, A. M., SAHNI, S. & RICHARDSON, D. R. 2015. Novel thiosemicarbazones regulate the signal transducer and activator of transcription 3 (STAT3) pathway: inhibition of constitutive and interleukin 6-induced activation by iron depletion. *Mol Pharmacol,* 87**,** 543-560.

LUO, J. L., KAMATA, H. & KARIN, M. 2005. IKK/NF-kappaB signaling: balancing life and death--a new approach to cancer therapy. *J Clin Invest,* 115**,** 2625-2632.

LUSHCHAK, V. I. 2014. Free radicals, reactive oxygen species, oxidative stress and its classification. *Chem Biol Interact,* 224**,** 164-175.

MAŁYSZKO, J., KOZŁOWSKA, K., KOZŁOWSKI, L. & MAŁYSZKO, J. 2016. Nephrotoxicity of anticancer treatment. *Nephrology Dialysis Transplantation,* 32**,** 924-936.

MARTINCUKS, A., ANDRYKA, K., KÜSTER, A., SCHMITZ-VAN DE LEUR, H., KOMOROWSKI, M. & MÜLLER-NEWEN, G. 2017. Nuclear translocation of STAT3 and NF-κB are independent of each other but NF-κB supports expression and activation of STAT3. *Cell Signal,* 32**,** 36-47.

MASHIMO, M., ONISHI, M., UNO, A., TANIMICHI, A., NOBEYAMA, A., MORI, M., YAMADA, S., NEGI, S., BU, X., KATO, J., MOSS, J., SANADA, N., KIZU, R. & FUJII, T. 2021. The 89-kDa PARP1 cleavage fragment serves as a cytoplasmic PAR carrier to induce AIF-mediated apoptosis. *J Biol Chem,* 296**,** 100046.

Matuz-Mares D, Riveros-Rosas H, Vilchis-Landeros MM, Vázquez-Meza H. Glutathione Participation in the Prevention of Cardiovascular Diseases. Antioxidants (Basel). 2021 Jul 29;10(8):1220. doi: 10.3390/antiox10081220. PMID: 34439468; PMCID: PMC8389000.

MCOYI, S., AMOAKO, D. G., SOMBORO, A. M., KHUMALO, H. M. & KHAN, R. B. 2020. The molecular effect of 1,4,7-triazacyclononane on oxidative stress parameters in human hepatocellular carcinoma (HepG2) cells. *J Biochem Mol Toxicol,* 34**,** e22607.

MENS, M. M. J. & GHANBARI, M. 2018. Cell Cycle Regulation of Stem Cells by MicroRNAs. *Stem Cell Rev Rep,* 14**,** 309-322.

MITCHELL, S., VARGAS, J. & HOFFMANN, A. 2016. Signaling via the NFκB system. *Wiley Interdiscip Rev Syst Biol Med,* 8**,** 227-241.

MITTAL, M., SIDDIQUI, M. R., TRAN, K., REDDY, S. P. & MALIK, A. B. 2013. Reactive Oxygen Species in Inflammation and Tissue Injury. *Antioxidants & Redox Signaling,* 20**,** 1126-1167.

MIZUSHIMA, N. & KOMATSU, M. 2011. Autophagy: renovation of cells and tissues. *Cell,* 147**,** 728-741.

MOHAMMAD, G. 2016. *Pyruvate Kinase M2 (PKM2) and Lactate Dehydrogenase A (LDHA) as Novel Diagnostic Markers and Therapeutic Targets for Pancreatic Cancer*.

MOK, M. T., ZHOU, J., TANG, W., ZENG, X., OLIVER, A. W., WARD, S. E. & CHENG, A. S. 2018. CCRK is a novel signalling hub exploitable in cancer immunotherapy. *Pharmacology & Therapeutics,* 186**,** 138-151.

MOOSAVI, B., ZHU, X.-L., YANG, W.-C. & YANG, G.-F. 2020. Genetic, epigenetic and biochemical regulation of succinate dehydrogenase function. *Biological Chemistry,* 401**,** 319-330.

MORRISON, P. W. J., PORFIRYEVA, N. N., CHAHAL, S., SALAKHOV, I. A., LACOURT, C., SEMINA, II, MOUSTAFINE, R. I. & KHUTORYANSKIY, V. V. 2017. Crown Ethers: Novel Permeability Enhancers for Ocular Drug Delivery? *Mol Pharm,* 14**,** 3528-3538.

MOTSUKU, L., CHEN, W. C., MUCHENGETI, M. M., NAIDOO, M., QUENE, T. M., KELLETT, P., MOHLALA, M. I., CHU, K. M. & SINGH, E. 2021. Colorectal cancer incidence and mortality trends by sex and population group in South Africa: 2002-2014. *BMC Cancer,* 21**,** 129.

NAVANEETHAKRISHNAN, S., ROSALES, J. L. & LEE, K. Y. 2019. ROS-Mediated Cancer Cell Killing through Dietary Phytochemicals. *Oxid Med Cell Longev,* 2019**,** 9051542.

OTTO, T. & SICINSKI, P. 2017. Cell cycle proteins as promising targets in cancer therapy. *Nat Rev Cancer,* 17**,** 93-115.

PERAZELLA, M. A. 2012. Onco-nephrology: renal toxicities of chemotherapeutic agents. *Clin J Am Soc Nephrol,* 7**,** 1713-1721.

PFEFFER, C. M. & SINGH, A. T. K. 2018. Apoptosis: A Target for Anticancer Therapy. *International journal of molecular sciences,* 19.

PHATAK, V. & MULLER, P. 2015. Metal toxicity and the p53 protein: an intimate relationship. *Toxicology Research,* 4**,** 576-591.

PICKHARDT, P. J., KIM, D. H., POOLER, B. D., HINSHAW, J. L., BARLOW, D., JENSEN, D., REICHELDERFER, M. & CASH, B. D. 2013. Assessment of volumetric growth rates of small colorectal polyps with CT colonography: a longitudinal study of natural history. *Lancet Oncol,* 14**,** 711-720.

RADI, R. 2018. Oxygen radicals, nitric oxide, and peroxynitrite: Redox pathways in molecular medicine. *Proceedings of the National Academy of Sciences,* 115**,** 5839-5848.

RAMESH, G. & REEVES, W. B. 2002. TNF-alpha mediates chemokine and cytokine expression and renal injury in cisplatin nephrotoxicity. *J Clin Invest,* 110**,** 835-842.

RAWLA, P., SUNKARA, T. & BARSOUK, A. 2019. Epidemiology of colorectal cancer: incidence, mortality, survival, and risk factors. *Prz Gastroenterol,* 14**,** 89-103.

REDZA-DUTORDOIR, M. & AVERILL-BATES, D. A. 2016. Activation of apoptosis signalling pathways by reactive oxygen species. *Biochimica et Biophysica Acta (BBA) - Molecular Cell Research,* 1863**,** 2977-2992.

SAKAMURU, S., ATTENE-RAMOS, M. S. & XIA, M. 2016. Mitochondrial Membrane Potential Assay. *Methods Mol Biol,* 1473**,** 17-22.

SALBITANI, G., BOTTONE, C. & CARFAGNA, S. 2017. Determination of Reduced and Total Glutathione Content in Extremophilic Microalga Galdieria phlegrea. *Bio-protocol,* 7**,** e2372.

SÁNCHEZ, M., SABIO, L., GÁLVEZ, N., CAPDEVILA, M. & DOMINGUEZ-VERA, J. M. 2017. Iron chemistry at the service of life. *IUBMB Life,* 69**,** 382-388.

SANNA, T., DALLOLIO, L., RAGGI, A., MAZZETTI, M., LORUSSO, G., ZANNI, A., FARRUGGIA, P. & LEONI, E. 2018. ATP bioluminescence assay for evaluating cleaning practices in operating theatres: applicability and limitations. *BMC Infect Dis,* 18**,** 583.

SATYO, L., AMOAKO, D. G., SOMBORO, A. M., SOSIBO, S. C., KUMALO, H. M., MHLONGO, N. N. & KHAN, R. B. 2020. Molecular Insights Into Di(2-Picolyl) Amine-Induced Cytotoxicity and Apoptosis in Human Kidney (HEK293) Cells. *Int J Toxicol,* 39**,** 341-351.

SCABINI, M., STELLARI, F., CAPPELLA, P., RIZZITANO, S., TEXIDO, G. & PESENTI, E. 2011. In vivo imaging of early stage apoptosis by measuring real-time caspase-3/7 activation. *Apoptosis,* 16**,** 198-207.

SHARIFI-RAD, M., ANIL KUMAR, N. V., ZUCCA, P., VARONI, E. M., DINI, L., PANZARINI, E., RAJKOVIC, J., TSOUH FOKOU, P. V., AZZINI, E., PELUSO, I., PRAKASH MISHRA, A., NIGAM, M., EL RAYESS, Y., BEYROUTHY, M. E., POLITO, L., IRITI, M., MARTINS, N., MARTORELL, M., DOCEA, A. O., SETZER, W. N., CALINA, D., CHO, W. C. & SHARIFI-RAD, J. 2020. Lifestyle, Oxidative Stress, and Antioxidants: Back and Forth in the Pathophysiology of Chronic Diseases. *Frontiers in Physiology,* 11.

SHARMA, G. N., GUPTA, G. & SHARMA, P. 2018. A Comprehensive Review of Free Radicals, Antioxidants, and Their Relationship with Human Ailments. *Crit Rev Eukaryot Gene Expr,* 28**,** 139-154.

SHI, D. & JIANG, P. 2021. A Different Facet of p53 Function: Regulation of Immunity and Inflammation During Tumor Development. *Frontiers in cell and developmental biology,* 9**,** 762651-762651.

SHI, T., VAN SOEST, D. M. K., POLDERMAN, P. E., BURGERING, B. M. T. & DANSEN, T. B. 2021. DNA damage and oxidant stress activate p53 through differential upstream signaling pathways. *Free Radical Biology and Medicine,* 172**,** 298-311.

SIES, H. 2015. Oxidative stress: a concept in redox biology and medicine. *Redox Biol,* 4**,** 180-183.

SIMON, K. 2016. Colorectal cancer development and advances in screening. *Clin Interv Aging,* 11**,** 967-976.

SINGH, N., BABY, D., RAJGURU, J. P., PATIL, P. B., THAKKANNAVAR, S. S. & PUJARI, V. B. 2019a. Inflammation and cancer. *Annals of African medicine,* 18**,** 121-126.

SINGH, R., LETAI, A. & SAROSIEK, K. 2019b. Regulation of apoptosis in health and disease: the balancing act of BCL-2 family proteins. *Nature reviews. Molecular cell biology,* 20**,** 175-193.

SIVANDZADE, F., BHALERAO, A. & CUCULLO, L. 2019. Analysis of the Mitochondrial Membrane Potential Using the Cationic JC-1 Dye as a Sensitive Fluorescent Probe. *Bio-protocol,* 9**,** e3128.

SOMBORO, A. M., AMOAKO, D. G., OSEI SEKYERE, J., KUMALO, H. M., KHAN, R., BESTER, L. A. & ESSACK, S. Y. 2019. 1,4,7-Triazacyclononane Restores the Activity of β-Lactam Antibiotics against Metallo-β-Lactamase-Producing Enterobacteriaceae: Exploration of Potential Metallo-β-Lactamase Inhibitors. *Applied and environmental microbiology,* 85**,** e02077-02018.

SPEARMAN, C. W. & SONDERUP, M. W. 2014. Preventing hepatitis B and hepatocellular carcinoma in South Africa: The case for a birth-dose vaccine. *S Afr Med J,* 104**,** 610-612.

SUBRAMANIAN, M., JONES, M. & LAL, A. 2013. Long Non-Coding RNAs Embedded in the Rb and p53 Pathways. *Cancers,* 5**,** 1655-1675.

SUN, S. C. 2017. The non-canonical NF-κB pathway in immunity and inflammation. *Nat Rev Immunol,* 17**,** 545-558.

SUN, X., ZHOU, X., DU, L., LIU, W., LIU, Y., HUDSON, L. G. & LIU, K. J. 2014. Arsenite binding-induced zinc loss from PARP-1 is equivalent to zinc deficiency in reducing PARP-1 activity, leading to inhibition of DNA repair. *Toxicology and applied pharmacology,* 274**,** 313-318.

SUNG, H., FERLAY, J., SIEGEL, R. L., LAVERSANNE, M., SOERJOMATARAM, I., JEMAL, A. & BRAY, F. 2021. Global cancer statistics 2020: GLOBOCAN estimates of incidence and mortality worldwide for 36 cancers in 185 countries. *CA Cancer J Clin*.

SZONDY, Z., SARANG, Z., KISS, B., GARABUCZI, É. & KÖRÖSKÉNYI, K. 2017. Anti-inflammatory Mechanisms Triggered by Apoptotic Cells during Their Clearance. *Frontiers in Immunology,* 8.

TAN, S. Y., ANG, C. Y. & ZHAO, Y. 2017. 5.17 - Smart Therapeutics Achieved via Host–Guest Assemblies. *In:* ATWOOD, J. L. (ed.) *Comprehensive Supramolecular Chemistry II.* Oxford: Elsevier.

TANIGUCHI, K. & KARIN, M. 2018. NF-κB, inflammation, immunity and cancer: coming of age. *Nat Rev Immunol,* 18**,** 309-324.

TOLOMEO, M. & CASCIO, A. 2021. The Multifaced Role of STAT3 in Cancer and Its Implication for Anticancer Therapy. *International journal of molecular sciences,* 22**,** 603.

TOMA, M., BELUŞICĂ, L., STAVARACHI, M., APOSTOL, P., SPANDOLE, S., RADU, I. & CIMPONERIU, D. 2012. Rating the environmental and genetic risk factors for colorectal cancer. *Journal of medicine and life,* 5**,** 152-159.

TSOTETSI, N., AMOAKO, D. G., SOMBORO, A. M., KHUMALO, H. M. & KHAN, R. B. 2020. Molecular mechanisms underlying the renoprotective effects of 1,4,7-triazacyclononane: a βeta-lactamase inhibitor. *Cytotechnology,* 72**,** 785-796.

URREGO, D., TOMCZAK, A., ZAHED, F., STÜHMER, W. & PARDO, L. 2014. Potassium channels in cell cycle and cell proliferation. *Philosophical transactions of the Royal Society of London. Series B, Biological sciences,* 369**,** 20130094.

VAKIFAHMETOGLU-NORBERG, H., OUCHIDA, A. T. & NORBERG, E. 2017. The role of mitochondria in metabolism and cell death. *Biochem Biophys Res Commun,* 482**,** 426-431.

VARADWAJ, P. R., VARADWAJ, A., PESLHERBE, G. H. & MARQUES, H. M. 2011. Conformational Analysis of 18-Azacrown-6 and Its Bonding with Late First Transition Series Divalent Metals: Insight from DFT Combined with NPA and QTAIM Analyses. *The Journal of Physical Chemistry A,* 115**,** 13180-13190.

VISCONTI, R., DELLA MONICA, R. & GRIECO, D. 2016. Cell cycle checkpoint in cancer: a therapeutically targetable double-edged sword. *J Exp Clin Cancer Res,* 35**,** 153.

WANG, X., CHEN, M., ZHOU, J. & ZHANG, X. 2014. HSP27, 70 and 90, anti-apoptotic proteins, in clinical cancer therapy (Review). *Int J Oncol,* 45**,** 18-30.

WANG, X., ZHU, J. & SMITHRUD, D. B. 2010. Synthesis and Investigation of Host-[2]Rotaxanes That Bind Metal Cations. *The Journal of Organic Chemistry,* 75**,** 3358-3370.

WILLIAMS, A. B. & SCHUMACHER, B. 2016. p53 in the DNA-Damage-Repair Process. *Cold Spring Harb Perspect Med,* 6.

WILLIAMS, R. A., TIMMIS, J. & QWARNSTROM, E. E. 2014. Computational Models of the NF-KB Signalling Pathway. *Computation,* 2**,** 131-158.

WONG, P. E. E., TETLEY, L., DUFÉS, C., CHOOI, K. W., BOLTON, K., SCHÄTZLEIN, A. G. & UCHEGBU, I. F. 2010. Polyamine Aza-Cyclic Compounds Demonstrate Anti-Proliferative Activity In Vitro But Fail to Control Tumour Growth In Vivo. *Journal of Pharmaceutical Sciences,* 99**,** 4642-4657.

YAMASHITA, T. & KANEKO, S. 2016. [Liver Cancer]. *Rinsho Byori,* 64**,** 787-796.

YANG, L., SHI, P., ZHAO, G., XU, J., PENG, W., ZHANG, J., ZHANG, G., WANG, X., DONG, Z., CHEN, F. & CUI, H. 2020. Targeting cancer stem cell pathways for cancer therapy. *Signal Transduction and Targeted Therapy,* 5**,** 8.

YANG, X., WANG, J., ZHOU, Y., WANG, Y., WANG, S. & ZHANG, W. 2012. Hsp70 promotes chemoresistance by blocking Bax mitochondrial translocation in ovarian cancer cells. *Cancer Lett,* 321**,** 137-143.

YOON, S., WOO, S. U., KANG, J. H., KIM, K., SHIN, H. J., GWAK, H. S., PARK, S. & CHWAE, Y. J. 2012. NF-κB and STAT3 cooperatively induce IL6 in starved cancer cells. *Oncogene,* 31**,** 3467-3481.

YU, H., LIN, L., ZHANG, Z., ZHANG, H. & HU, H. 2020. Targeting NF-κB pathway for the therapy of diseases: mechanism and clinical study. *Signal Transduct Target Ther,* 5**,** 209.

YU, H., PARDOLL, D. & JOVE, R. 2009. STATs in cancer inflammation and immunity: a leading role for STAT3. *Nat Rev Cancer,* 9**,** 798-809.

YU, L., LI, L., MEDEIROS, L. J. & YOUNG, K. H. 2017. NF-κB signaling pathway and its potential as a target for therapy in lymphoid neoplasms. *Blood reviews,* 31**,** 77-92.

YUAN, X., GAJAN, A., CHU, Q., XIONG, H., WU, K. & WU, G. S. 2018. Developing TRAIL/TRAIL death receptor-based cancer therapies. *Cancer and Metastasis Reviews,* 37**,** 733-748.

ZAHRA, K. F., LEFTER, R., ALI, A., ABDELLAH, E.-C., TRUS, C., CIOBICA, A. & TIMOFTE, D. 2021. The Involvement of the Oxidative Stress Status in Cancer Pathology: A Double View on the Role of the Antioxidants. *Oxidative Medicine and Cellular Longevity,* 2021**,** 9965916.

ZAMAN, S., WANG, R. & GANDHI, V. 2014. Targeting the apoptosis pathway in hematologic malignancies. *Leuk Lymphoma,* 55**,** 1980-1992.

ZHANG, J., HU, W., DING, C., YAO, G., ZHAO, H. & WU, S. 2019. Deferoxamine inhibits iron-uptake stimulated osteoclast differentiation by suppressing electron transport chain and MAPKs signaling. *Toxicol Lett,* 313**,** 50-59.

ZHAO, H., WU, L., YAN, G., CHEN, Y., ZHOU, M., WU, Y. & LI, Y. 2021. Inflammation and tumor progression: signaling pathways and targeted intervention. *Signal Transduction and Targeted Therapy,* 6**,** 263.

ZHAO, R. Z., JIANG, S., ZHANG, L. & YU, Z. B. 2019. Mitochondrial electron transport chain, ROS generation and uncoupling (Review). *Int J Mol Med,* 44**,** 3-15.

ZOROVA, L. D., POPKOV, V. A., PLOTNIKOV, E. Y., SILACHEV, D. N., PEVZNER, I. B., JANKAUSKAS, S. S., BABENKO, V. A., ZOROV, S. D., BALAKIREVA, A. V., JUHASZOVA, M., SOLLOTT, S. J. & ZOROV, D. B. 2018. Mitochondrial membrane potential. *Analytical biochemistry,* 552**,** 50-59.

APPENDICES

Appendix 1: Cell viability of Hek239 cell

Hek293 cells were treated with a range concentration of Hexacyclen (0 – 500 µM) for 48 hours. Cell viability of Hek293 cells decreased in a dose-dependent manner and an IC_{50} and IC_{20} of 138µM and 6µM were recorded (Appendix Table 1)

Hexacyclen Concentration (µg/ml)	Average Absorbance	% Viability	Log [Hexacyclen]
0	1.63	100	
25	1.10	59	1.40
50	0.91	52	1.70
100	0.69	41	2.00
200	0.73	44	2.40
300	0.72	45	2.70
400	0.72	47	2.88
500	0.59	37	3.00

Appendix 2: Cell viability of Caco2 cells

Caco2 cells were treated with a varying range of Hexacyclen concentrations (0 – 50 µM) over 48 hours. A dose-dependent decrease was revealed by the MTT assay and an IC50 and IC20 of 5µM and 1.2µM were detected (Appendix Table 2).

Hexacyclen Concentration (µg/ml)	Average Absorbance		% Viability	Log [Hexacyclen]
0	2.69		100	
2.5	1.69		63	0.40
5	1.15		43	0.70
10	0.48		18	1.00
20	0.45		17	1.30
30	0.43		16	1.48
40	0.62		23	1.60
50	0.45		17	1.70

Appendix 3: Nitrate standard curve

Table 3: The determination of the nitrates and nitrites standard.

Nitrite Standard Concentration (µM)	Absorbance		Average absorbance
0	0	0	0
25	0.138	0.146	0.142
50	0.271	0.281	0.276
75	0.303	0.388	0.3455
100	0.445	0.526	0.4855
125	0.679	0.606	0.6425
150	0.711	0.733	0.722
175	0.754	0.789	0.7715
200	0.827	0.935	0.881

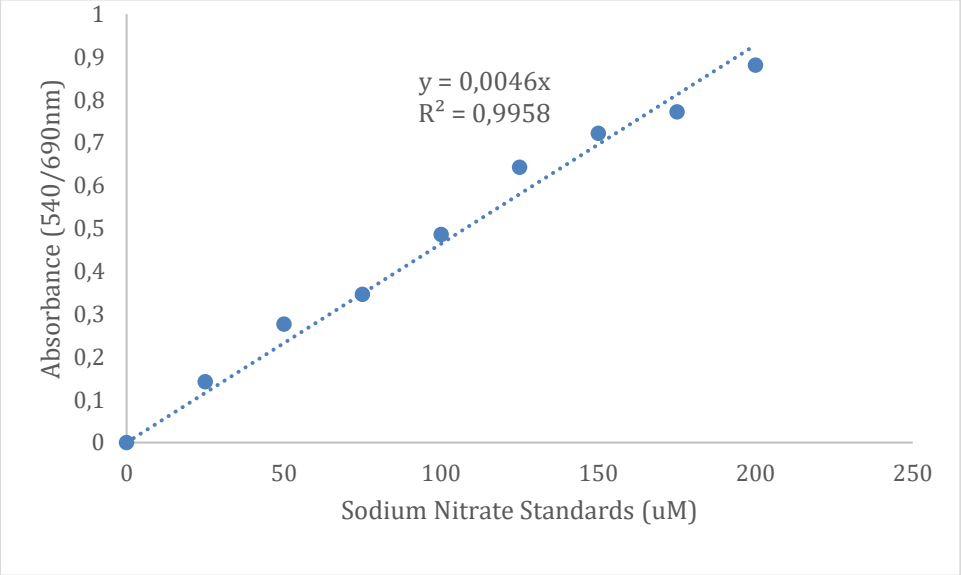

***Figure 1**: Standard curve generated from nitrates and nitrites standards and was used to determine nitrates and nitrites concentration in samples.*

Appendix 4: Protein standard curve

Bovine Serum Albumin (BSA) was used for protein quantification and standardisation

Concentrations	OD1	OD2	Average	Avg-Blank
0	0.069	0.075	0.072	0
0.2	0.133	0.136	0.1345	0.0625
0.4	0.188	0.193	0.1905	0.1185
0.6	0.218	0.219	0.2185	0.1465
0.8	0.277	0.281	0.279	0.207
1	0.274	0.344	0.309	0.237

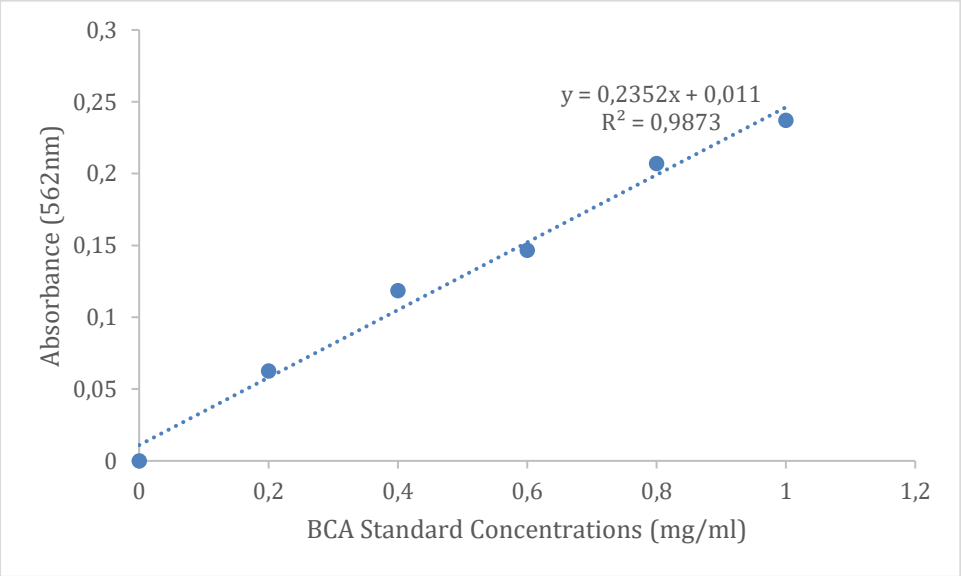

Figure 2: *standard curve generated from BSA standard and used to determine protein concentrations in samples.*

Appendix 5: Bax protein expression in Hek293 cells

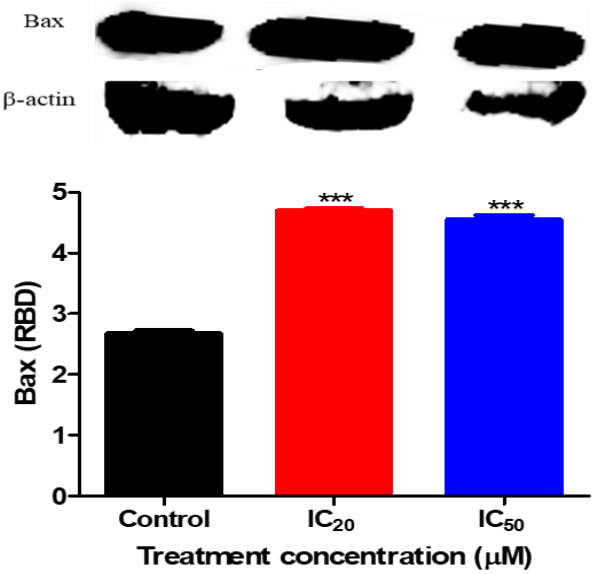

Figure 3: *Hexacyclen induced a significant increase in Bax activity at IC_{20} and IC_{50} in Hek293 cells treated for 48 hours (**p < 0.0001, **p= 0.0002, using an unpaired t-test with Welch's correction).*

Appendix 6: Activity of PARP-1 and cPARP-1

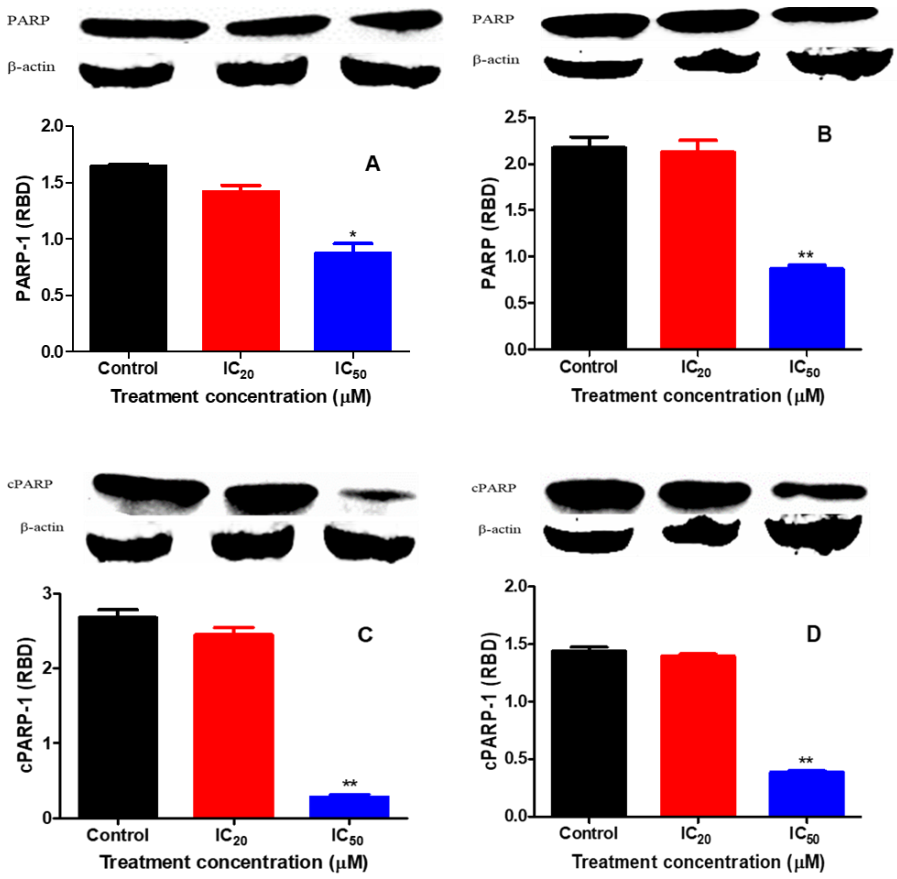

***Figure 4**: A non-significantly decline was triggered at IC_{20} in PARP-1 and cPARP-1 of Hek293 and Caco2 cells while an IC_{50} caused a significant decreased after 48-hour treatment period (*p= 0.0134, **p= 0.0020, **p= 0.0086, **p= 0.0012, using an unpaired t-tests with Welch's correction).*

Appendix 7 protein activity of STAST-3 and pSTAST-3

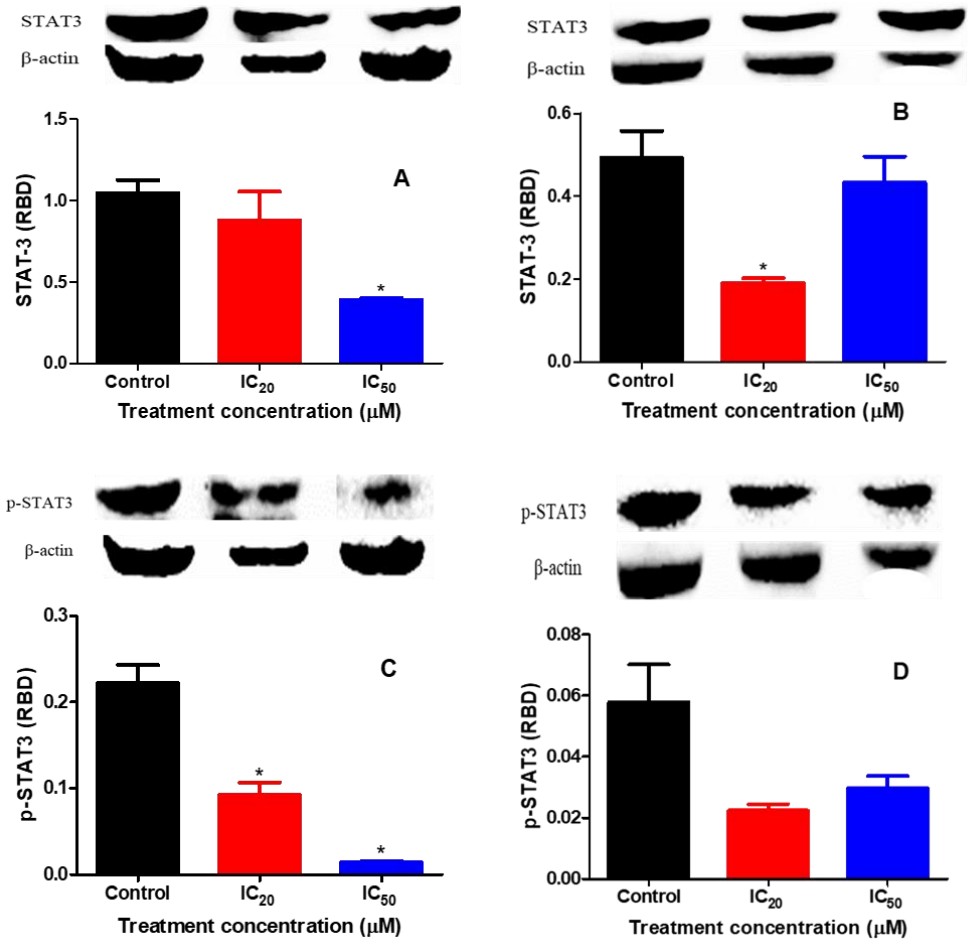

***Figure 5**: Stat-3 activity was significantly decreased by the IC_{50} in Hek293 cells while it was significantly decreased by the IC_{20} in Caco2 cells (*p= 0.0146, *p= 0.0458). In Hek293 cells, P-Stat3 was significantly reduced at IC20 and IC50 meanwhile in Caco2 cells was decreased non-significantly (*p= 0.0147, *p= 0.0103, using an unpaired t with Welch's correction).*